An Experimental Investigation of Multi-Functional Z-Pinned Carbon-Epoxy Composites

A thesis submitted in fulfilment of the requirements for the degree of Doctor of Philosophy

Fabio Pegorin

BEng, MEng (University of Padua)

School of Aerospace Mechanical and Manufacturing Engineering

College of Science Engineering and Health

RMIT University

September 2016

Declaration

I certify that except where due acknowledgement has been made, the work is that of the author alone; the work has not been submitted previously, in whole or in part, to qualify for any other academic award; the content of the thesis is the result of work which has been carried out since the official commencement date of the approved research program; any editorial work, paid or unpaid, carried out by a third party is acknowledged; and, ethics procedures and guidelines have been followed.

Fabio Pegorin
September 14th 2016

Acknowledgements

Thanks to the ones who cared about me and my work.

Table of Contents

List of figures

AN EXPERIMENTAL INVESTIGATION OF MULTI-FUNCTIONAL Z-PINNED CARBON-EPOXY COMPOSITES

FABIO PEGORIN

BEng, MEng (University of Padua)

Abstract

Carbon fibre reinforced epoxy composites have high specific strength, stiffness and fatigue resistance whilst being durable and corrosion resistant, and these properties make them suitable for light-weight aerospace structures. Despite the many advantages, there are some properties that limit the use of composites in aircraft structures. Carbon-epoxy laminates are susceptible to delamination cracking due to the low strength and toughness properties of the epoxy matrix and the fibre-matrix interface. Delamination cracks can grow under relatively low interlaminar loads resulting in a potential threat to the structural integrity and safety of composite structures. Other problems with using carbon-epoxy composites in aircraft structures are their low electrical and thermal conductivities, particularly in the through-thickness direction.

This PhD project aims to experimentally characterise a novel multi-functional carbon fibre-epoxy laminate that uniquely combines high delamination resistance with increased thermal and electrical conductivities. These properties are controllably improved using z-pins, which are thin composite or metal rods inserted in the through-thickness direction of the laminate. The effects of the volume content, diameter, length and material properties of z-pins on the delamination fracture toughness, fatigue resistance, impact damage tolerance, and interlaminar strengthening mechanisms are systematically investigated. In addition, the influence of the material properties and volume content of z-pins on the through-thickness electrical and thermal conductivities of carbon-epoxy laminates is determined. Using this information, it is possible to design multi-functional composites with tailored damage tolerant and electrical/thermal properties.

An extensive literature review is presented in this PhD thesis into the processes used to manufacture z-pinned composites. The benefits of z-pinning for improving the interlaminar fracture toughness and delamination fatigue resistance of laminates is reviewed using both

experimental and finite element modelling research. The thesis also reviews the adverse effect of z-pins on the microstructure and in-plane mechanical properties of laminates.

An experimental study into the improvements to the mode II interlaminar fracture toughness and fatigue properties of z-pinned carbon-epoxy laminates is presented. The effect of z-pin material on the mode II delamination properties is investigated using thin rods made of carbon fibre composite, stainless steel, titanium or copper. Irrespective of the material, the z-pins are highly effective at increasing the mode II fracture toughness and fatigue resistance. However, z-pins made of carbon fibre composite prove more effective than metal pins at improving the mode II delamination properties. Fracture toughening and fatigue strengthening occurs by the z-pins forming a large-scale crack bridging zone, and these mechanisms are determined.

A follow-on study systematically explores the effects of the volume content, diameter and length of z-pins on the mode II interlaminar fracture toughness and delamination fatigue resistant properties of carbon-epoxy laminate. The mode II fracture toughness increases rapidly with the volume content of z-pins (by 200-300% for every 1% increase in volume content), and this is due to an increasing number of pins generating bridging traction loads along the delamination crack. However, there is limiting volume content of z-pins beyond which no further improvements are gained due to a transition in the mode II fracture mechanism from single to multiple delamination cracks. The mode II fracture toughness is also influenced by the diameter of z-pins; with thicker pins being more effective by increasing the length of the crack bridging zone. The z-pin length also affects the delamination toughness and fatigue properties, and this is examined.

The delamination toughness and fatigue properties of z-pinned laminates are also investigated under mixed mode I/II interlaminar loading. The toughness and fatigue properties increase with the mode I component of the mixed I/II loading, revealing that z-pins are more effective at resisting the growth of delamination cracks under mode I than mode II (both monotonic or cyclic loads).

The parameters which control the impact damage resistance and post-impact compressive properties of z-pinned laminates are experimentally investigated. The effect of the z-pin material (carbon fibre composite, stainless steel, titanium and copper) and z-pin length (2, 4 and 7 mm) on the barely visible impact damage response and in-plane compressive properties (pre- and post-impact) are studied. A large reduction (up to 70%) to the impact damage area was achieved

using z-pins, with pins made of carbon fibre composite being more effective than metal pins. The percentage reduction in the amount of impact-induced damage gained by the z-pins increases with the incident impact energy, and this is because the pins are more effective at resisting the growth of long delaminations. Pre-impact compression testing reveals the z-pins did not change significantly the compressive modulus and strength of the laminate. The compression-after-impact strength of the z-pinned laminates is higher (20% on average) than the unpinned material, and this is due to the impact damage area being smaller.

The effects of the material type and volume content of z-pins on the electrical conductivity of carbon-epoxy laminates is investigated experimentally and analytically. The electrical conductivity was determined in the through-thickness, longitudinal and transverse directions. The through-thickness conductivity increases at a linear rate with the z-pin content. The conductivity is also controlled by the z-pin material, and increases in the order of carbon fibre composite (least conductive), stainless steel, titanium and copper (most conductive). However, the z-pins did not change significantly the in-plane (longitudinal and transverse) electrical conductivity of the laminate, and this was due to the inability of the discrete z-pins to create a continuous pathway for the electric current to flow. A simple model based on rule-of-mixtures analysis is found to approximate the through-thickness and in-plane electrical properties of z-pinned laminates.

The effects of the material properties and volume content of z-pins on the through-thickness thermal diffusivity of carbon-epoxy laminates are investigated. The flash laser method is implemented into an FE model and used to calculate the thermal diffusivity of the laminates, and from this the thermal conductivity is computed. An analytical based on the rule-of-mixture is also developed to predict the effect of z-pins on the thermal properties of the laminate. Analysis performed using the FE and analytical models give results that show that the through-thickness thermal conductivity is increased by z-pins, which create a pathway for accelerated heat flow through the laminate.

This PhD project demonstrates for the first time that by the judicious choice of the volume content, diameter, length and material properties of z-pins it is possible to controllably tailor the mode I/II delamination fracture toughness, mode I/II delamination fatigue resistance, impact damage resistance, post-impact compressive properties, and through-thickness electrical and thermal conductivities. Such flexibility will potentially enable aircraft designers to manufacture

z-pinned composites with improved mechanical, electrical and thermal properties for light-weight, damage tolerant structures.

List Of Publications

F. Pegorin, K. Pingkarawat, S. Daynes and A.P. Mouritz. Multi-functional fibre-polymer composites using z-pins. Proceeding of the 16th European Conference on Composite Materials (ECCM-16); Seville, Spain, 06/2014.

F. Pegorin, K. Pingkarawat, S. Daynes, A.P. Mouritz. Mode II interlaminar fatigue properties of z-pinned carbon fibre reinforced epoxy composites. Composites Part A: Applied Science and Manufacturing. 2014; 67:8-15.

F. Pegorin, K. Pingkarawat, A.P. Mouritz. Comparative study of the mode I and mode II delamination fatigue properties of z-pinned aircraft composites. Materials & Design. 2015; 65:139-46.

F. Pegorin, K. Pingkarawat, S. Daynes, A.P. Mouritz. Influence of z-pin length on the delamination fracture toughness and fatigue resistance of pinned composites. Composites Part B: Engineering. 2015; 78:298-307.

F. Pegorin, K. Pingkarawat, S. Daynes, A.P. Mouritz. Delamination fatigue properties of z-pinned carbon-epoxy laminate using metal or composite rods. Proceedings of the 20th International Conference on Composite Materials (ICCM20); Copenhagen, Denmark, 07/2015.

A.P. Mouritz, K. Pingkarawat, F. Pegorin, G. Stegschuster, B. Wendland. Improving the delamination fatigue properties of textile composites using through-thickness reinforcement. Proceeding of the 12th International Conference On Textile Composites (TEXCOMP-12); Raleigh, USA, 05/2015.

F. Pegorin, K. Pingkarawat, S. Daynes, A.P. Mouritz. Delamination fatigue properties of z-pinned carbon-epoxy laminate using metal or composite rods. Composite Science & Technology. (Under Review).

Chapter 1: Introduction

1.1 Project Background

For about 30 years, carbon fibre polymer matrix composites have been successfully used in aircraft structures. Despite their long use there are some factors limiting the use of composites. Inferior impact damage resistance and low through-the-thickness mechanical properties of composites when compared to other aerospace materials such as aluminium and titanium alloys limit their use in some critical aircraft structures which are subjected to high interlaminar stresses and that are likely to be impacted (e.g. leading edges of wings, inlet fan blades to engines). Low interlaminar mechanical properties lead to delamination, which is a long standing problem for composites. Carbon fibre reinforced epoxy composites used in aircraft structures are susceptible to delamination cracking due to the low strength and fracture toughness of the polymer matrix and fibre-matrix interface. Delamination cracks are caused by in-service damage events such as bird strike and other impact events, and due to their adverse effect on the structural properties of composites there are stringent aviation safety regulations on their management. The Federal Aviation Administration (FAA) [1, 2] mandates damage tolerant regulations which specify that delamination cracks within aircraft composites above a critical size must be repaired or the damaged structures replaced. (The critical size depends on several parameters including the loading and geometry of the structure and the location of the damage). FAA regulations permit short delamination cracks to be left unrepaired provided they do not grow under operational loading and environmental conditions over a specified period of time. However, aircraft composites are prone to rapid fatigue cracking under relatively low interlaminar cyclic loads due to the brittle epoxy matrix. Delamination cracks can grow under mode I or mode II interlaminar fatigue loads [3-5], and this severely limits the allowable damage size for aircraft composite structures. New materials are needed to increase the delamination fracture toughness and fatigue damage tolerance of aerospace composite structures.

Many techniques have been developed to minimize or overcome the delamination problem and low impact resistance. Techniques include high performance matrix systems (chemical or rubber toughening), thermoplastic interleaving and plasma treatment of fibres. Driven by the need to decrease the manufacturing costs and time, increase the impact damage resistance and through-the-thickness mechanical properties, various approaches to manufacture composites using three-

dimensional fibre architectures have also been investigated. The through-the-thickness reinforcement techniques include 3D weaving, stitching, 3D braiding, tufting and z-anchoring. These techniques are all effective at increasing the interlaminar fracture toughness and impact resistance of composites, however they cannot readily be used on prepreg materials. This is a serious limitation because many of the highly-loaded aerospace composite components are made using carbon-epoxy prepreg tape. The only technique that can be used on prepreg materials in large commercial quantities is z-pinning. Z-pins are thin rods made of high strength and stiffness material such as carbon fibre composite or metals.

Z-pins are inserted in the through-the-thickness direction of uncured prepreg laminates, although the technique can also be used to reinforce fabrics (prior to resin infusion), which are then cured in an autoclave. The z-pins create an interlocking mechanism between plies through a combination of adhesion and friction which improves significantly the delamination resistance of composites.

Modern aircraft structures require multi-functional materials able to provide high structural/mechanical properties combined with suitable thermal and electrical performance. Increased engine performance and increased flight speed are only two of the reasons why the thermal load on modern aircraft is increasing and is estimated to reach 10 MW within the next few years [6, 7]. Cooling of components such as leading edges to supersonic aircraft, surrounding areas to the auxiliary power unit (APU), and hydraulic pump enclosures all need high heat transfer capability to efficiently and rapidly dissipate heat. A limitation of carbon fibre composites is their low in-plane and through-thickness thermal conductivities, which is much lower than aircraft grade aluminium alloys. The need exists to tailor the thermal properties of composite to increase their thermal management for aircraft structures. One possible but not yet investigated solution, is to increase the through-thickness thermal conductivity using z-pins.

There is also a desire to provide composite materials with, among other integrated functions, improved electrical conductivity. Compared to aluminium, composite materials are more susceptible to damage caused by lightning strikes due to their lower electrical conductivity [8]. A lightning strike can deliver 10-200 kA in less than a second, and this large amount of energy must be rapidly dissipated from an aircraft. The concern is not just limited to the damage of the composite, but there is also the risk involving damage to electronic on-board equipment. This includes damage from current flowing into the on-board systems such as hydraulic fuel lines,

electrical wiring, fuel and vent tubes. It is feasible that z-pins can be used to improve the electrical conductivity of composites, along it remains to be proven.

1.2   Aim and Scope of PhD

This PhD project aims to develop and characterise a novel multi-functional composite material for aerospace structures that combines high structural performance and damage tolerance with thermal and electrical management. These properties will be controllably tailored in composites using the through-the-thickness reinforcement technology known as z-pinning. Z-pins are currently used on a few military aircraft types (FA-18 E/F Super Hornet) and F1 cars, although their functionality has been limited to increased damage tolerance and joining.

This PhD project makes a major technological advance in the characterisation of a new class of z-pinned composite that combines multi-functional properties including thermal management, high electrical conductivity, improved delamination toughness, delamination fatigue resistance and damage tolerance whilst retaining high in-plane mechanical performance (e.g. tension/compression stiffness and strength) and light-weight. The project involves an experimental study into the increased delamination toughness and delamination fatigue resistance obtained by z-pins under different interlaminar loading conditions. The project also involves an original study into the analysis and experimental evaluation into the use of z-pins to controllably tailor the through-thickness thermal and electrical properties of composites. It is shown that z-pins can be used for the thermal management (increased thermal conductivity) and electrical management (increased electrical conductivity). Increased thermal conductivity will allow composites to dissipate heat more readily, which will potentially increase their applications in high temperature components. Increased electrical conductivity will allow composites to dissipate more effectively electrical charges resulting from lightning strikes, potentially eliminating the current requirement for expensive metallic meshes used in composites aerospace structures. However, more extensive research is needed before z-pins can be considered as an effective approach to prevent damage from lightning strikes on composite aircraft. The vision that the mechanical, electrical and thermal properties can be controlled using z-pins depends on extensive and in-depth research and development of these composite materials. The work presented in this PhD thesis makes some progress towards this vision

1.3   Format of PhD Thesis

An extensive review of the scientific and technical literature on z-pinned composites is presented in Chapter 2. Aspects such as the need to find large-scale and cost-effective techniques to improve

the damage tolerance on composites are described, and the z-pinning technique is introduced. The most relevant published research works performed into the manufacture, microstructure, damage tolerance and mechanical properties of z-pinned composites are reviewed.

Chapters 3, Chapter 4 and 5 present experimental investigations into the mode II and mixed mode I/II interlaminar fracture toughness and delamination fatigue resistant properties of z-pinned composites. The effects of the material, volume content, length and diameter of z-pins on the interlaminar properties on the mode II and mixed mode I/II interlaminar properties are determined. In addition, the effect of these z-pin parameters on the fracture toughening and fatigue strengthening mechanisms are identified.

The effect of the material and the length of z-pins on the impact damage resistance and in-plane compression properties of carbon-epoxy laminates is experimentally investigated in Chapter 6. Z-pinned composites were impacted at different incident energy levels and their post-impact compressive properties were determined. Z-pins increase the impact damage resistance of composite laminates, with the percentage improvement being dependent on the length. The in-plane compressive properties are not significantly affected by the z-pins, although because of the reduced impact damaged area the post-impact compressive strength is higher for z-pinned laminates.

Chapter 7 presents an experimental investigation into the electrical properties of z-pinned laminates. Z-pins create preferential paths for current flow in the through-thickness direction thereby proving an effective technique to increase the electrical conductivity. On the other hand, it was found that the in-plane electrical properties are not affected significantly by z-pins. Similar conclusions can be drawn when referring to the thermal diffusivity of z-pinned laminates reported in Chapter 8. An FE model is developed and used to calculate the effects of the volume content and material type of z-pins on the thermal properties of carbon-epoxy laminates. Z-pins, which are characterized by high heat transfer properties, have a significant effect on the through-thickness thermal diffusivity of composites.

Chapter 9 summarises the major findings and conclusions of the PhD project.

Chapter 2: Literature Review

2.1   Z-pinned Composites

Light-weight, high in-plane stiffness, strength and fatigue resistance as well as corrosion resistance are some of the properties that make composite materials useful for aerospace structures. However, composites have some drawbacks; in particular their susceptibility to delamination cracking due to the low strength and fracture toughness of the polymer matrix and fibre-matrix interface. The amount and type of damage caused by an impact event depends on many parameters, including the properties and ply orientations of the composite, the shape and kinetic energy of the impacting object, and the boundary conditions [9]. Wang et al. [10] showed experimentally and numerically that impact-induced delamination cracks in carbon–epoxy composites can significantly reduce the tensile properties. Delaminations caused by impact can also reduce the compression properties and buckling resistance [11].

Z-pins (Figure 2.1) are generally made from carbon fibre composite or metal (e.g. steel, titanium alloy). Once inserted and cured within the prepreg laminate, the pins will provide a locking mechanism between the plies through a combination of friction and adhesion. The volume content, diameter, length and material properties of the z-pins can be controllably tailored to achieve the desired level of damage resistance.
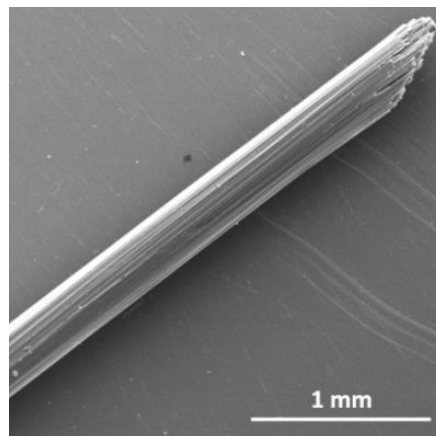
Figure 2.1. SEM photograph of a composite z-pin.

Z-pins are currently used on the F-18 E/F Superhornet jet fighter (Figure 2.2) as a substitute to titanium fasteners in the air inlet ducts and engine bay doors [12]. This has resulted in a cost saving of about $83,000 as well as in a modest weight reduction of 17 kg for each aircraft [13]. Partridge et al [13] estimated that using z-pins in aircraft can reduce the expenses of drilling and installation of metal fasteners by about 70%. The only non-aerospace application of z-pins technique is for Formula 1 cars (Figure 2.3) where they have been used to reinforce the composite roll cage [14].

Figure 2.2. Super Hornet F/A-18E/F fighter: Carbon fibre composite z-pins used in the air inlet ducts, which is circled.
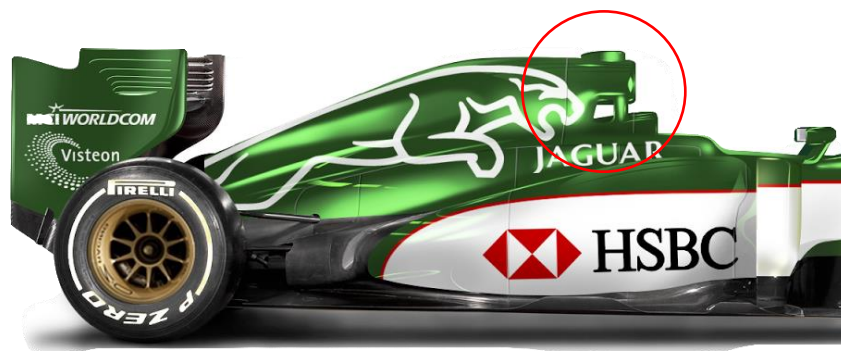
Figure 2.3. Jaguar R3 F1 Car. Z-pinned roll hoop, which is circled. [14].

2.2   Z-pinned Laminates: Manufacturing

Z-pinning is currently the only technique capable of the through-thickness reinforcement of prepreg-based carbon fibre-epoxy composites in large commercial quantities. Z-pins are inserted in the through-the-thickness direction of uncured prepreg laminates; although different insertion

techniques can be used. The most common technique is the Ultrasonically Assisted Z-Fiber®
process (UAZ), which is schematically represented in Figure 2.4.
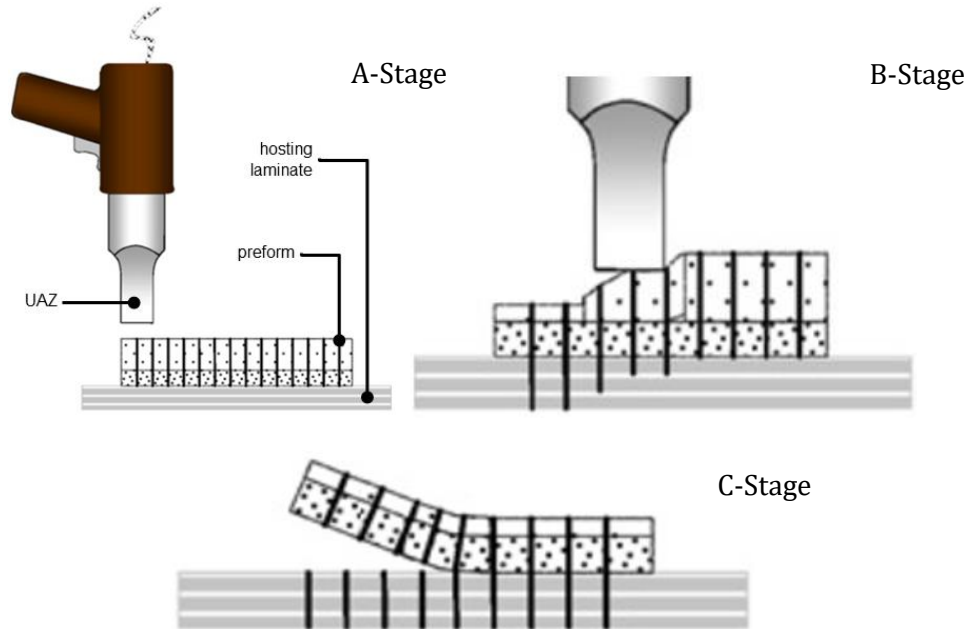
Figure 2.4. Schematic representation of the UAZ z-pinning process. Low density foam carrying z-pins is placed onto the uncured laminate (A-stage). UAZ through several steps is used to push the z-pins into the laminate (B-stage). Z-pin length in excess is sheared away with a cutting tool (C-stage) [15].

A two-layer foam consisting of an upper dense foam (such as 51IG Rohacell) is used to accurately
locate the z-pins and lower density foam is used to collapse under the pressure of an UAZ tool to
force the pins into the uncured prepreg. The flat head of the tool vibrates at 20 kHz, and this
induces an axial vibration to the z-pins. The pins are gently inserted via the combination of
applied pressure and vibration-induced heat which softens the uncured polymer matrix. After the
z-pins are inserted the collapsed foam and the excess z-pin length is sheared away using a cutting
tool. Other techniques have been used to insert z-pins into prepreg material. The low density z-pin foam carrier can be compressed via vacuum bagging and the overpressure generated by an
autoclave [16]. The combined heat and high pressure force the foam to collapse and thereby
insert the z-pins into the laminate.

2.3   Microstructure of Z-pinned Laminates

After inserting fibrous or metal z-pins into an uncured prepreg, the microstructure of the
laminate is changed. Generally the microstructural changes have an adverse effect on the in-plane

mechanical properties. In this section, research into the effect of z-pins on the microstructure of composites is reviewed.

2.3.1 Fibre waviness and crimping

One of the main changes to the microstructure due to z-pinning is fibre waviness. Fibres are pushed aside to create space for the z-pins, thereby creating fibre waviness (Figure 2.5). Fibre misalignment is higher at the flanks of the resin pockets [17]. The amount and extent of fibre waviness is dependent on the volume content and diameter of the z-pins, respectively. Chang [18] experimentally measured the effects of the volume content and diameter of z-pins on the fibre waviness. It was found that the volume fraction of fibre waviness increases linearly with the z-pin content (Figure 2.6a) and the waviness length (W_x) and misalignment (Θ) increases linearly with the z-pin diameter (Figure 2.6b).

(a)

(b)
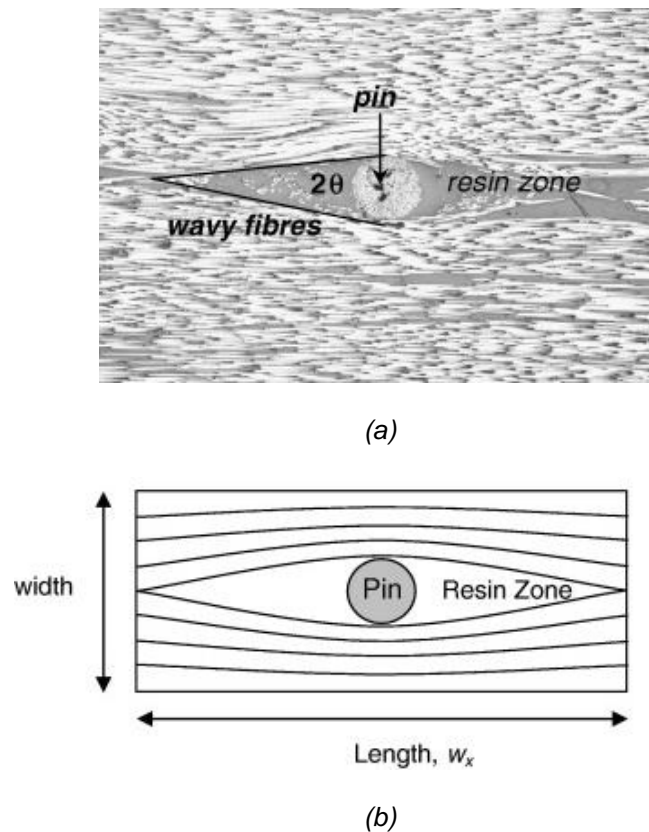
Figure 2.5. (a) SEM photo and (b) schematic of region of wavy fibres surrounding a z-pin [15].

(a)   *(b)*
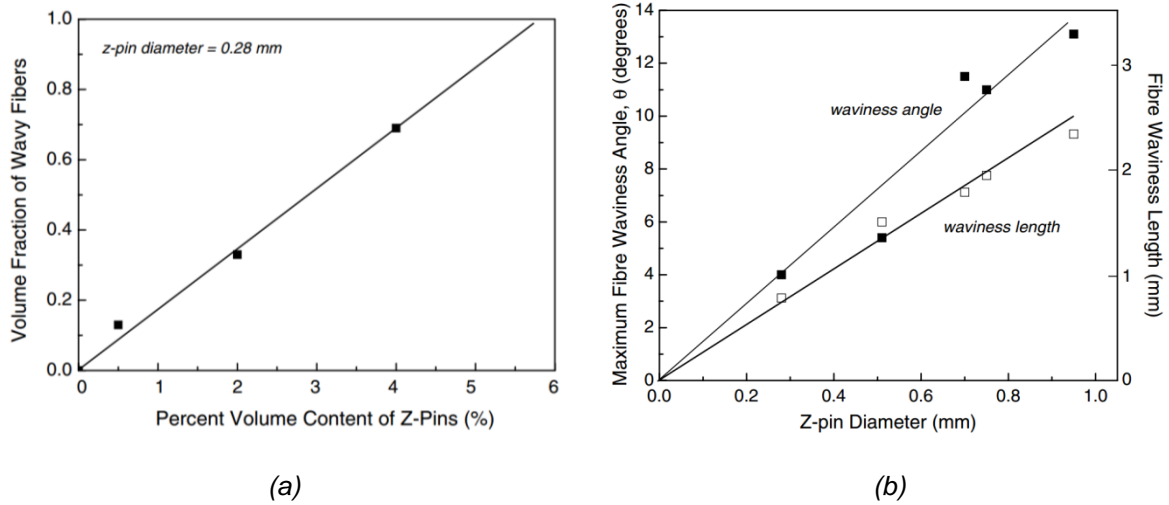
Figure 2.6. Effects of (a) volume content and (b) diameter of z-pins on fibre wavinaess in a unidirectional carbon-epoxy laminate [18].

Crimping of fibres in the z-pin insertion direction is another type of microstructural change to laminates (Figure 2.7). Crimping is caused by the z-pins pushing segments of the in-plane fibres towards the through-thickness direction.

(a)   *(b)*
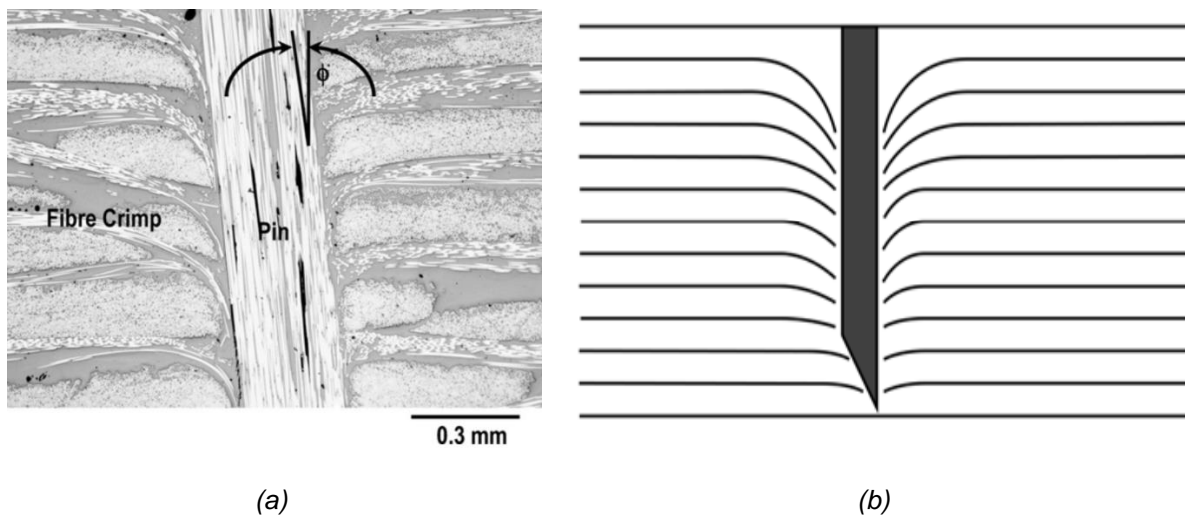
Figure 2.7. (a) SEM photo and (b) schematic of a cross-section of a z-pinned laminate showing fibre crimping [15].

2.3.2 Resin-rich zones

The formation of resin-rich region is a consequence of fibre waviness in the proximity of z-pins. The z-pins create voids which are subsequentially filled with resin during curing of the laminate (Figure 2.5). In laminates with high z-pin volume content, the pins are very close to each other

(around 1 mm) and this can cause continuous resin-rich channels to form in the fibre direction (Figure 2.8).
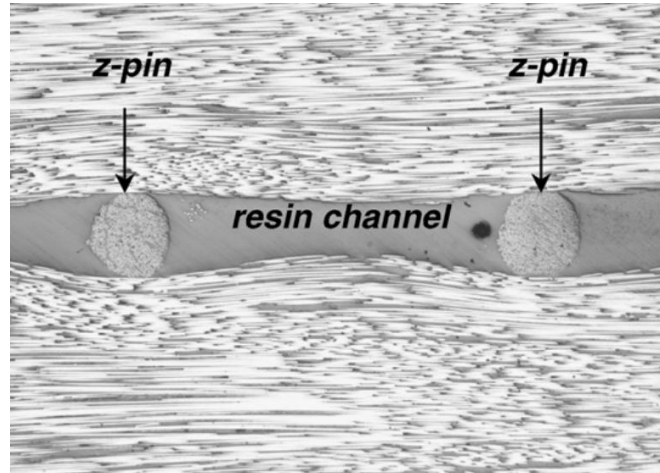
Figure 2.8. Resin-rich channel along a row of z-pins [15].

2.3.3 Z-pin interfacial micro-cracking

Due to the different thermal expansion coefficients of z-pins and the host laminate, the pins can experience interfacial debonding during curing (Figure 2.9). Sweeting and Thomson [19] used FE analysis to predict that cracks occur at or near the matrix z-pin interface because the residual tensile stress surrounding z-pins is about four times higher than the far-field residual stress. The residual stress at the laminate/z-pin interface is larger than the laminate/z-pin interface strength causing partial or complete interfacial cracking.
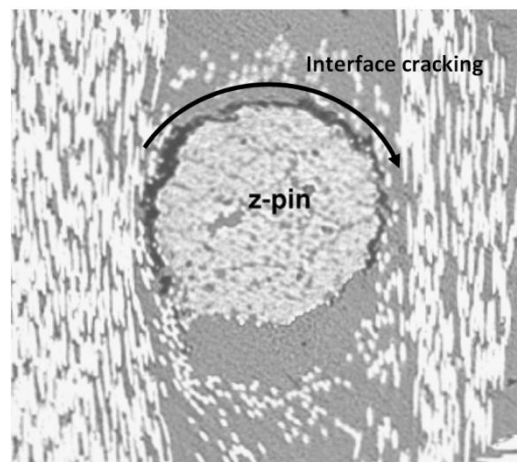
Figure 2.9. Z-pin laminate interfacial cracking [15].

2.3.4 Laminate swelling

Swelling is the average reduction of fibre volume content of the laminate caused by z-pins [13, 20, 21]. It is caused by the laminate expanding in order to accommodate the z-pins as well as the z-pins opposing through-thickness consolidation of the laminate during curing within an autoclave.

2.3.5 Z-pin misalignment

Despite the foam carrier which laterally supports and precisely locates the z-pins during insertion, the pins are unlikely to be perfectly aligned in the through-thickness direction. This is due to lateral loads being inadvertently applied during insertion combined with lateral forces applied during shear cutting of the excess pin length after insertion. When manual UAZ® is used for the insertion, the z-pins are inclined over a range of angles from the through-thickness direction (Figure 2.10).
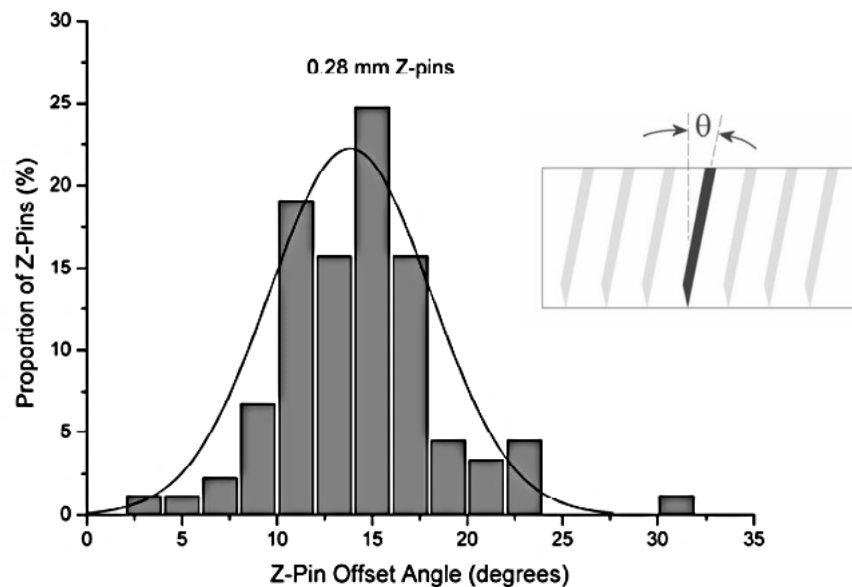
Figure 2.10. Z-pins off-set angle distribution in a carbon-epoxy laminate [18].

2.4 Z-pinned Laminates: Improvement to Mechanical Properties

2.4.1 Introduction

A large amount of experimental, numerical and analytical research has been conducted to evaluate the mechanical properties and failure mechanisms of z-pinned composites. Studies have

mainly focused on the improvements to the interlaminar properties such as delamination fracture toughness and impact damage resistance.

2.4.2 Experimental determination of the delamination fracture toughness

Delamination cracking is one of the main failure modes for composite materials and structures. Crack propagation in a composite can results in a loss in stiffness and strength, and potentially leads to catastrophic failure. A large number of numerical and experimental studies have been performed on the modes I and II interlaminar fracture toughness properties and delamination toughening mechanisms of z-pinned composites [15, 22-37]. The Double Cantilever Beam (DCB), the End Notch Flexure (ENF) and the Mixed-Mode Bending (MMB) tests are the most common techniques used to experimentally measure respectively the mode I, mode II and mixed I/II delamination properties of z-pinned composites and other types of fibre-polymer laminates (Figure 2.11).
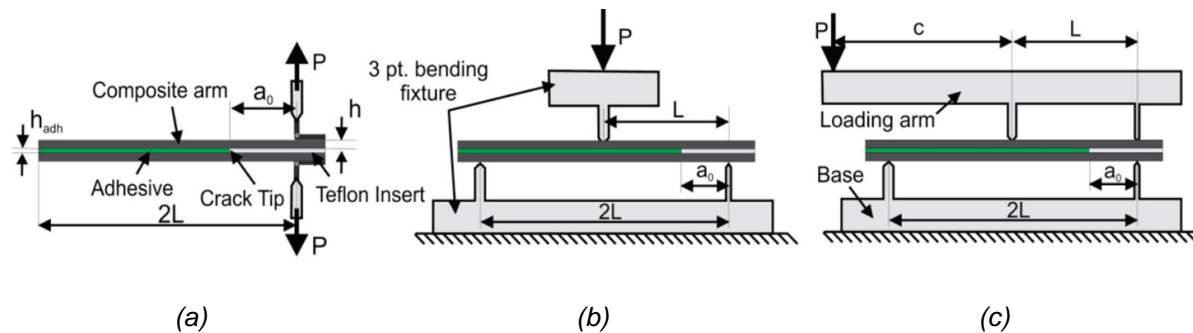
Figure 2.11. (a) Double Cantilever Beam (DCB), (b) End Notch Flexure (ENF) and (c) Mixed-Mode Bending (MMB) tests.

The mode I, mode II and mixed I/II delamination toughness of z-pinned composites increase with delamination crack length up to a steady-state toughness condition [6, 22, 23, 25, 28, 36-46] (Figure 2.12). The progressive increase in fracture toughness is due to the formation of a large-scale crack bridging zone in which an increasing number of z-pins bridge the delamination. Cartié et al. [34] have experimentally determined the mode I and mode II delamination toughness properties of an aircraft-grade carbon-epoxy laminate. Examples of the improvements to the fracture toughness (G_{Ic}, G_{IIc}) properties due to z-pins is shown in Figure 2.13. In this study, the mode I and mode II delamination toughness are improved by 15 and 8 times respectively, and both toughness properties increase linearly with the volume content of z-pins. Z-pins create a large-scale bridging zone along the delamination which reduces the stress acting at the crack tip and thereby increases the interlaminar fracture toughness.

There is a transition in the stability of the fracture process with z-pinning. Cracking of z-pinned laminates usually occurs as stick-slip propagation. The crack slows down when reaching the z-pin locations (stick), and once the pin has debonded from the laminate and pulled-out at the rear of the bridging zone then the crack advances (slip). In comparison, unpinned laminates with a brittle polymer matrix experience unstable (rapid) delamination failure. A different fracture sequence is involved for z-pinned composites where the crack shows stick-slip behaviour. Scanning electron micrograph revealed substantial changes in the failure mode of the z-pins for the different loading conditions. Under mode I the z-pins debond and are pulled-out with increasing crack opening (Figure 2.14). In-plane shear tests performed by Cartié et al. [34] under mode II loading the z-pins initially debond from the laminate and then are damaged by splitting and shear fracture (Figure 2.15).
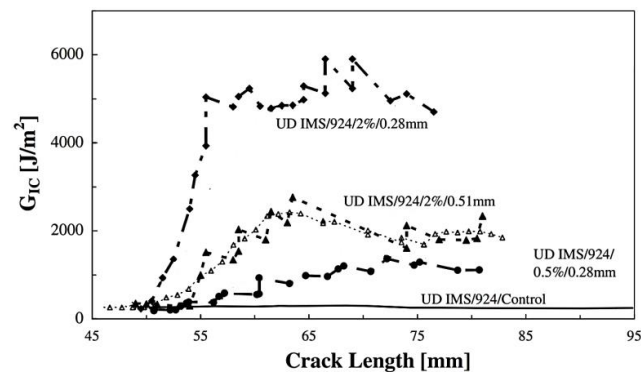
(a)
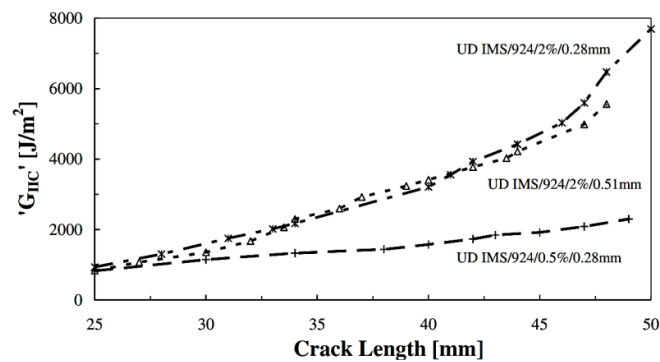
(b)

Figure 2.12. R-curves showing the effects of the volume content and diameter of z-pins on the (a) mode I and (b) mode II delamination toughness (G_{Ic}, G_{IIc}). UDIMS/924 identifies the carbon-epoxy tape used whilst 2%/0.51 mm identify the volume content and diameter (in mm) of the z-pins [34].
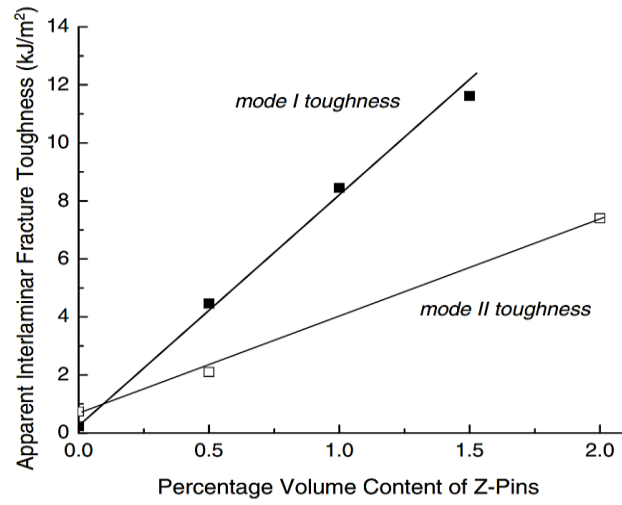
Figure 2.13. Effect of the z-pin volume content on the mode I and mode II delamination toughness. Carbon-epoxy composite was reinforced with composite z-pins 280 µm in diameter [15].
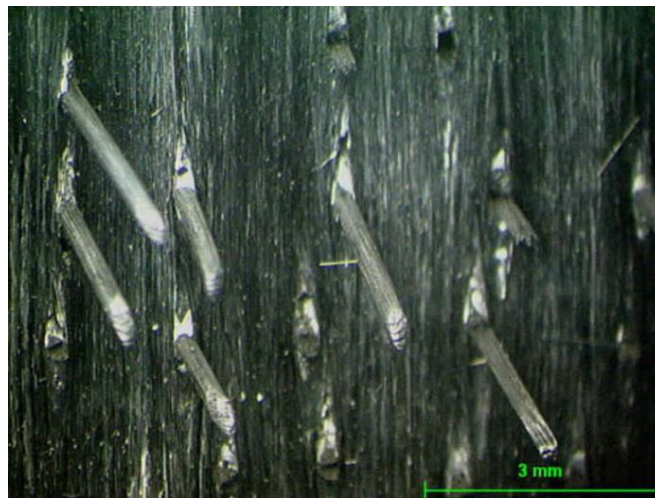
Figure 2.14. Optical microscope image showing the crack surface of a z-pinned composite which experienced mode I delamination cracking [35].
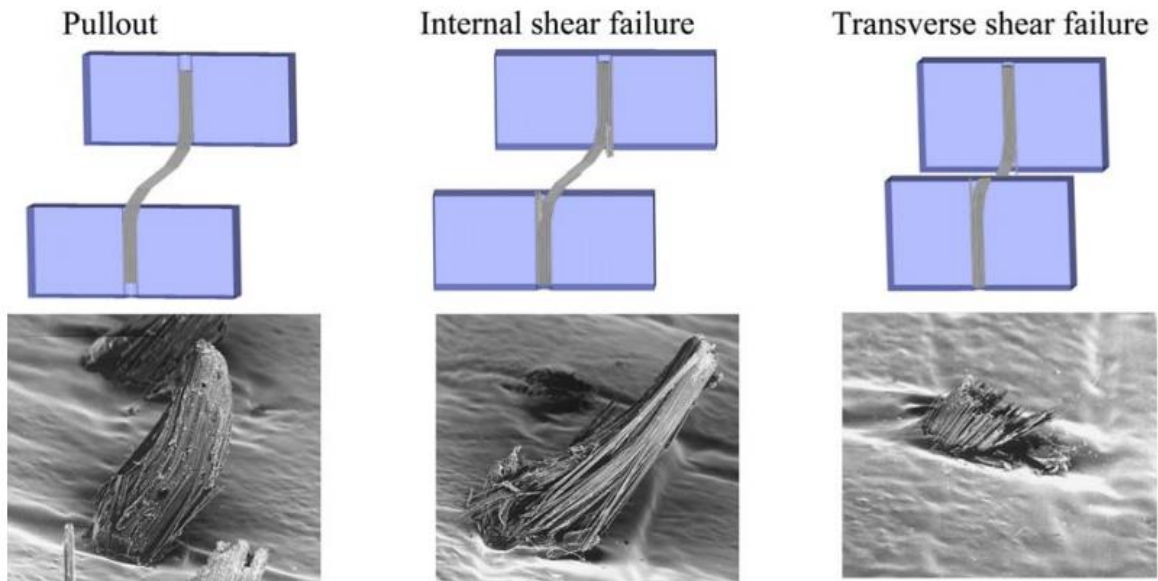
Figure 2.15. Sequence of the failure mechanism for a z-pin loaded in mode II. The z-pin partially debonded from the laminate and then experienced partial pull-out, splitting and finally shear rupture under increasing crack sliding displacement [34].

Mouritz and Koh [29] developed an analytical model to calculate the mode I bridging force generated by z-pins that takes into account parameters such as the misalignment, interfacial cracking and porosity (Figure 2.16). As mentioned, z-pin offset insertion angle is due to the manufacturing process. Interfacial cracking around z-pins is mainly due to residual stresses generated by a large difference in the thermal expansion coefficients of the z-pins and host laminate. The model also accounts for porosity in z-pins. The z-pin traction loads calculated using mechanical analysis are compared against experimental loads measured using pull-out test and are shown in Figure 2.17. The agreement between the predicted values and experimental data was good for the z-pinned laminate used in the study, and the modified traction load can be used to provide a good prediction of the effects of length, porosity, misalignment and interfacial cracking of z-pins.
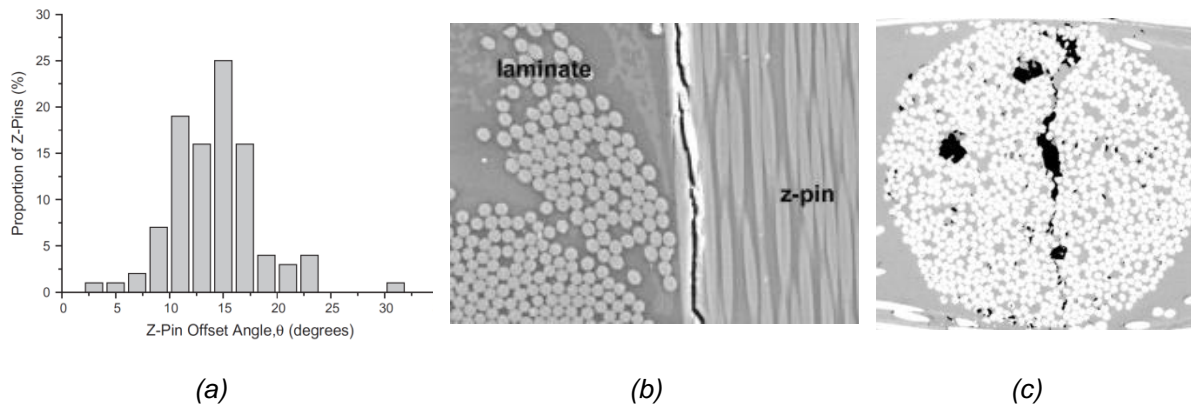
Figure 2.16. Microstructural parameters affecting the z-pin traction properties. (a) Typical off-angle distribution percentage of z-pins, (b) z-pin/laminate interface crack and (c) voids in a z-pin [29].
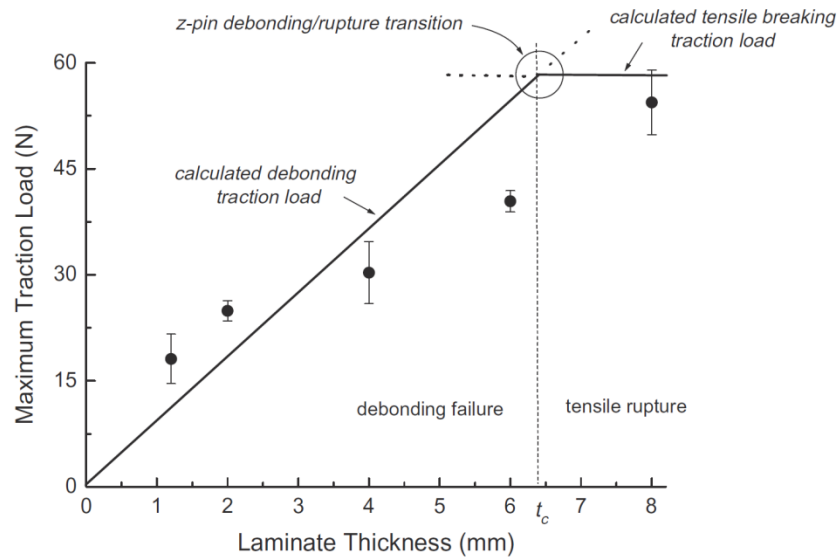
Figure 2.17. Effect of laminate thickness on the mode I maximum traction load and failure mode of a z-pin. The predicted values compared with experimental test data [29].

Cartié et al. [36] investigated the z-pin bridging toughening mechanisms under increasing crack opening (mode I) and crack sliding (mode II) displacements. Titanium and carbon fibre z-pins were embedded into cuboidal-shaped coupons containing a pre-existing delamination crack along the mid-plane. The coupons were bridged by a single z-pin. Under crack opening loading the z-pin always pulled out from one side of the coupon, with barely visible splitting of the laminate. Under mode I loading the failure mechanism is dominated by elastic tensile deformation of the z-pin (initial linear region of the bridging traction in Figure 2.18a), debonding of the z-pin, followed by pull-out from the laminate. Shear tests also exhibited three main stages of failure. Prior to pull-out, and then the z-pin elastically shear deforms and then starts to debond. It was

found that the angle of insertion affected the mode II failure mechanisms of the z-pin, which experienced pull-out or shear fracture when aligned with or against the nap, respectively (Figure 2.19).
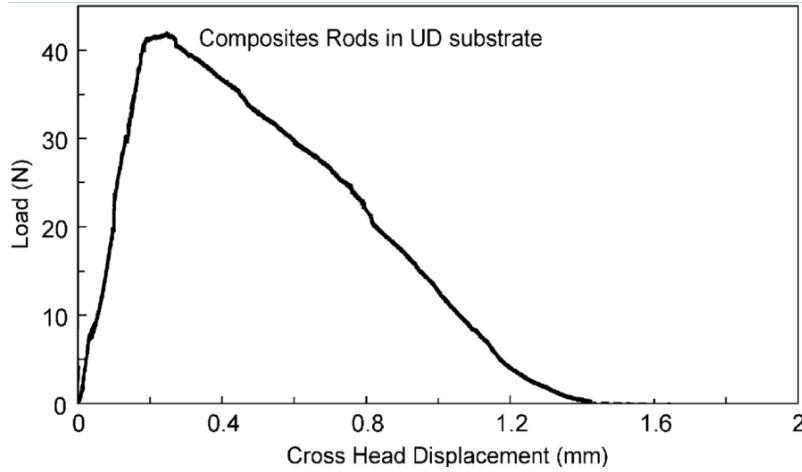
(a)
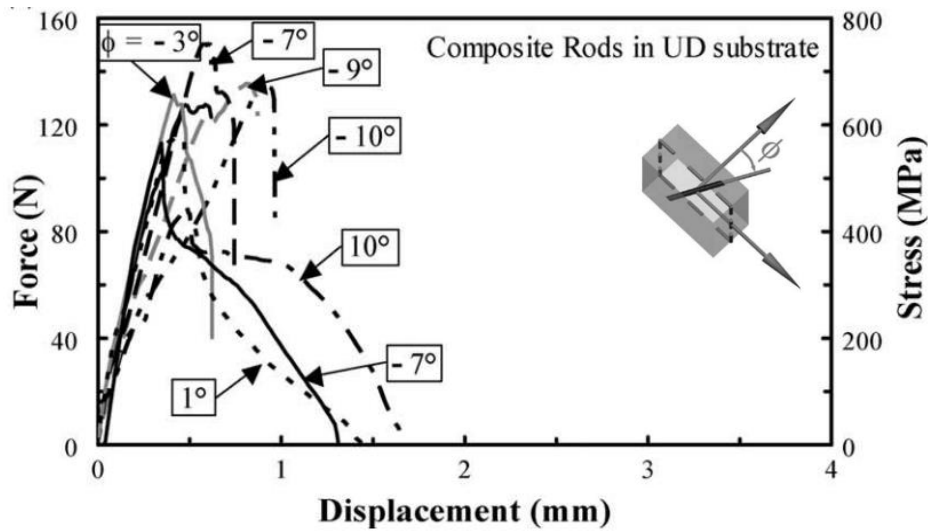
(b)

Figure 2.18. Crack bridging traction load-displacement curves for (a) mode I and (b) mode II of a single carbon-fibre z-pin.The numbers on Figure b indicate the z-pin angle [36].

(a)   *(b)*
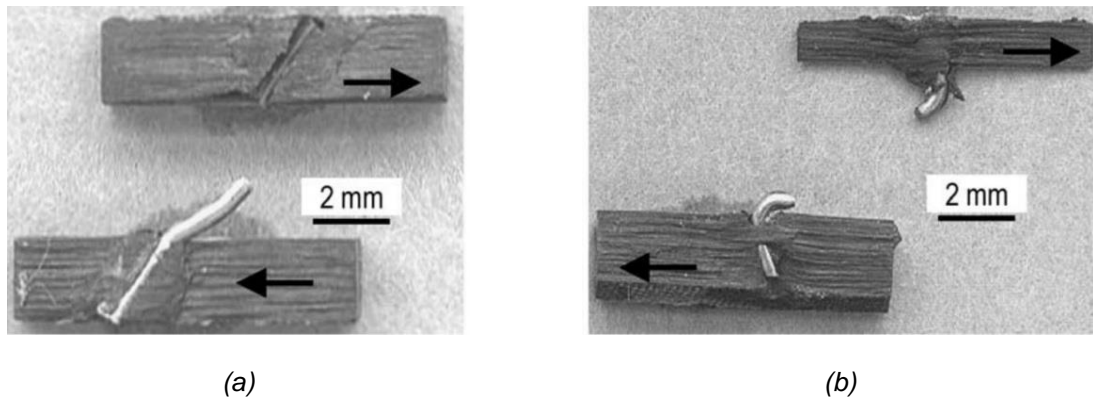
Figure 2.19. Effect of z-pin misalignment on the shear fracture mechanisms (a) with the nap and (b) against the nap [36].

2.4.3 Modeling the delamination fracture toughness of z-pinned laminates

Many research studies have been published aiming to model the delamination fracture behaviour of z-pinned composites, and different modelling approaches have been used. Some finite element models analyse the z-pinned delamination region as a cohesive zone with the fracture toughness computed by averaging the pin bridging forces over the entire crack area [26, 47]. Other models use non-linear springs located at the z-pins to compute the crack bridging traction loads, and from this the fracture toughness is computed [22, 23, 48].

In this section, published research into modelling the delamination fracture properties of z-pinned composites is reviewed. The double cantilever beam is the most common geometry used to model the mode I delamination toughness of z-pinned composites (Figure 2.20). Grassi and Zhang [44] developed a micro-mechanical FE model consisting of thick shell elements to model the laminate and non-linear interface elements to simulate the z-pins. The model is capable of analysing mixed-mode loading and different z-pin insertion angles. The model also computed the traction forces generated during pull-out and lateral ploughing of the z-pins. The numerical output of the FE model is a relation between the z-pin traction loads at the delamination surface and the crack opening displacement, and close agreement is found with the experimental data (Figure 2.21).
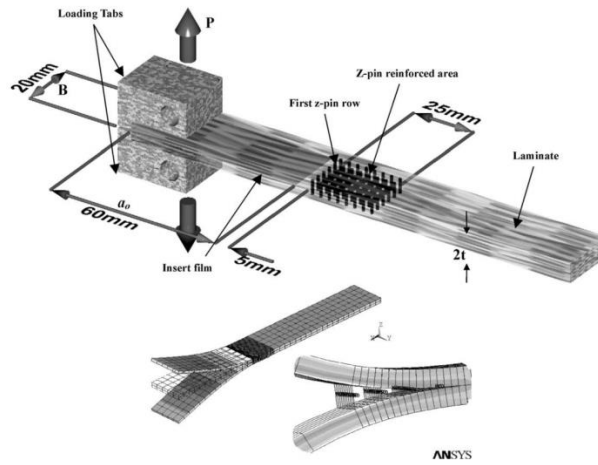
Figure 2.20. Schematic representation of the FE model for a z-pinned DCB laminate [44].
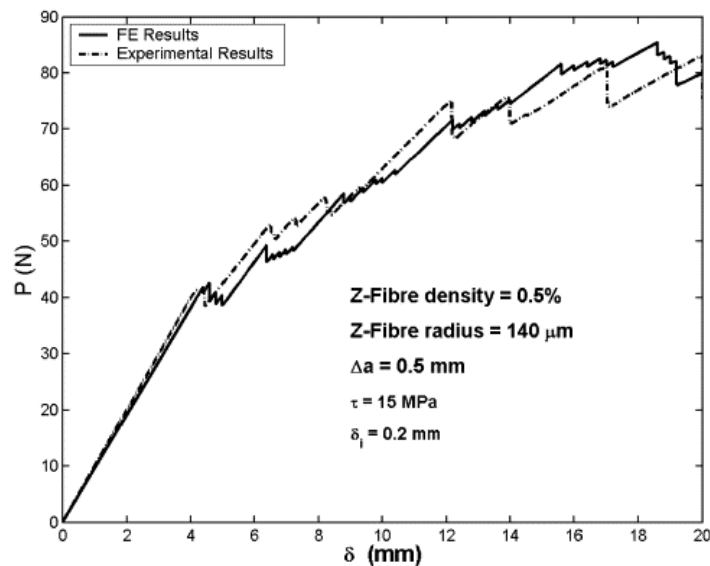
Figure 2.21. Load (P)-displacement (δ) curves for a z-pinned DCB laminate. Experimental results are accurately predicted with the FE model [44].

FE models are capable of analysing the three main toughening mechanisms induced by z-pins under mode I loading: elastic deformation, debonding and pull-out from the laminate (Figure 2.22a). Z-pin pull-out is the main toughening mechanism under mode I loading; accounting for ~80% of the total toughening effect [30]. Toughening under mode II loading is more complex, with the carbon fibre composite z-pins experiencing longitudinal splitting to accommodate large transverse shear deformations and, depending on the pin arrangement, the pins will subsequently pull-out or shear fracture (Figure 2.22b). While experiencing pull-out an enhanced

traction stress is generated, known as snubbing, induced by z-pin being pushed laterally into the laminate [33].

Cui et al. [32] developed a FE model to analyse the crack bridging mechanisms of z-pinned laminates subjected to mixed I/II loads. The cohesive zone method was used to compute the longitudinal splitting/rupture of z-pins. It was computed that shear traction loads generated by bridging z-pins increase with the mode II ratio because of the snubbing effect close to the delamination crack. The FE model was validated, showing good agreement with the experimental results for different mixed-mode ratios. Figure 2.23 presents the calculated opening load applied to the cracked-end of the z-pinned DCB coupon against the opening displacement generated at the same location. The model is validated for both the unpinned and z-pinned laminates.

(a)   *(b)*
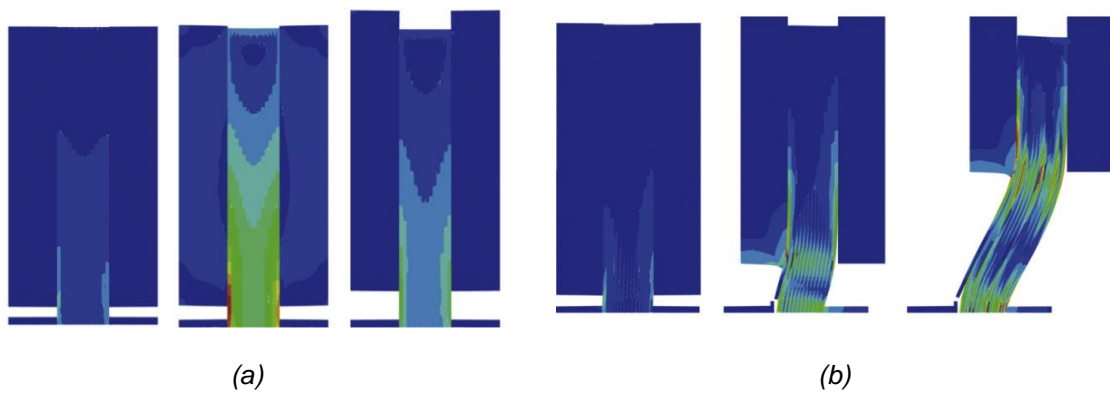
Figure 2.22. FE modelling of the (a) mode I and (b) mode II failure mode of a z-pin [32].

(a)
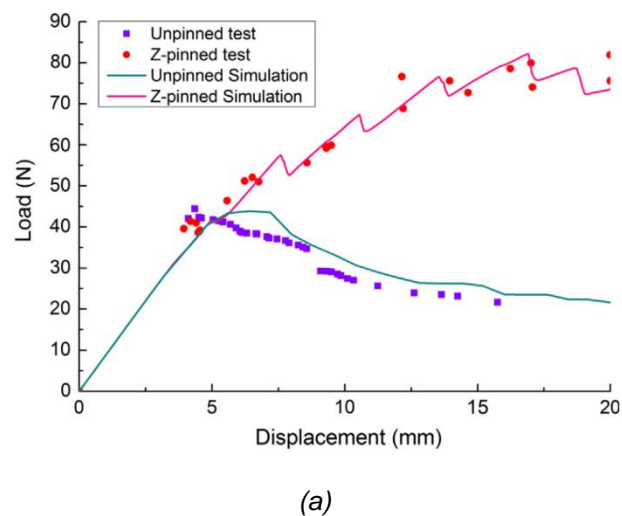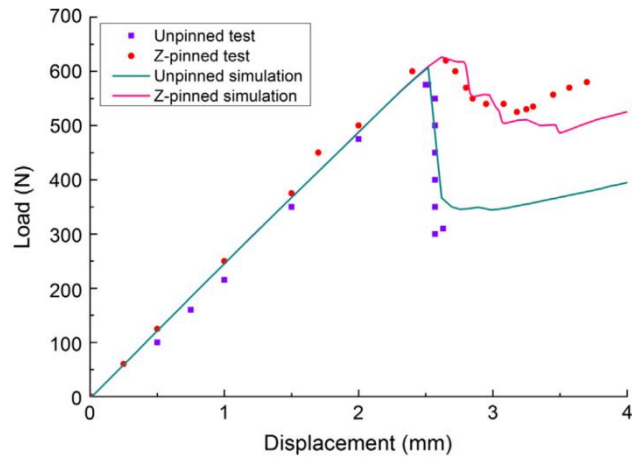
(b)
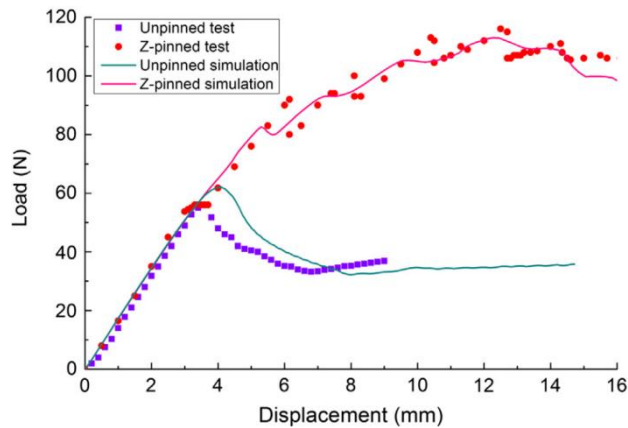
(c)

Figure 2.23. Load-displacement curves for unpinned and z-pinned laminates subjected to (a) mode I, (b) mode II and (c) mixed I/II loads ($G_{II}/G_{TOT} = 20\%$) [49].

Yan et al. [50] performed FE modelling using non-linear springs to simulate the z-pins (Figure 2.24a). The z-pins are defined using a non-linear spring system, with the springs uniformly distributed and arranged on the nodes. Mode I DCB tests performed by Cartié and Partridge [51] were used as reference experimental data to prove the accuracy of the FE model, and excellent agreement was found (Figure 2.24b).

(a)

(b)
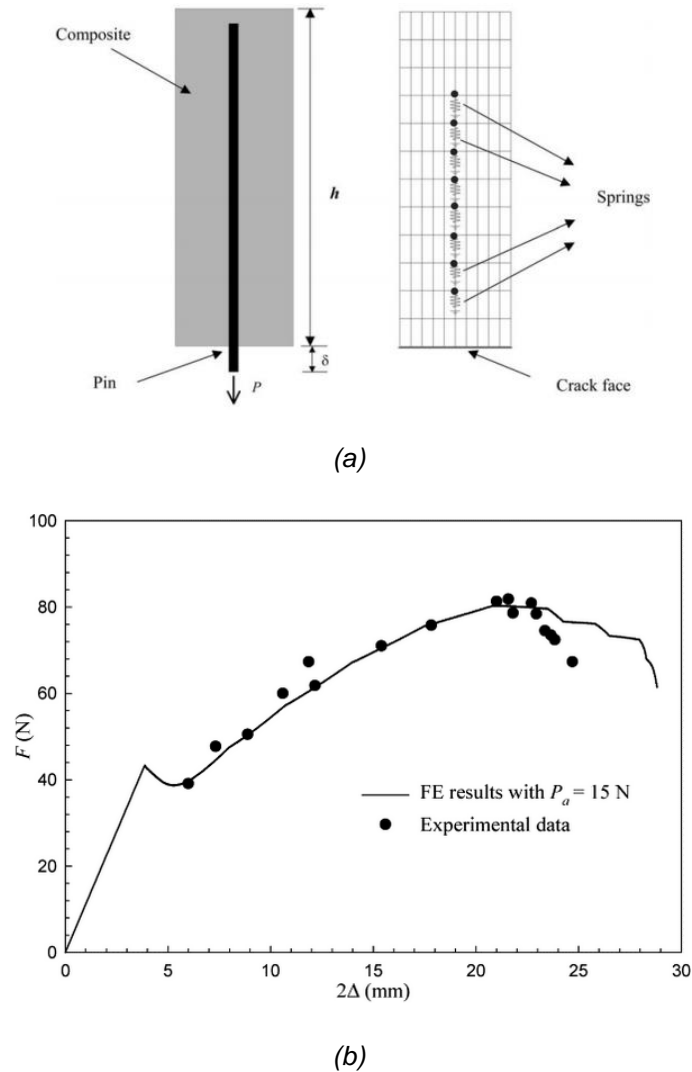
Figure 2.24. (a) FE model for the cross-section of the pin-laminate and (b) comparison between the experimental data and model predictions z-pinned DCB coupon [50].

Bianchi and Zhang [52] developed a FE model to calculate the mode II delamination fracture toughness of z-pinned composites. The model implements two distinct crack bridging traction-separation laws to compute the mode II interlaminar toughness. The toughness of the unpinned laminate governs the law for the unpinned region whereas for the z-pinned region a multi-scale model was developed accounting for the z-pin failure modes of rupture or pull-out. The resultant bridging laws are implemented into a full-scale ENF model of the z-pinned laminate (Figure 2.25). The FE model accounts for lateral elastic deformation of the composite when the pin is laterally deflected (Figure 2.26). The lateral elastic coefficient is determined by the stiffness of the surrounding material. The model was validated by comparison with experimental data resulting

in a good prediction for both the bridging effect and the load-displacement response for the ENF model of the z-pinned laminate (Figure 2.27).

(a)

(b)
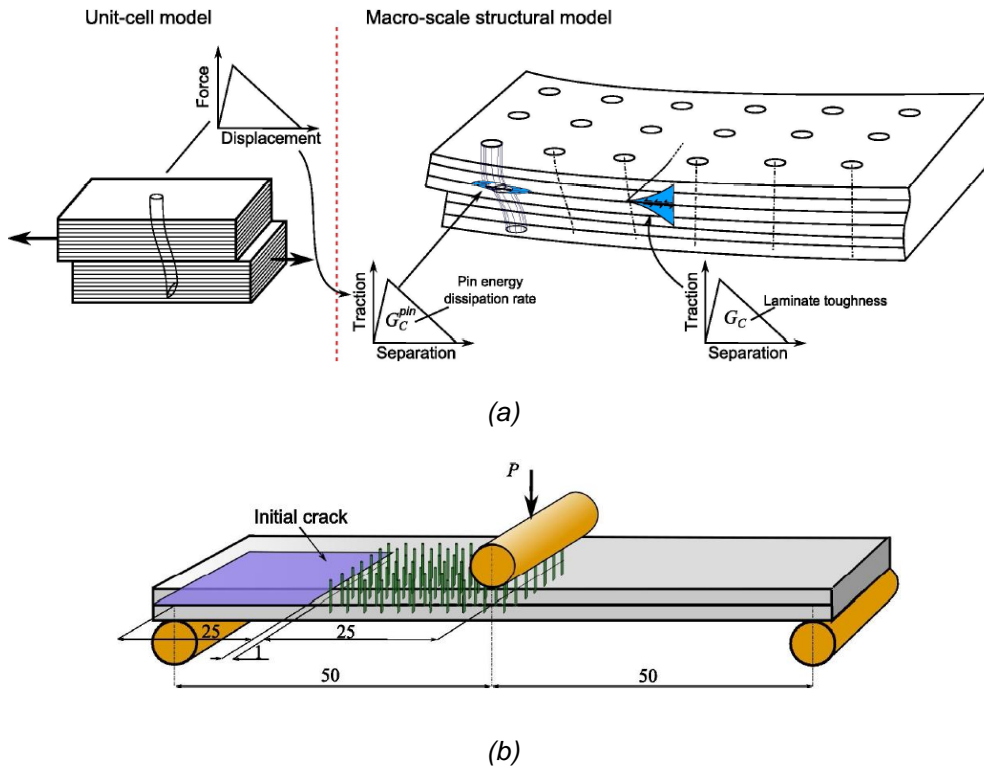
Figure 2.25. (a) Unit-cell model used to determine the mode II bridging traction laws implemented into (b) full-scale ENF model of the z-pinned laminate [52].
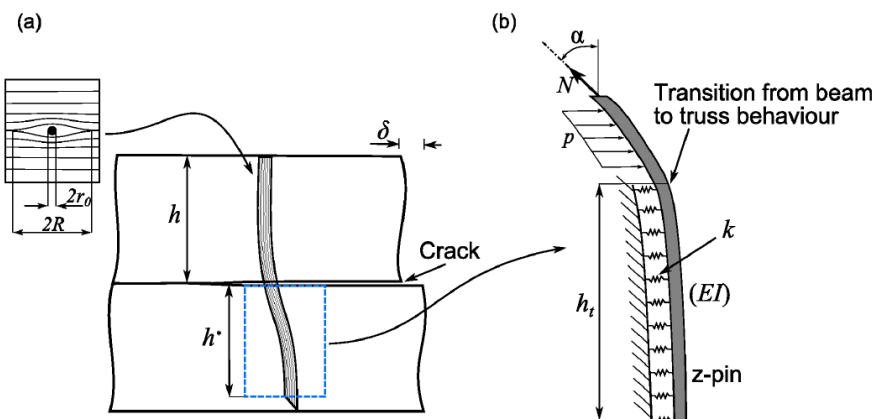
Figure 2.26. Details for the single-pin mode II unit-cell for the evaluation of the mode II crack bridging zone along a delamination [52].

(a) *(b)*
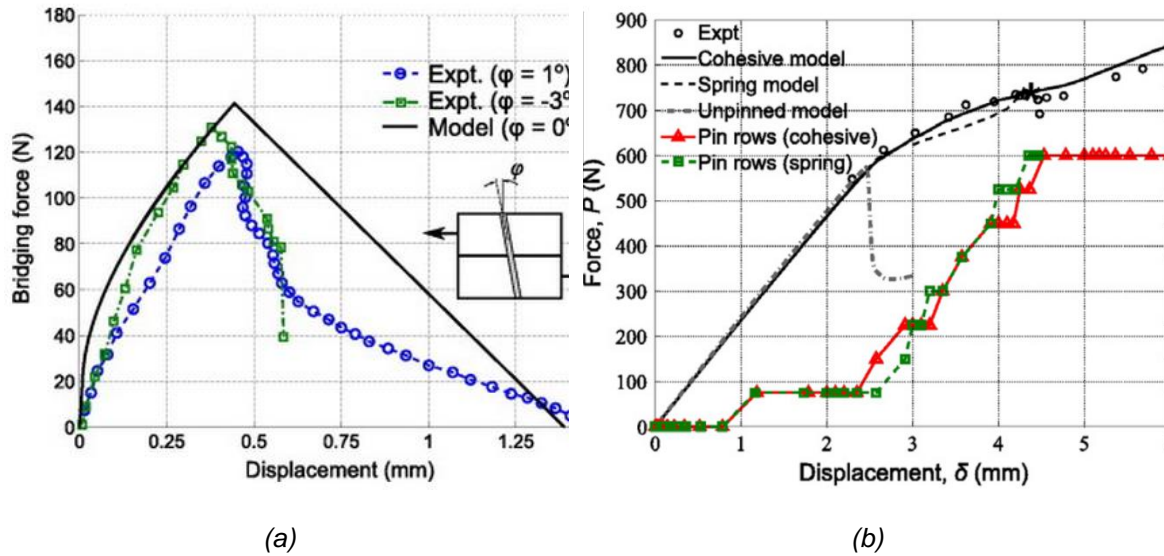
Figure 2.27. Comparison between experimental and FE predictions for the (a) unit-cell model and (b) ENF sliding force-displacmeent curve [52].

2.4.4 Delamination fatigue properties of z-pinned laminates

Delamination cracks can grow under relatively low cyclic interlaminar stresses caused by fatigue loading [3-5, 53]. Once a delamination has reached a certain length then catastrophic failure can occur via rapid, unstable crack growth through the composite. The delamination properties of z-pinned composites under fatigue loading are not well known, and there is only a small amount of published research work that has investigated the fatigue properties and fatigue strengthening mechanisms.

Cartié et al. [35] experimentally investigated the improvements to the mode I and II delamination fatigue resistance of carbon-fibre epoxy laminates reinforced with carbon fibre z-pins. Interlaminar fatigue tests were performed on laminates reinforced with two z-pin contents (2 and 4 vol%), and the fatigue results were compared against an unpinned material. The research revealed that increasing the volume content of z-pins slows the crack growth rate per load cycle because of bridging loads generated by the pins. However, a direct comparison between the fatigue resistance of the z-pinned composites and unpinned laminate was not possible because of inconsistency of the test procedure. Fatigue tests were performed under displacement control and load control for the unpinned and z-pinned materials, respectively, making it impossible to directly compare the crack growth rates (Figure 2.28).
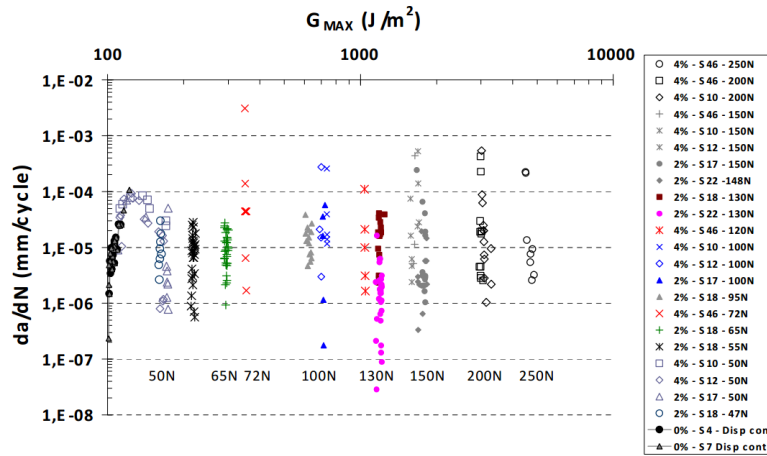
Figure 2.28. Mode I fatigue crack growth rates for unpinned and z-pinned composites [35, 54].The legend indicates the type of material tested and the loading-control conditions.

As previously discussed, when an increasing mode I crack opening load is applied then the z-pin response usually involves three stages: elastic deformation, debonding and finally pull-out. Fractographic examination of the DCB fatigued samples performed by Cartié et al. [35] revealed that z-pins when subjected to mode I fatigue loading do not pull-out, but instead fracture close to the delamination crack plane, as shown in Figure 2.29.

(a)

(b)
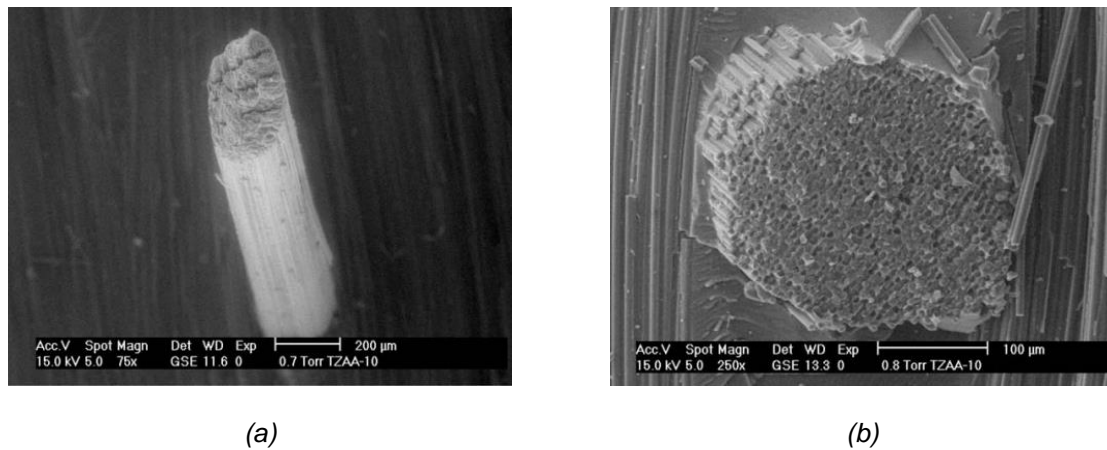
Figure 2.29. Mode I (a) static and (b) fatigue failure mechanisms of a z-pin [35].

Pingkarawat and Mouritz [28] experimentally studied the mode I delamination fatigue properties of z-pinned composites. The effects of the volume content (0.5, 2 and 4%), diameter (280 and 510 µm) and length (2, 4 and 8 mm) of z-pins on the fatigue properties and fatigue strengthening mechanisms were determined. Paris curves showing the effect of these parameters is presented

in Figure 2.30. Z-pins significantly increase the mode I delamination fatigue resistance over the entire range of cyclic stress intensity factors, from the threshold cyclic stress intensity required to initiate delamination cracking to the stress intensity range necessary to cause unstable crack growth. The delamination crack growth rate rapidly slows down with increasing volume content of z-pins content up to a limiting value of 2%, above which the fatigue process transitioned from a single to multiple cracks growing in parallel. This was believed to be caused by the delamination fatigue resistance being so high that was energetically more favourable to split into multiple crack paths (Figure 2.31). Fatigue loading caused z-pin/laminate interfacial cracking, and this occurred irrespective of the volume content. Cracks developed at the interface between the z-pins and laminate and then progress in length along the interface until the z-pins has completely pulled-out (Figure 2.32b).

(a)

(b)

(c)
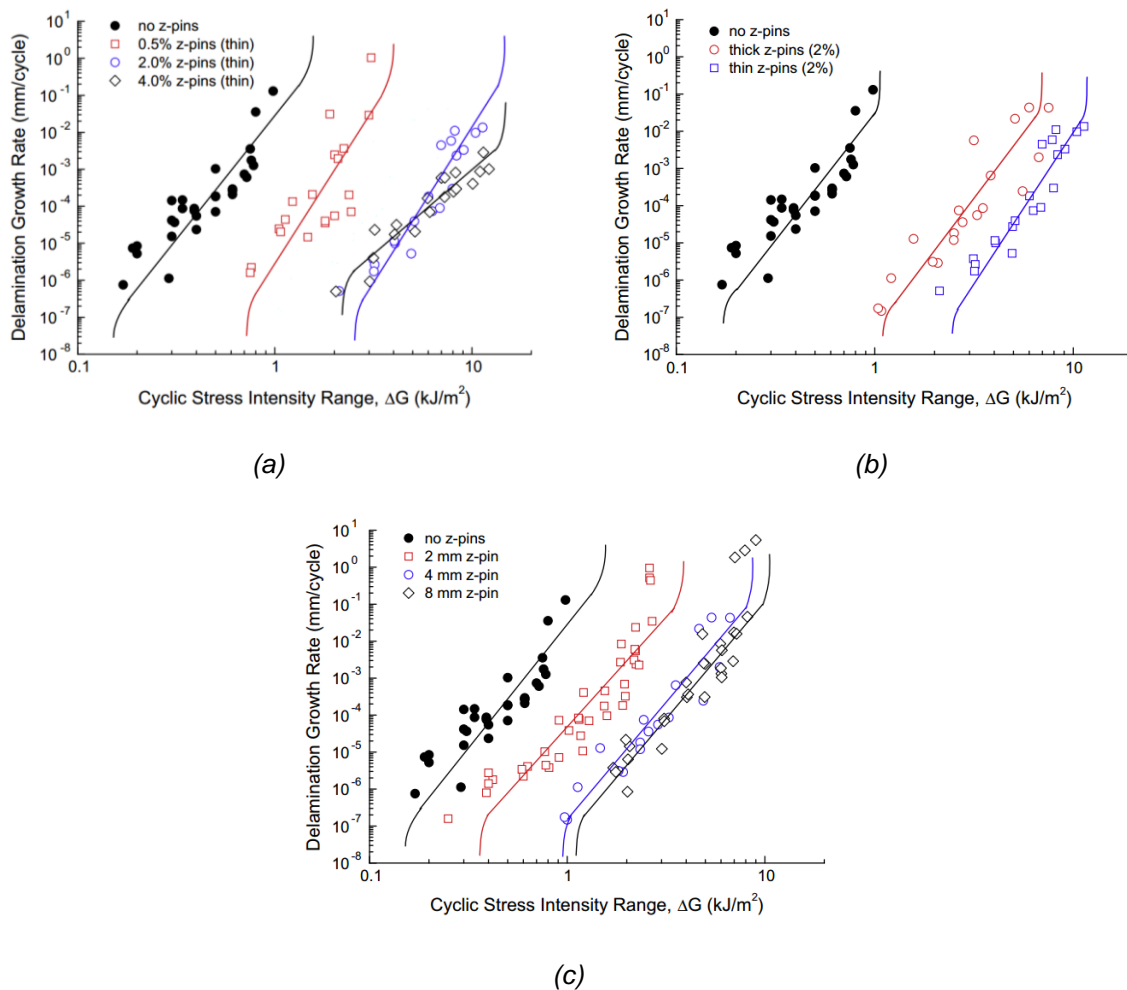
Figure 2.30. Effects of the (a) volume content, (b) diameter and (c) length of z-pins on the mode I Paris curves of carbon-epoxy laminate [28].

(a)

(b)
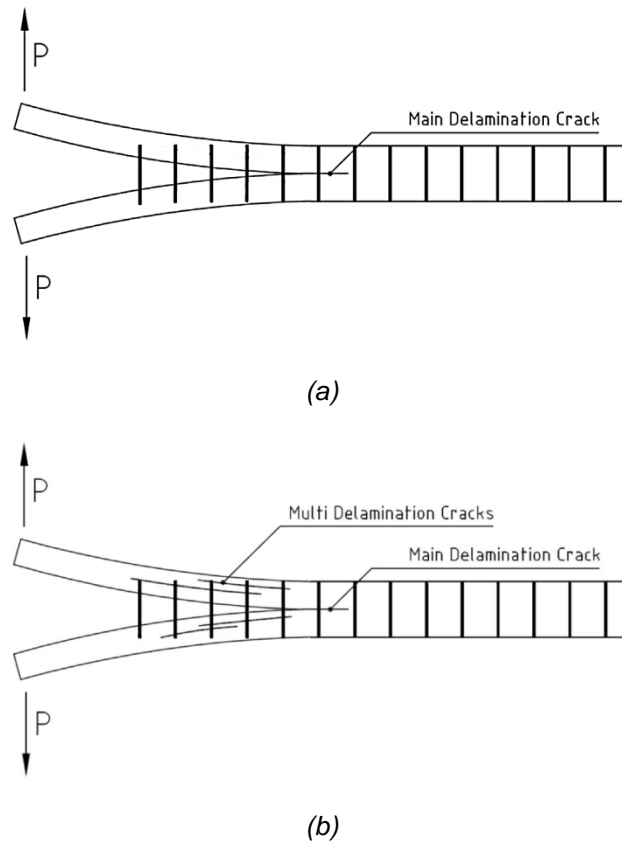
Figure 2.31. Transition in the delamination fatigue cracking process from (a) single crack to (b) multiple cracks with increasing z-pin content [28].

The mode I delamination fatigue resistance is also affected by the z-pin diameter. It was found by Pingkarawat and Mouritz [28] that thin z-pins were the more effective at resisting fatigue cracking because of the higher interfacial contact area compared to thicker pins (Figure 2.30b). Paris curves reveal that the fatigue resistance increased rapidly with the z-pin length up to 4 mm, beyond which no further improvements were obtained (Figure 2.30c). This occurred because of the high interface strength for long (8 mm) z-pins which causes them to rupture instead of pulling-out. The fracture and fatigue failure mode are also dependent on the material properties of z-pins. Pingkarawat and Mouritz [55] found that the fatigue strengthening capacity was dependent on the material properties of the z-pins, and increased in the order of: copper (being the least effective), titanium, stainless steel and carbon fibre.

(a) *(b)*
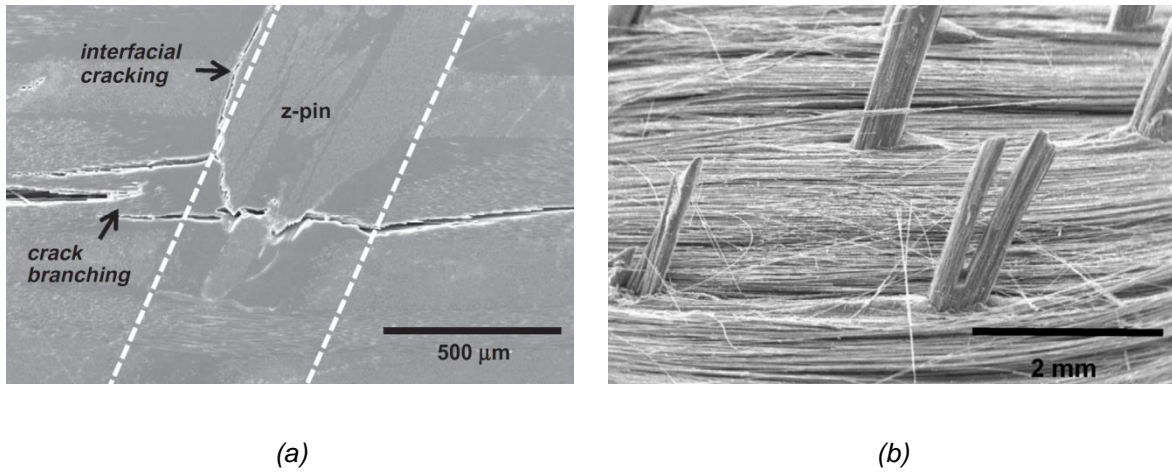
Figure 2.32. (a) Cross-section of a z-pin bridging a mode I fatigue delamination crack and (b) mode I delamination fatigue crack surface showing pull-out of z-pins [28].

Zhang et al. [54] experimentally investigated the deterioration of the mode I crack bridging traction loads of z-pins due to fatigue. Carbon-epoxy laminates were reinforced using two volume contents (0.5, 2%) and diameter (280, 510 μm) of z-pins, and were then tested under cyclic opening (mode I) loading. Reductions to the debonding and friction pull-out forces of the z-pins was measured over a range of fatigue crack opening displacements (50% and 80% of the ultimate debonding displacement). It was found that the maximum debonding and frictional forces decreased with increasing number of load cycles, however, the frictional force degraded at a higher rate (Figure 2.33).

(a) *(b)*
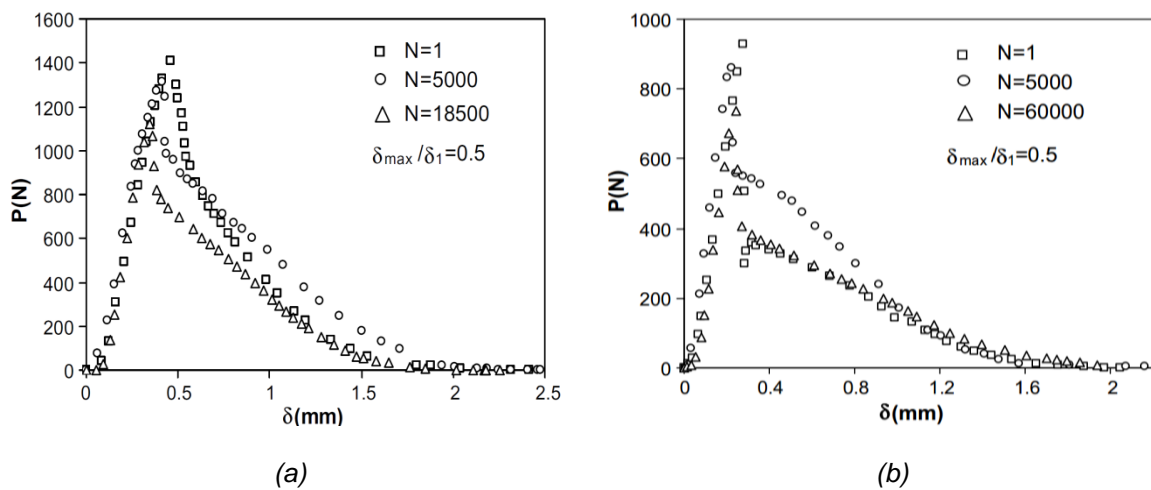
Figure 2.33. Pull-out load-displacement curves for (a) thick and (b) thin z-pins after increasing number (N) of mode I load cycles [54].

2.4.5 Compression properties and impact resistance of z-pinned laminates

Experimental research has proven that z-pins can reduce the amount of delamination damage caused by impact events from low energy objects, ballistic projectiles and large hailstones [43, 56, 57], and this is because of the improved interlaminar fracture toughness properties. Zhang et al. [58] investigated the impact damage resistance and the pre- and post-impact compression properties of z-pinned laminates. Z-pinned samples were made using carbon-epoxy with different thickness (2, 4 and 6 mm), and impacts were performed at several energy levels. It was found that z-pins were effective at increasing the impact damage resistance, with the impact damage area being reduced by between 19% and 64% depending on the laminate thickness and impact energy (Figure 2.34). Also, z-pins can increase the post-impact compressive strength by about 45% (Figure 2.35), although the amount of improvement depends on the thickness/impact configuration.
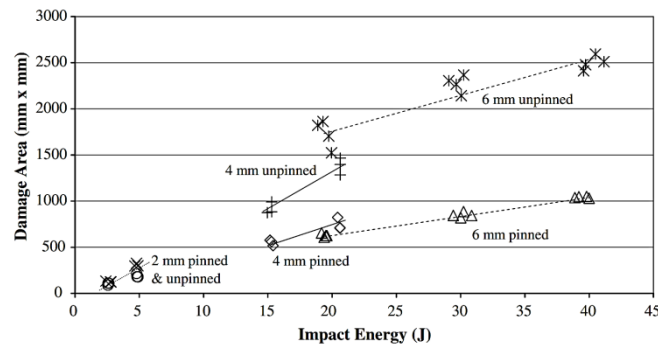
Figure 2.34. Effect of impact energy and laminate thickness on the impact damage area for unpinned and z-pinned laminates [58].
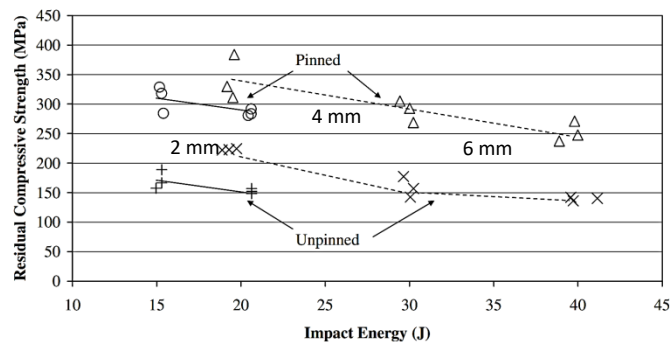
Figure 2.35. Effect of impact energy and laminate thickness on the post-impact compressive strength for unpinned and z-pinned laminates [58].

Isa et al. [59] experimentally investigated the impact damage resistant properties of quasi-isotropic carbon fibre-epoxy composite reinforced with different volume contents of z-pins (0, 0.5, 2 and 4%). The composites were impacted at different energies, and the damage resistance was quantified by ultrasonically measuring the impact damage area. The damaged area was reduced significantly by z-pins (up to about 50%), however the z-pins were ineffective at impact energies below ~17 J (Figure 2.36). This phenomenon was due to z-pins not significantly increasing the mode I and II delamination toughness for short delamination cracks (up to 10 mm). For higher impact energies the impact damage increases in size (above 10 mm) and then z-pins become effective and larger improvements were observed.
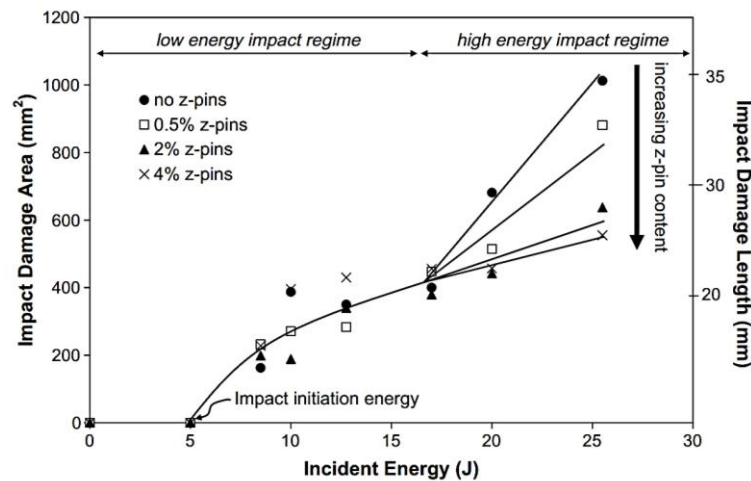
Figure 2.36. Effect of incident impact energy and volume content of z-pins on impact damaged area and length. Z-pins are effective when impact energy is above 17 J [59].

Compression fatigue tests were performed by Isa et al. [59] at different maximum cyclic stress levels ranging from 80% (close to the fatigue endurance limit) to 98% of the ultimate compressive strength (UCS). Compression fatigue tests show that z-pins have a detrimental effect on the in-plane compression properties. The fatigue life, compression modulus and strength decrease with increasing volume content of z-pins, and there is no improvement in the post-impact compressive properties on samples impacted at low energy levels (under ~17 J). However, following high-energy impact loading the compression strength and fatigue resistance are higher for z-pinned laminates, and the benefits improve with the pin content and this is because of their capacity to reduce the impact damage area.

All the studies performed on z-pins have considered solid rods of circular section embedded in prepreg materials. Knaupp and colleagues [60] experimentally investigated the impact damage resistant properties of composites reinforced with circular or rectangular z-pins (Figure 2.37). The damage area was reduced by up to 60% with rectangular z-pins. Knaupp et al. claim that rectangular z-pins provide laminates with higher impact damage resistance compared to circular z-pins due to a presence of twice as many rectangular pins for a given areal density compared to circular pins, which only reduce the damage by ~35% (Figure 2.38a). The post-impact compression strength of composites with rectangular z-pins were also higher (Figure 2.38b).

(a)   (b)
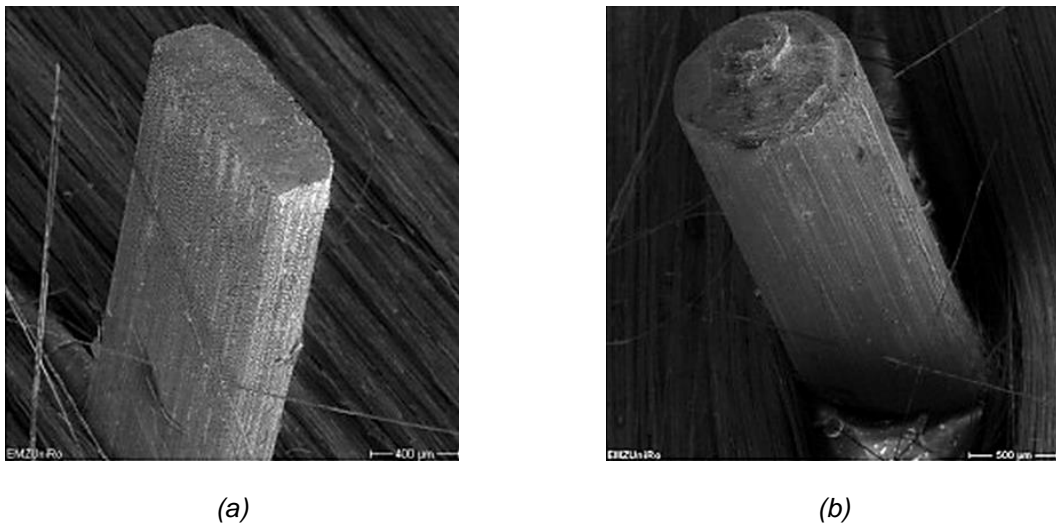
Figure 2.37. SEM photo showing (a) rectangular and (b) circular z-pin [60].

(a)   (b)
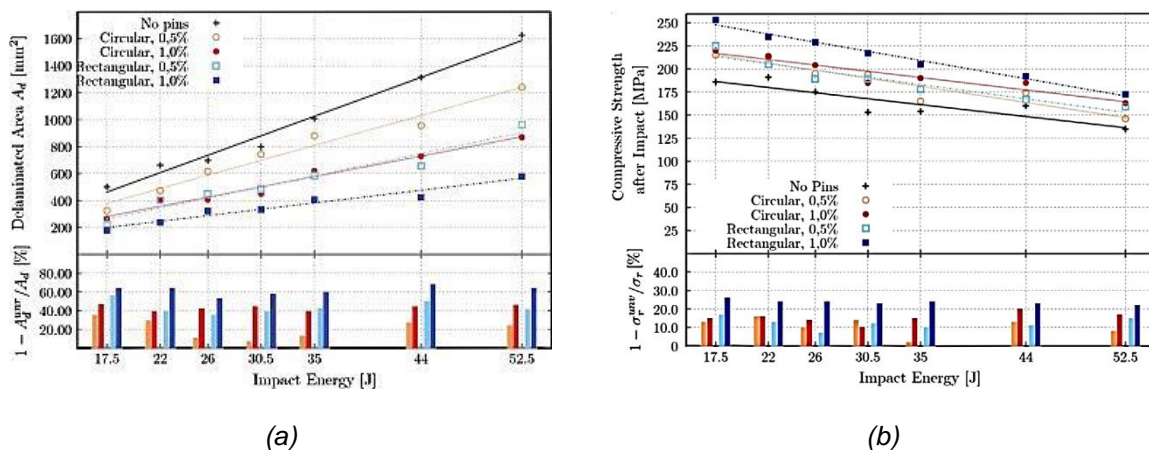
Figure 2.38. Effect of impact energy on the (a) impact damage area and (b) post-impact compressive strength for unpinned laminate and composites containing circular or rectangular z-pins [60].

The effect of hot (75°C) and wet (85% relative humidity) environmental conditions on the impact damage resistance of z-pinned composite was experimentally investigated by Mouritz [30]. It was found that both increasing the impacting energy (Figure 2.39) and the hot-wet (Figure 2.40) exposure time lead in increased impact damage.
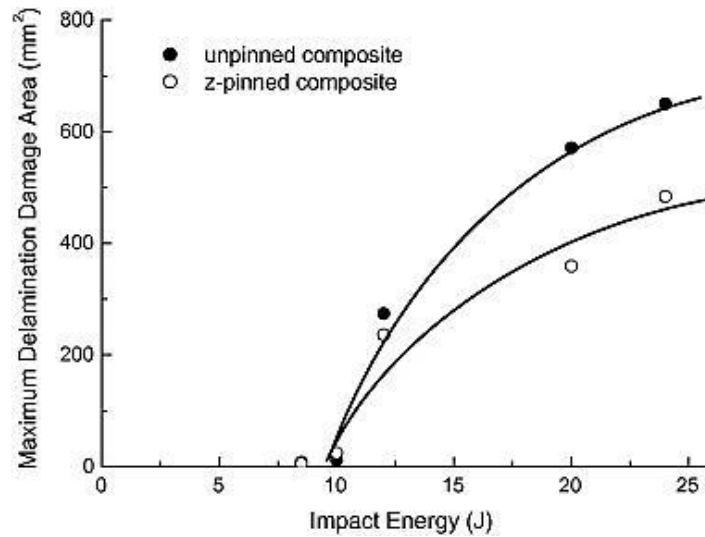
Figure 2.39. Effect of the incident impact energy on the delamination damage on unpinned and z-pinned laminates [30].

(a)   (b)
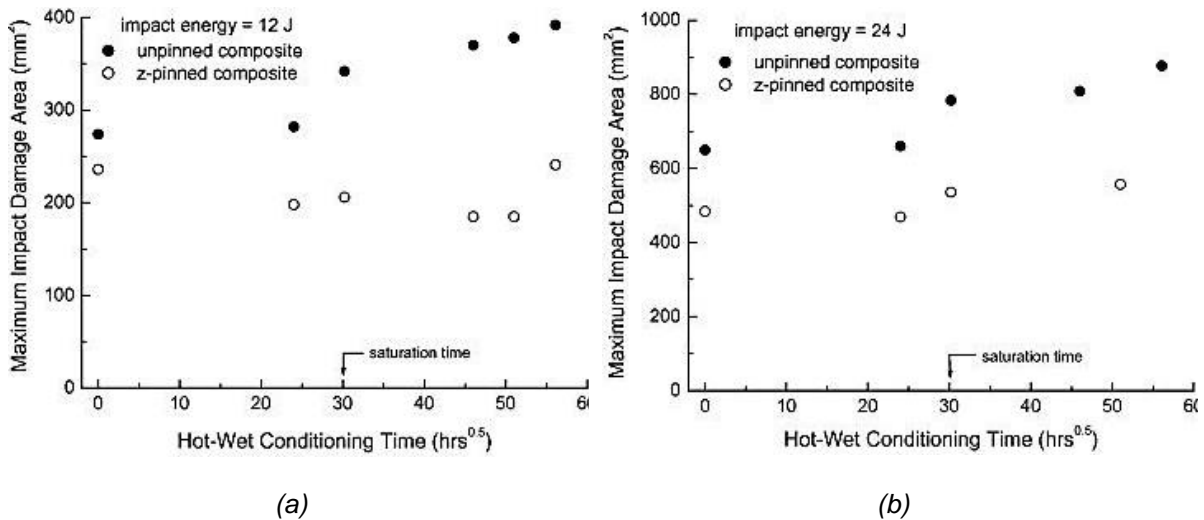
Figure 2.40. Effect of the hot-wet exposure time on the impact damage area for the unpinned and z-pinned laminates impacted at (a) 12 and (b) 24 J [30].

2.5   In-Plane Mechanical Properties of Z-Pinned Laminates

While z-pinning is efficient at improving the interlaminar properties of composites, there are some adverse effects which are a direct consequence of changes to the laminate microstructure caused by the pins. Changes to the microstructure can reduce the in-plane mechanical properties such as elastic modulus, ultimate strength and fatigue life [16, 17, 21, 43, 61-68]. Reviewed is the most significant published research into the in-plane mechanical properties of z-pinned laminates.

2.5.1 In-plane tensile properties of z-pinned laminates

The effect of z-pins on the tensile strength and modulus was experimentally and numerically determined by Craig et al. [68]. It was found that the z-pinned laminates experienced an early failure due to stress concentration surrounding the pin sites, and this was reflected in the tensile strength being reduced by up to about 27% at a z-pin volume content of 2%. Craig et al. also reported that z-pins do not have any effect on the in-plane tensile modulus. Mouritz and Chang [67] experimentally investigated the effect of z-pin content on the tensile modulus and strength of carbon/epoxy laminates. The effect of different ply stack sequence (i.e. unidirectional, quasi-isotropic and bias) was also determined. It was found that the tensile modulus was largely unaffected by the z-pins up to a volume content of 4% (Figure 2.41a), although it is suggested that the stiffness could be reduced at higher contents. The tensile strength reduced at a linear rate with increasing z-pin content (Figure 2.41b), with a unidirectional laminate being more sensitive than the other ply orientation.

(a)   *(b)*
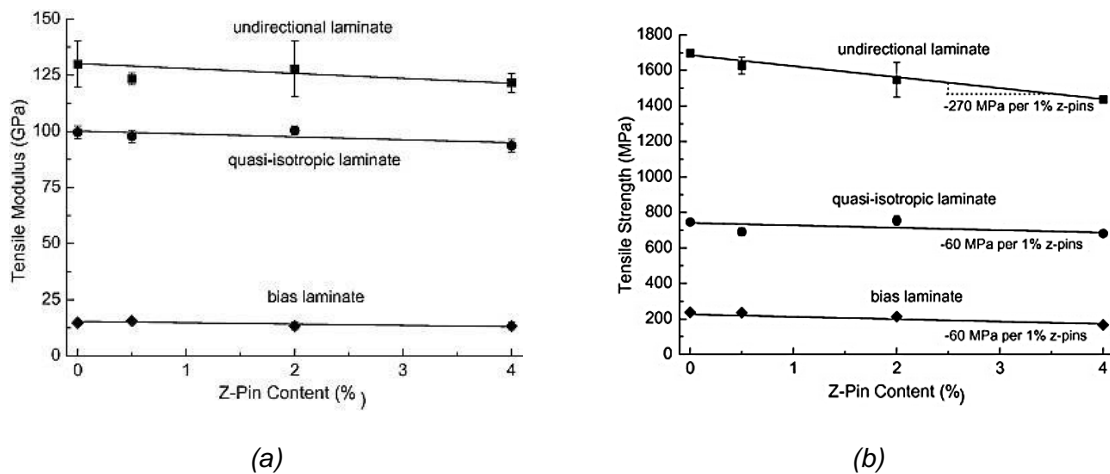
Figure 2.41. Effect of z-pin volume content on the (a) elastic modulus and (b) tensile strength of carbon-epoxy laminates with different ply orientations [67].

The tensile fatigue properties of z-pinned laminates have also been investigated. S-N curves show that there is a significant reduction in the fatigue life of laminates due to z-pins (Figure 2.42). The percentage reduction in fatigue performance is larger for fibre dominated laminates (i.e. unidirectional) due to different mechanisms controlling the initiation and growth of fatigue damage.
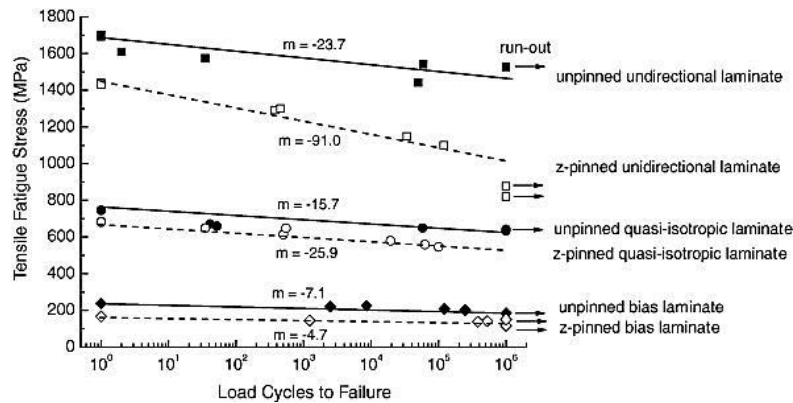
Figure 2.42. Effect of the stacking sequence for the unpinned and z-pinned materials on the tensile fatigue life. The z-pinned laminates were reinforced with a volume content of 4% [67].

Other studies have also reported small reductions to the in-plane properties due to z-pinning. Dickinson et al. [63] used a FE model of a z-pinned laminate to calculate the reduction to the in-plane and through-thickness elastic properties. Four different laminate stack sequences were analysed: cross-ply [0/90], bias [45/-45], unidirectional [0/0] and quasi-isotropic [45/0/-45/90]. The effect of z-pins on the longitudinal and transverse elastic modulus is shown in Figure 2.43. As reported by Mouritz and Chang [67], the percentage reduction to the longitudinal modulus is greater for fibre dominated laminates (5 to 10% in reduction). It was found that z-pins do not have a significant effect on the through-thickness modulus.

Other studies such as the 3D finite element model developed by Grassi et al [64] predicted that the tensile modulus is reduced by up to 10 % with z-pinning (Figure 2.44), which agrees with the other research work.
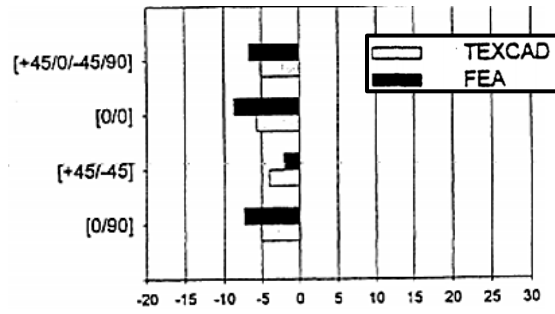
(a)
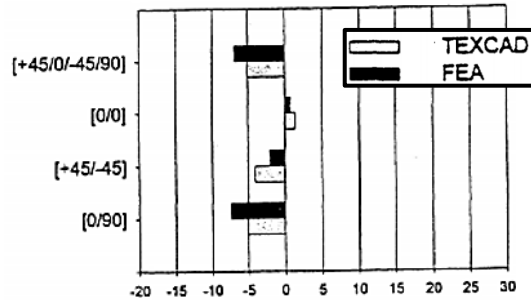
(b)

Figure 2.43. Percentage effect of z-pins on the (a) longitudinal and (b) transverse modulus of carbon-epoxy laminate with different ply orientations calculated using FE analysis. The values give the difference compared to the unpinned laminate. The model assumes a volume fraction and diameter for the z-pins of 1.9% and 0.6 mm, respectively [63].
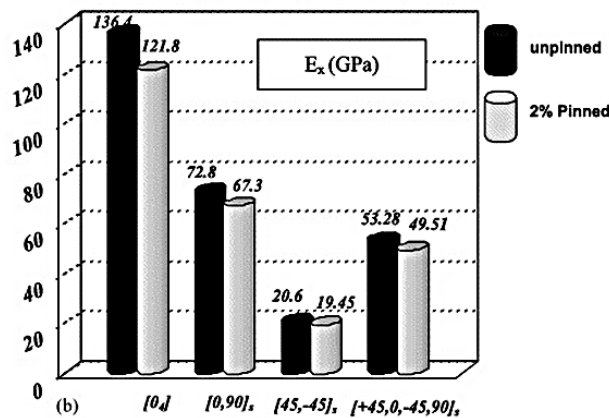
Figure 2.44. Effect of 2 %volume content of z-pin on the Young's modulus of carbon epoxy laminates with different ply stacking sequences [64].

2.5.2 In-plane compression properties of z-pinned laminates

The benefits of z-pins opens the opportunity for z-pinned laminates being used in compression-loaded aircraft structures. However, research show that the in-plane compressive properties can

be reduced significantly by z-pins [17, 43, 64-66, 68]. O'Brien and Krueger [66] developed a FE model to determine the effects of the volume content and diameter of z-pins on the compression strength of carbon fibre-epoxy laminates. Results show that increasing the volume content is more detrimental than increasing the diameter of z-pins (Figure 2.45).
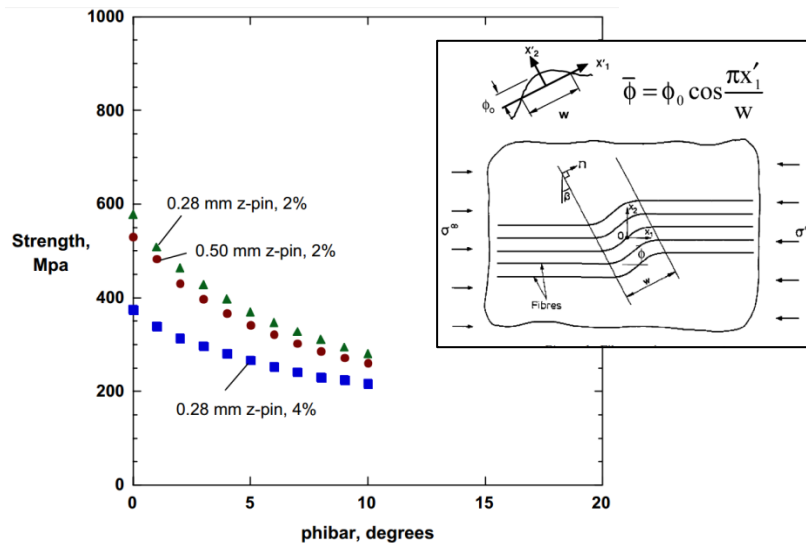
Figure 2.45. Effect of volume content, diameter and misalignment angle of z-pins on the compressive strength of a carbon-epoxy laminate [66].

Craig et al. [68] experimentally measured a knock-down of approximately 30% to the compressive strength due to z-pins. They found a clear correlation between the reduction in compressive strength and fibre waviness, which also depends on the z-pin pattern (fibre waviness is less severe when z-pin rows are parallel with the compression load direction). Mouritz [65] experimentally determined the effect of increasing z-pin content on the open-hole compressive properties of carbon-epoxy laminates. It was found that the compressive modulus decreases linearly with increasing volume content and diameter of the z-pins, and this was due to increased fibres waviness and laminate swelling. A similar study was numerically performed by Grassi and Zhang [44] who predicted using FE analysis a similar trend for laminates with different lay-ups. Similar effect was found for the compressive strength of laminates, which decrease with increasing volume content and diameter of z-pins (Figure 2.47). The compression fatigue life is also reduced significantly by z-pinning, with the S-N curves dropping to lower cyclic stress levels with increasing pin content and diameter. Fatigue life is reduced because of fibre waviness and laminate swelling, which reduces the capacity of a z-pinned laminate to withstand compressive fatigue loading (Figure 2.48).

(a)

(b)
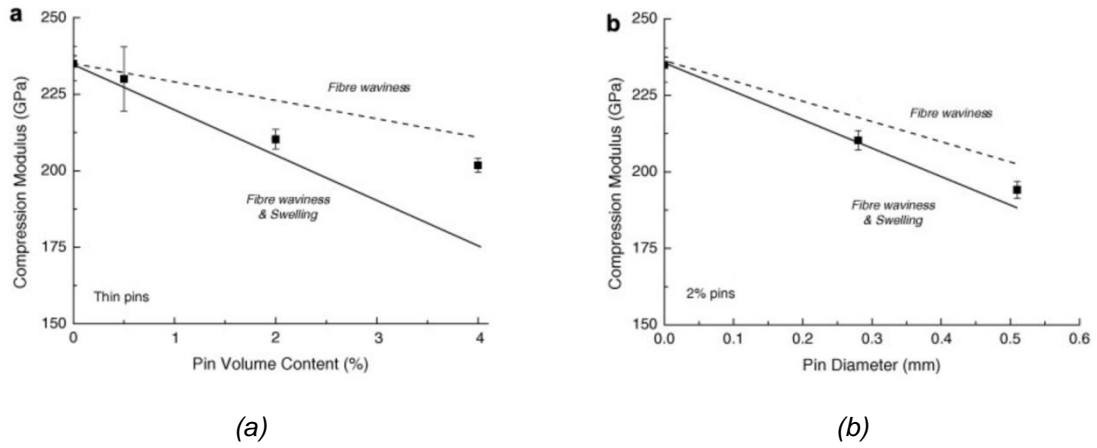
Figure 2.46. Effect of (a) volume content and (b) diameter of z-pins on the compression modulus of carbon-epoxy laminate [65]. The lines show the calculated reduction in modulus due to fibre waviness alone or with laminate swelling.

(a)

(b)
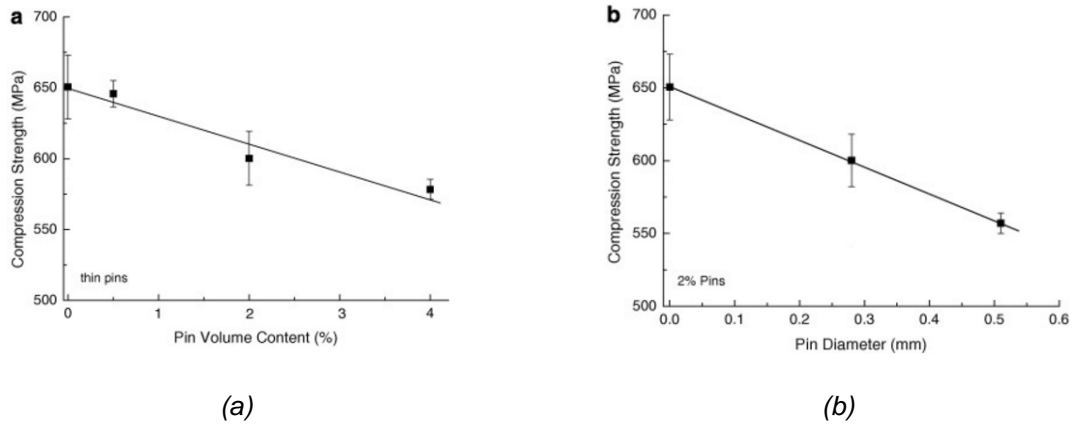
Figure 2.47. Effect of (a) volume content and (b) diameter of z-pins on the compression strength of a carbon-epoxy laminate [65].

(a)

(b)
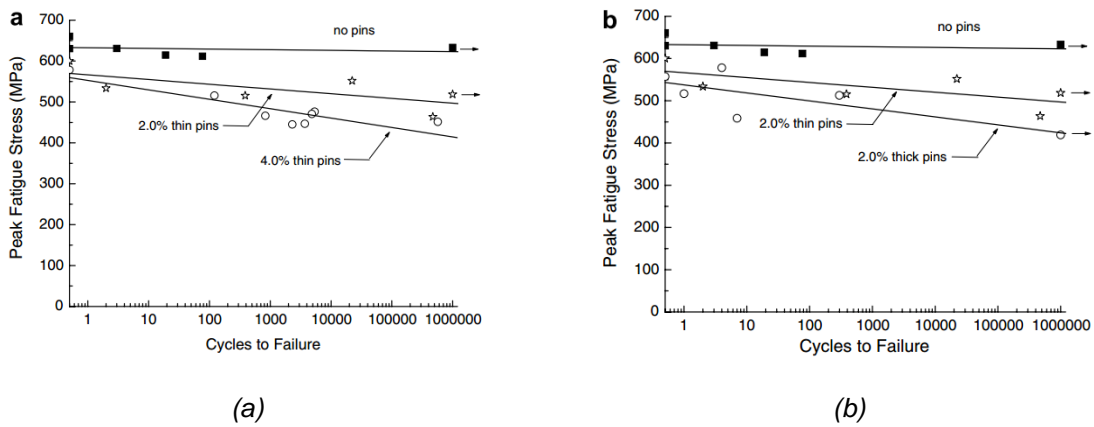
Figure 2.48. Effect of (a) volume content and (b) diameter of z-pins on the S-N curves for a carbon-epoxy laminate [65].

2.6   Concluding Remarks

This literature review has presented a large amount of experimental and numerical research work that proves z-pinning is an effective technique for increasing the delamination toughness, delamination fatigue resistance and impact tolerance of composite materials. However, z-pins modify the microstructure of composites and this can have a negative effect on the in-plane mechanical properties, although usually out-weighed by the higher improvements to the interlaminar properties.

However, there is not a significant amount of published work into the delamination fatigue resistance and fatigue strengthening mechanisms of z-pinned laminates, especially under mode II and mixed mode I/II cyclic loadings. Filling this knowledge gap is vital because of the cyclic loads applied to many aircraft components. The effect of parameters such as volume content, length, diameter and material properties of z-pins on these delamination fatigue properties is not well understood.

While a significant amount of research work have been performed to improve the thermal conductivity of composite through the addition of carbon [69-78], metallic [79-81] and ceramic [82-84] based fillers, there is no reported work that has investigated the effect of z-pins on the thermal conductivity. Similar conclusions can be drawn for the electrical conductivity, with nanoparticles including nanotubes (CNTs) [85-88], carbon nano fibres (CNFs) [89, 90] and graphene nano-sheets (GNSs) [91, 92] being used. It is feasible that z-pins can also be used to increase the electrical conductivity, although this has not been proven.

The research work presented in the following chapters aims to fill these research gaps through a comprehensive experimental investigation on the fatigue delamination properties, impact tolerance, and thermal and electrical properties of z-pinned laminates.

Chapter 3: Mode II Delamination Fracture and Fatigue Properties of Z-pinned Composites: Effect of Z-pin Material

3.1 Abstract

Presented in this chapter is an experimental study into the improvements to the mode II delamination fracture and delamination fatigue properties of carbon fibre-epoxy laminate reinforced through-the-thickness with z-pins made of different materials. The z-pins were made of unidirectional carbon fibre composite, copper, stainless steel or titanium. The mode II interlaminar fracture and fatigue properties were measured under static and cyclic displacement control conditions using the end notch flexure (ENF) test. The carbon fibre and metal z-pins were effective in improving the mode II delamination toughness and at resisting the initiation and growth of delamination cracks under fatigue loads. The properties were improved by the z-pins forming of a large-scale extrinsic bridging zone along the fatigue crack. The influence of the material properties of the z-pins on their strengthening capacity and failure mode are determined.

The research presented in this chapter has been submitted for publication:
F. Pegorin, K. Pingkarawat, S. Daynes, A.P. Mouritz. Delamination fatigue properties of z-pinned carbon-epoxy laminate using metal or composite rods. Composite Science & Technology. (Under Review).
and published:
F. Pegorin, K. Pingkarawat, S. Daynes, A.P. Mouritz. Delamination fatigue properties of z-pinned carbon-epoxy laminate using metal or composite rods. Proceedings of the 20th International Conference on Composite Materials (ICCM20); Copenhagen, Denmark, 07/2015.

3.2 Introduction

As mentioned in Chapter 2, delamination cracking is a long standing problem with laminated composite materials due to the low strength and toughness of the polymer matrix and matrix/fibre interface. Delaminations can grow rapidly in brittle matrix composites under low interlaminar fatigue loads, often with the cracks being undetectable via visual inspection [5, 93,

94]. A large number of numerical and experimental studies have proven that z-pinning is an effective through-thickness reinforcement method for increasing the modes I and II interlaminar fracture toughness properties of laminates [23, 24, 26, 30, 34, 44, 54]. Several studies have also reported that z-pinning can increase the delamination fatigue resistance of laminates under mode I and II cyclic loads [28, 31, 35, 54], as reviewed in Chapter 2. The improvements to the mode I fracture toughness and fatigue strength depend on several parameters, including the volume content [35], diameter [28, 54], embedded length [28] and material properties [55] of the z-pins. Experimental research using carbon fibre z-pins has revealed that the mode I fatigue resistance increases with the volume content and length of the z-pins (up to limiting values), and also increases when the diameter of the z-pins is reduced [28]. Carbon fibre z-pins increase the fatigue resistance by generating a large-scale extrinsic crack bridging zone until they eventually fail.

However, research performed to date has focused almost entirely on laminates reinforced with carbon fibre z-pins. The improvements to the mode II delamination toughness and fatigue resistance gained by z-pins made of different material types have not been thoroughly assessed. In Chapter 2 it was mentioned that Cartié et al. [36] showed that titanium z-pins are highly effective at increasing the mode II fracture toughness of laminates, and plastically deform in shear at high crack sliding displacements. More recently, Chio and colleagues investigated the improvement to the fatigue resistance of a composite single-lap joint reinforced in the bonded region with thin stainless steel rods [95, 96]. Apart from these few studies, the delamination toughness and fatigue properties of composites reinforced with metal z-pins have not been thoroughly studied. It is not known whether the fatigue strengthening effect for metal z-pins is similar, better or worse than the more studied carbon fibre z-pins.

This chapter presents an experimental study into the influence of the z-pin material on the mode II delamination toughness and fatigue resistance of z-pinned carbon-epoxy laminates. Z-pin materials with different elastic modulus, yield stress, ultimate stress, and fatigue strength properties were used. These were copper, stainless steel, titanium and unidirectional carbon fibre composite. The study presented in this chapter aims to experimentally determine the effect of these different z-pin materials on the delamination toughness, fatigue properties and strengthening mechanisms under mode II interlaminar static and cyclic loads.

3.3 Materials and Experimental Methodology

3.3.1 Z-pinned composite materials

Unpinned and z-pinned composite specimens were manufactured to measure the mode II delamination fracture toughness and fatigue properties. The specimens were made using unidirectional (UD) T700 carbon fibre-epoxy prepreg tape (VTM264 supplied by Advanced Composite Group). The main mechanical properties of a unidirectional laminate made using this prepreg are given in Table 3.1. The prepreg was laid-up in a 0° fibre dominated ply pattern. 0° plies were located at the centre-line of the laminates (which is the plane for delamination growth) and adjoining 90° plies to prevent excessive fibre bridging along the crack during fracture and fatigue testing. The uncured plies were stacked in a $[0_6/[90/0]_2]_s$ ply sequence. The laminate was debulked after the lay-up of every four plies via vacuum bagging for five minutes, and this was to prevent that air pockets were trapped within the material prior to autoclave cure.

Table 3.1. Mechanical properties for the unidirectional VTM264 prepreg.The properties are referred to the fibre direction [97].

Tensile Strength (MPa)	2459	Compression Strength (MPa)	1102
Tensile Modulus (GPa)	118	Compression Modulus (GPa)	107
Tensile Strain-to-Failure (%)	2.07	In Plane Shear Strength (MPa)	83.6
Flexural Strength (MPa)	1677	In Plane Shear Modulus (GPa)	4.07
Flexural Modulus (GPa)	110		

The uncured prepreg laminate was reinforced in the through-thickness direction with z-pins made of unidirectional carbon fibre-bismaleimide (BMI), copper (99.9% purity), titanium (grade 1; 99.5% purity) or stainless steel (316L). The tensile properties of these z-pin materials are given in Table 3.2. The spacing (3.2 mm), diameter (510 μm), orientation (orthogonal), volume content (2%), and embedded length (4 mm) of the different z-pins were the same; the only difference was the z-pin material.

The carbon fibre z-pins were inserted into the uncured laminate using the ultrasonically assisted pinning (UAZ) process. As described in Chapter 2, the UAZ process involves placing a low density foam carrier containing the z-pins over the uncured prepreg laminate. The foam (51LG Rohacell-type) is made of two layers; an upper dense foam with the purpose of holding the z-pins in place and a lower dense foam which collapses under the pressure exerted by the UAZ tool (Figure 3.1). The tool head is placed over the foam. Vibrations at a frequency of 20 kHz combined with the pressure applied by the operator causes the foam to collapse and drive the z-pins into the

laminate. Once the insertion process is completed, the excess length of z-pins protruding from the laminate surface along with the foam is sheared away using a blade.

Table 3.2. Mechanical properties of the z-pin materials [98, 99].

Material	Tensile Modulus [GPa]	Yield Stress 0.2% Offset [MPa]	Ultimate Tensile Strength [MPa]	Elongation to Failure [%]	Shear Modulus [MPa]
Cu (99.9% purity)	117	70	162	86	48
Titanium (grade 1; 99.5% purity)	105	309	590	24	45
Stainless Steel (316L)	200	170	782	55 (sheet)	82
Carbon fibre-BMI	140	-	2300	1.6	-

The metal z-pins were individually and manually inserted into the uncured laminate (Figure 3.2). Before insertion, the metal z-pins were cleaned and then surface treated with an organosilane-coupling agent (3-methacryloxypropyl-trimethoxysilane) to promote bonding with the epoxy matrix to the laminate. Coupling agents such as organo-silanes have an organic portion which bonds with the organic resin (epoxy matrix) and an inorganic portion which adheres to the metal pins, thus increasing the pin/composite interfacial strength. After the metal z-pins were inserted, the pinned laminates were debulked and this allowed to cut the z-pins length in excess so that there was not significant protrusion into the tabbing material. The carbon fibre and metal z-pins were inserted in a grid pattern with the longitudinal and transverse pin rows aligned parallel with the 0° and 90° fibre directions to the laminate, respectively (Figure 3.3).

(a)

(b)
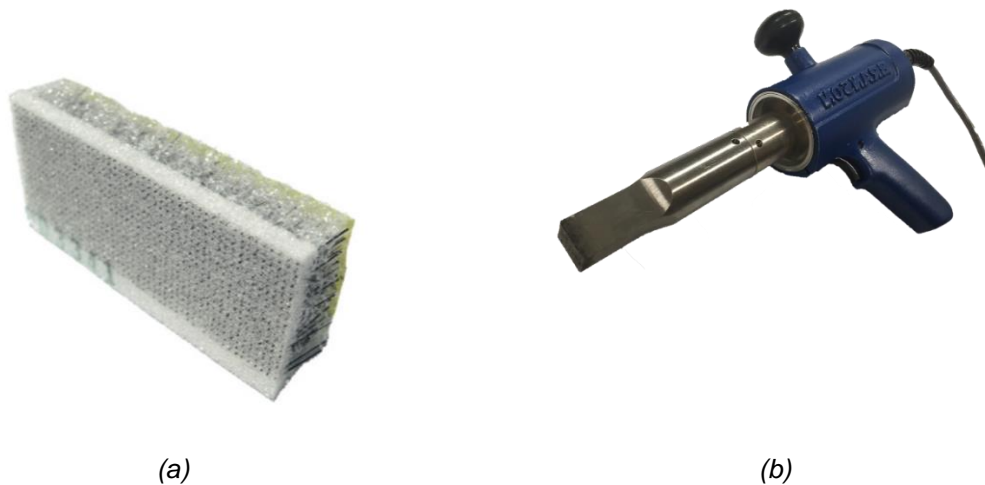
Figure 3.1. (a) Bi-layer carrier foam containing the carbon fibre composite z-pins and (b) UAZ tool used for the z-pin insertion.
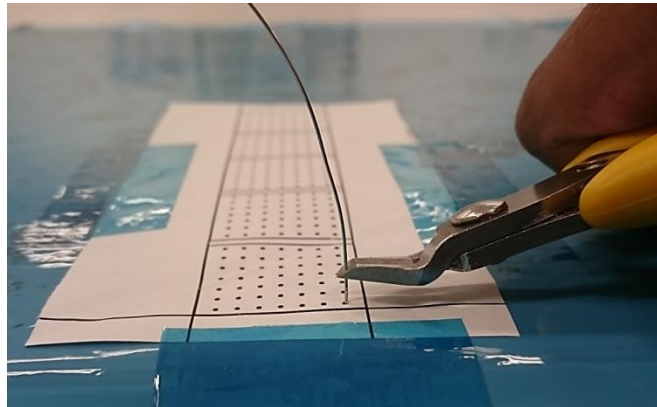
Figure 3.2. Insertion process for the metal pins.
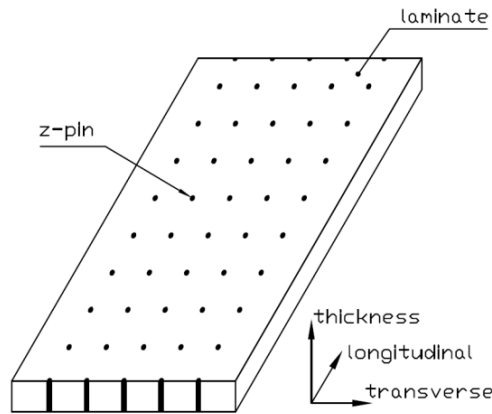
Figure 3.3. Schematic of the z-pin square insertion pattern.

While the z-pins made of carbon fibre composite and metals were inserted using different methods, microstructural examination of the z-pinned laminates did not reveal any significant differences. Specifically, the amount of crimp, distortion and localised breakage of carbon fibres in the composites was not noticeably different when reinforced using the carbon fibre or metal z-pins. It is expected, however, that the residual stresses near the interface between the laminate and z-pins will be different due to differences in the coefficients of linear thermal expansion of the carbon fibre (-1×10^{-6} K^{-1}), copper (16.6×10^{-6} K^{-1}), stainless steel (16×10^{-6} K^{-1}) and titanium (8.6×10^{-6} K^{-1}).

In the manufacture of the test specimens, the z-pinned laminates were sandwiched between two unpinned unidirectional carbon-epoxy tabs (each 4.5 mm thick) to prevent failure of the

specimen arms during fracture and fatigue testing, as shown in Figure 3.4. A control material consisting of the unpinned $[0_6/[90/0]_2]_s$ carbon-epoxy laminate, and it was made to the same dimensions as the z-pinned composites. Previously published research has shown that z-pins do not change significantly the mechanical properties of cross-ply and quasi-isotropic laminates. The unpinned and z-pinned laminates were cured and consolidated in an autoclave at 120°C and 620 kPa for one hour (Figure 3.5). The volume content of carbon fibres for the different laminates was about the same at ~58%.

(b)
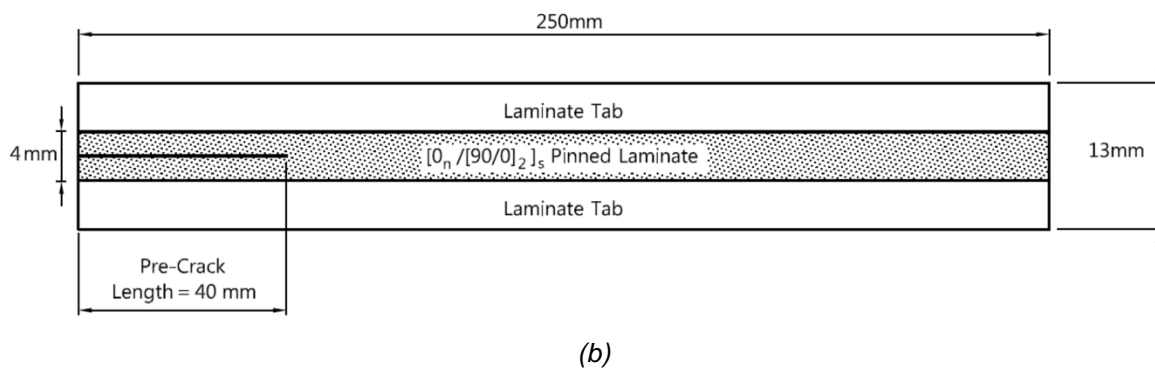
Figure 3.4. Schematic of the z-pinned ENF specimen. The specimen was 25 mm wide.
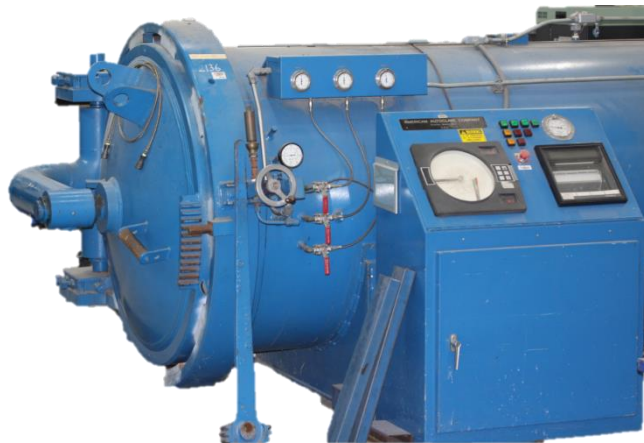
Figure 3.5. Autoclave used to cure the unpinned and z-pinned laminates.

3.3.2 Mode II delamination fracture toughness and fatigue testing

The mode II delamination fracture toughness and fatigue resistance of the unpinned and z-pinned materials were measured using the end notched flexure (ENF) test, which is shown in Figure 3.6. Several test methods can be used to determine the mode II interlaminar properties, including the

end loaded split (ELS) and four-point end notched flexure (4ENF) tests. In the project the ENF test used because it is the most widely used technique for measuring mode II fracture toughness, including the testing of materials with through-thickness reinforcement including z-pinned composites. The mode II ENF specimens contained a 40 mm long artificial crack created by a Teflon film (20 μm in thickness) inserted at the mid-plane (as indicated in Figure 3.4). The mode II fracture toughness was measured by applying a monotonically increasing downward displacement (rate of 0.5 mm/min) at the mid-length of the sample, as shown in Figure 3.6.

The delamination crack was forced to propagate at short intervals (5-10 mm) along the mid-plane of the ENF sample, and at each increment the mode II strain energy release rate was calculated using the beam equation [100]:

$$G_{II} = \frac{9a^2 P_{II} \delta_{II}}{2b(2L^3 + 3a^3)} \qquad\qquad (3.1)$$

where δ_{II} is the applied bending displacement, P_{II} is the measured applied force, b is the sample width and a is the total crack length. Three or four samples of the unpinned laminate and each of the different types of z-pinned composites were tested.

(a)

(b)
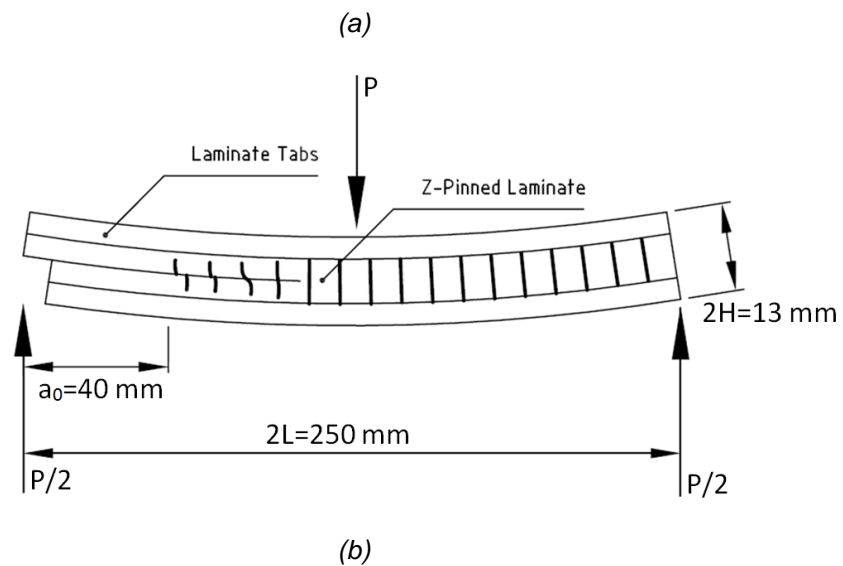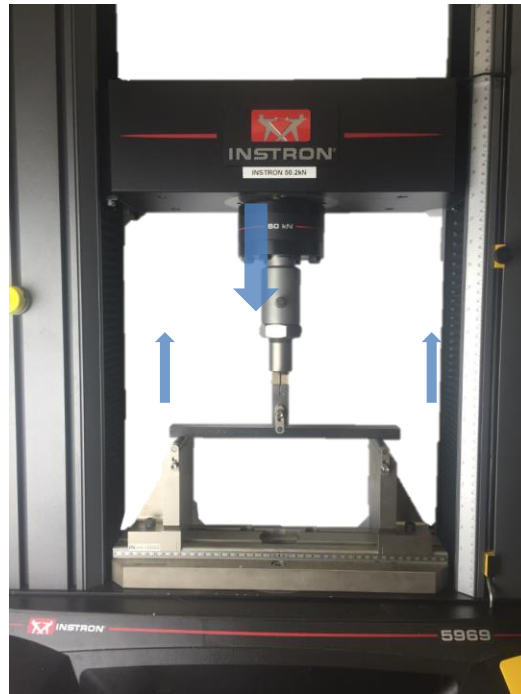
Figure 3.6. (a) Photograph and (b) illustration of the three-point bend mode II ENF test.

Before fatigue testing, the ENF sample was cyclically loaded in mode II to extend the delamination 30-40 mm from the artificial crack tip. By growing the delamination this length, an almost-fully matured z-pin bridging zone was created before fatigue testing. Fatigue crack growth started from the tip of this fully matured bridging zone to ensure the delamination fatigue properties were independent of the bridging zone length. The unpinned and z-pinned ENF specimens were then cyclically loaded in displacement control at a frequency of 10 Hz and R ratio of 0.1, which is defined as the ratio between the minimum and maximum displacements per load cycle. The specimens were fatigued under constant cyclic displacement conditions to allow the delamination to grow by 5-10 mm, which is approximately equivalent to 2-3 rows of z-pins. The fatigue testing under a fixed cyclic strain energy release rate (ΔG_{II}) commenced with the crack tip located very close to or at a transverse row of z-pins. The crack proceeded to grow from this row for at least another two or three rows of z-pins under the constant ΔG_{II} value. The total number of load cycles needed to cause the crack extension was used to determine the crack growth rate (da/dN). In some cases it was difficult to precisely determine whether the crack started growing at a transverse row of z-pins, and could have occurred about mid-way between two rows, and this would cause some scatter to the measured crack growth rate. The growth of the fatigue crack was monitored continuously during testing, and its length was measured using a travelling optical microscope located to one-side of the ENF specimen. The accuracy of the crack length measurements made using the travelling optical microscope were determined using through-thickness ultrasonics. The length of the cracks measured using the two techniques were very similar, giving confidence that the optical microscopy provided a reliable means of measuring the delamination length. This process was repeated over a wide range of cyclic strain energy release rate values spanning from the fatigue (no-growth) threshold condition to the fast fatigue fracture condition (unstable growth). Two or three samples of the unpinned laminate and the different types of z-pinned composites were fatigue tested under mode II cyclic loading.

The mode II cyclic strain energy release rate range (ΔG_{II}) was calculated from the difference between the maximum and minimum interlaminar strain energy release rate (G_{II}) values within one fatigue cycle:

$$\Delta G_{II} = G_{II(max)} - G_{II(min)} \tag{3.2}$$

where

$$G_{II(\text{max})} = \frac{9a^2 P_{II(\text{max})} \delta_{II(\text{max})}}{2b(2L^3 + 3a^3)}$$ (3.3)

and

$$G_{II(\text{min})} = \frac{9a^2 P_{II(\text{min})} \delta_{II(\text{min})}}{2b(2L^3 + 3a^3)}$$ (3.4)

$\delta_{II(max)}$ and $\delta_{II(min)}$ are the maximum and minimum bending displacements, and $P_{II(max)}$ and $P_{II(min)}$ are the maximum and minimum bending loads.

3.3.3 Z-pin crack bridging shear traction testing

Pure shear tests were performed on the composite and metal z-pins to measure their mode II bridging traction properties, as illustrated in Figure 3.7. The shear specimen consisted of two carbon epoxy laminates with a step-shaped profile separated by 20 μm thick-Teflon film (to mimic a delamination) and held together just by the z-pins. The laminates were made using the same carbon-epoxy prepreg used for the ENF specimens. The central region of the specimens was reinforced with 28 pins (4 mm long) arranged in a 7x4 grid pattern and equally spaced in the *x* and *y* directions by 3.2 mm, which is the same pin spacing that was used in the ENF specimens. Samples were reinforced with z-pins made of carbon fibre composite, copper, titanium or stainless steel. The samples were loaded in the in-plane direction (x-direction) at a monotonically increasing displacement rate of 1 mm/min to a maximum value of 0.68 mm, which was about the maximum crack sliding displacement that occurred in the mode II static tests performed on the z-pinned ENF samples (as described later).
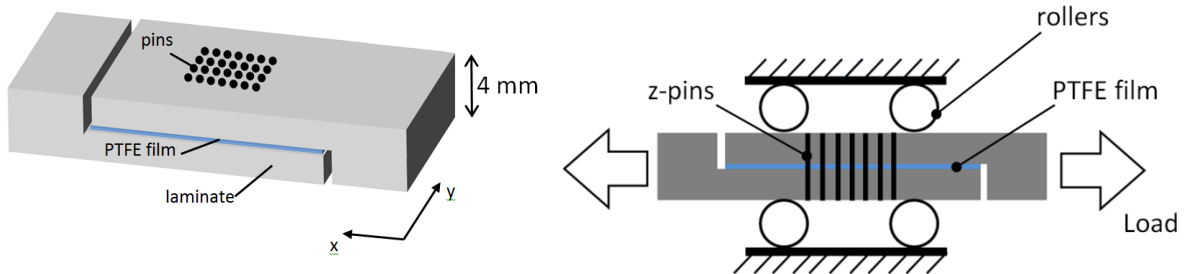
Figure 3.7. Schematic of the mode II z-pin bridging traction test.

Roller bearings were used to prevent crack opening displacement and to minimise the friction effect between the specimen and the supporting rig (as schematically shown in Figure 3.7). The sliding between the two laminates generated a low friction force (∼15 N) which was much lower than the mode II traction force generated by the z-pins (up to ∼1200-4000 N depending on the pin type). The measured shear load-crack sliding displacement curve was used to determine the mode II bridging traction properties of the different types of z-pin.

3.3.4 Fractographic analysis

Both the fracture surface and cross-section of the ENF samples were examined using a scanning electron microscope (FEI Quanta 200 ESEM) at the RMIT Microscopy and Microanalysis Facility. Specimens were cut to a short length (35 mm) and then diamond polished (Ra ≈ 0.025) prior to gold coating.
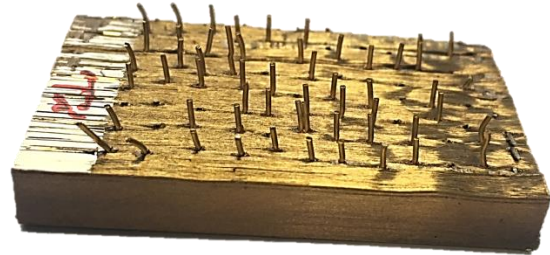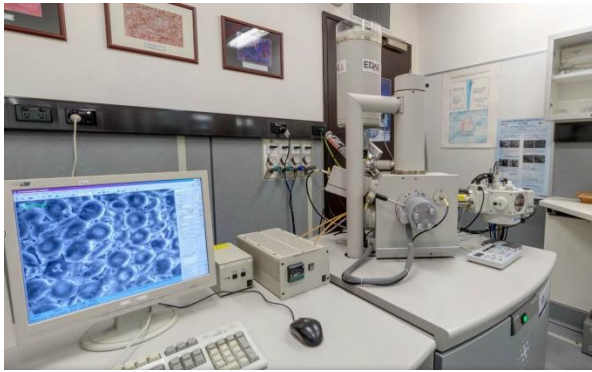
Figure 3.8. (a) RMIT FEI Quanta ESEM and (b) gold coated z-pinned sample for SEM examination.

3.4   Results and Discussion

3.4.1 Mode II delamination toughness properties

The ENF samples, when loaded in a three-point bending configuration, elastically deform until reaching a critical point when there is sufficient internal strain energy to cause crack growth. Delamination growth in the unpinned laminate was unstable (rapid), which is characterised by a large and sudden load drop due to large-scale crack extension (Figure 3.9). For the unpinned material only one data point per sample could be recorded due to the large and rapid crack growth. There is a transition in the fracture process from the unpinned laminate to the z-pinned composites. Regardless of the z-pin material, crack growth occurs in a stick-slip manner rather than rapid unstable growth. The crack quickly propagated between the pin rows (slip) – resulting

in a drop in the bending load due to an increase in the ENF sample compliance, and then the crack arrested in proximity of the next pin row. Compliance is defined as the ratio between the bending displacement (δ) and load (L);

$$C = \frac{\delta}{L} = \frac{3a+4L}{8bh^3E_{11}} \qquad\qquad (3.5)$$

where a is the total crack length, L half the distance between the three-point bending support points, h is half-thickness of the ENF sample, and E_{11} is the longitudinal modulus of the composite.

Figure 3.10 shows plots of the mode II interlaminar fracture toughness vs delamination crack length (R-curves) experimentally measured for the unpinned and z-pinned laminates reinforced with different z-pin materials. The mode II strain energy release rate (G_{II}) is plotted against the crack length (Δa), which is the difference between the total delamination crack length and the initial crack length (40 mm). The delamination toughness of the unpinned material rapidly reached the steady-state value indicating that the delamination crack length does not have a significant effect on the mode II fracture toughness. The mode II toughness was increased significantly by the z-pins, and this is because of shear bridging traction loads generated by the pins. The delamination toughness for the z-pinned laminates increases with the delamination length, and for both the composite and metal pins the steady-state toughness condition was not reached meaning that the bridging zone has not fully developed despite the long crack length generated during the test ($\sim$ 60 mm).
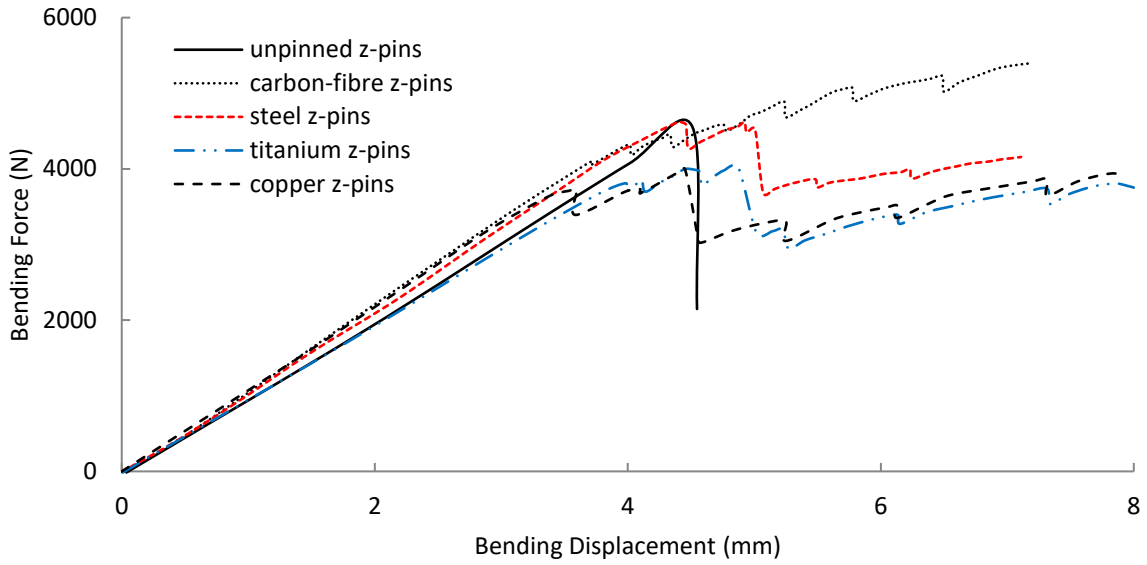
Figure 3.9. Load vs displacement curves for the unpinned and z-pinned ENF specimens.
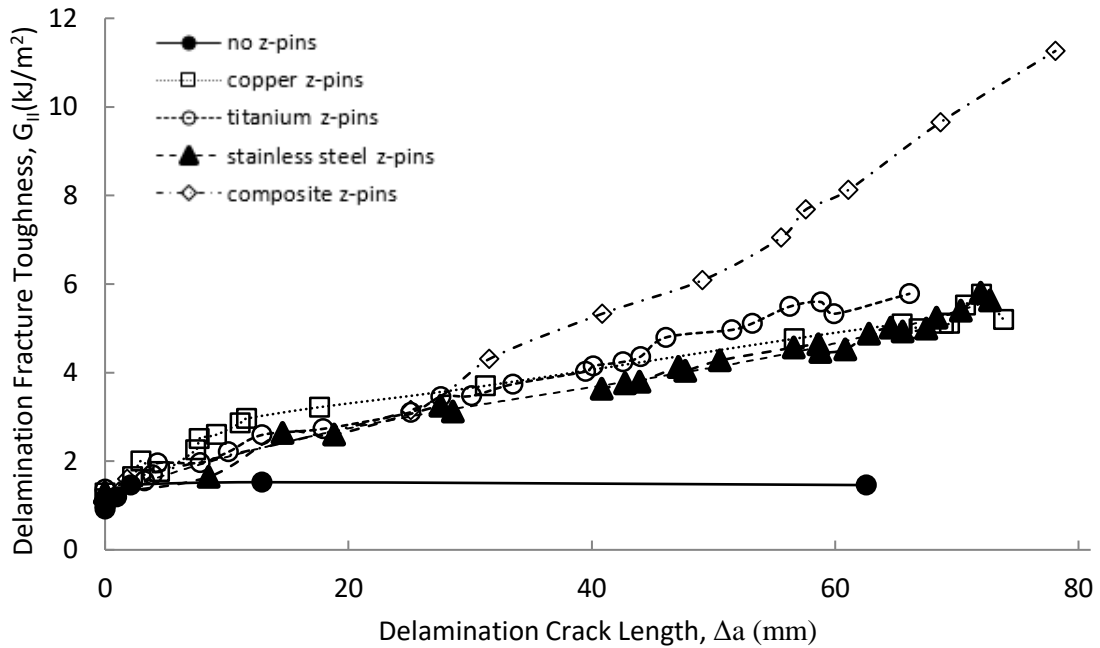
Figure 3.10. Mode II crack growth resistance curves for the unpinned and z-pinned laminates.

Table 3.3 gives the measured values for the mode II strain energy release rate for crack initiation (fracture toughness calculated at the first non-linear point of the applied load vs displacement curve) and at long length (Δa = 50 mm). It was found that the mode II delamination toughness

was higher for the composite reinforced with the carbon fibre z-pins, and there was no significant difference between the different types of metal pins.

Under increasing crack sliding displacement, both the composite and metal z-pins deformed and debonded from the surrounding laminate, as shown in Figure 3.11. With increasing displacement the metal z-pins experienced localised plastic shear deformation whereas the carbon fibre z-pins fractured without pull-out (Figure 3.12). The difference in the fracture mechanisms is due to the higher shear modulus and higher pin/laminate interface strength [55] of composite pins compared with metal pins; revealing that shear modulus, shear strength and pins/laminate interface strength are all important parameters in controlling the mode II fracture toughness of z-pinned composites.

Table 3.3. Mode II fracture properties of the unpinned and z-pinned laminates. The number in brackets shows the times improvement compared to the unpinned material.

	Fracture Toughness Initiation (kJ/m^2)	Fracture Toughness (Δa=50 mm) (kJ/m^2)	Z-Pin Bridging Zone Length (mm)	Z-Pin Failure Mode
no-pins	0.9 ± 0.2	1.3 ± 0.1		
copper	1.2 ± 0.2	4 ± 0.2 (4.4x)	> 60 mm	pull-out
steel	1.2 ± 0.2	3.8 ± 0.3 (4.2x)	> 60 mm	pull-out
titanium	1.4 ± 0.2	4.5 ± 0.2 (4.9x)	> 60 mm	pull-out
carbon	1.3 ± 0.2	6.7 ± 0.9 (7.3x)	> 60 mm	pull-out

(a)   *(b)*
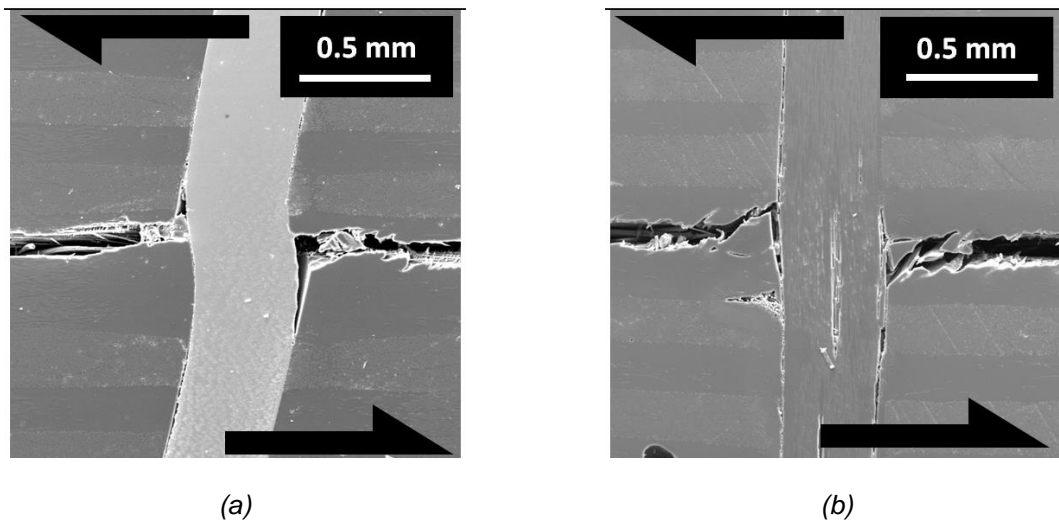
Figure 3.11. Cross-sectional photographs showing (a) titanium and (b) carbon fibre composite z-pins at the same mode II delamination crack location (Δa = 50 mm). Arrows indicate the sliding directions. For the different metal pins the failure mechanism was the same hence only one type of metal is reported.

The mode II interlaminar fracture toughness properties were improved by the z-pins forming a large-scale bridging zone along the delamination crack. The mode II shear traction load-crack sliding displacement curves for the different z-pins are shown in Figure 3.13. These curves were measured using the test method described in section 3.3.3. Irrespective of the material used, there is an initial linear region indicating the elastic deformation of the z-pins at low crack sliding displacement. Following elastic shear deformation, the metal z-pins experience plastic deformation whereas the carbon fibre z-pins undergo longitudinal splitting (Figure 3.141). This can be seen from the mode II traction load curves being smooth and jagged for the metal and carbon fibre z-pins, respectively. During the mode II interlaminar fracture test the maximum applied sliding displacement was approximately 0.68 mm, and this was not sufficient to cause shear failure of the metal z-pins although this displacement severely damaged the carbon fibre pins. Shear test reveals that titanium and copper z-pins fail for respectively 0.72 and 0.79 mm whereas no failure was observed for the stainless steel pin.

(a)   (b)
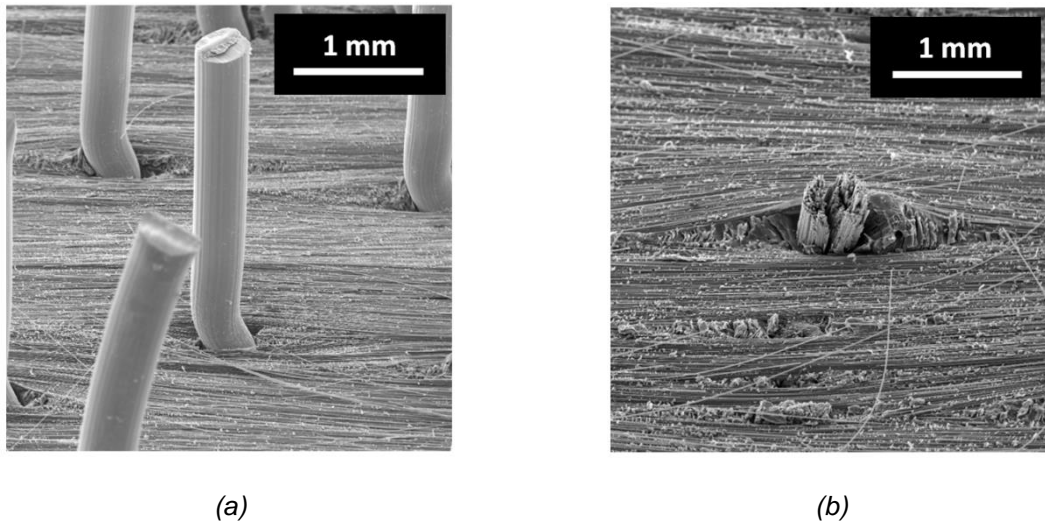
Figure 3.12. Photographs of a mode II crack surface showing the failure mode for the (a) titanium and (b) carbon fibre z-pins. The samples reinforced with metal z-pins were manually split opened after test to show the deformation localized at the crack plane.

Table 3.4 gives the maximum shear traction load and energy (defined by the area under the curve ($\delta < 0.68$ mm)) values measured for the different z-pins. The mode II traction energy of the z-pins increased in the order: copper, stainless steel, titanium and carbon fibre. This correlates with the order for the measure improvements to the mode II fracture toughness properties.
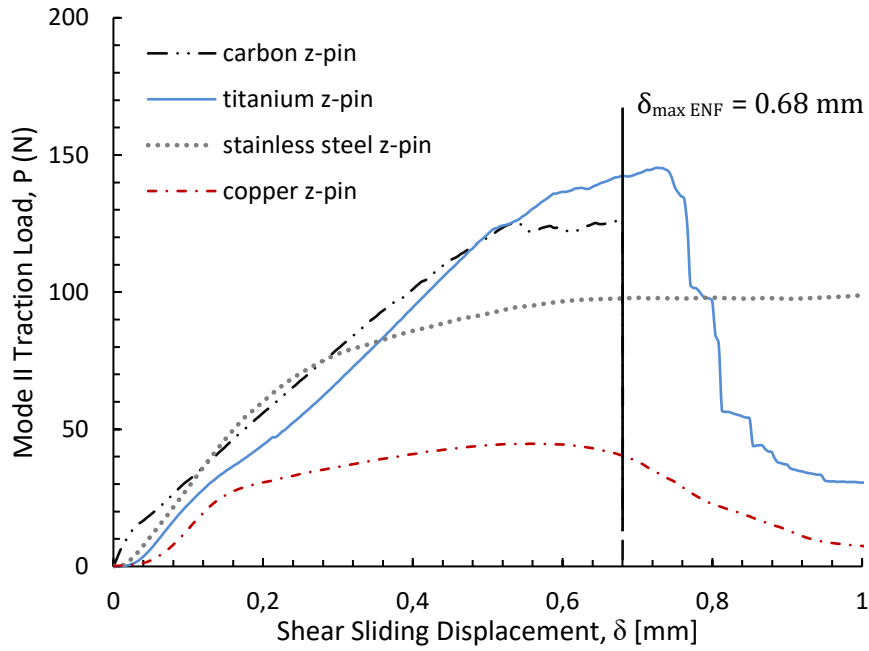
Figure 3.13. Mode II bridging traction load-displacement curves for the different z-pins.

(a)   (b)
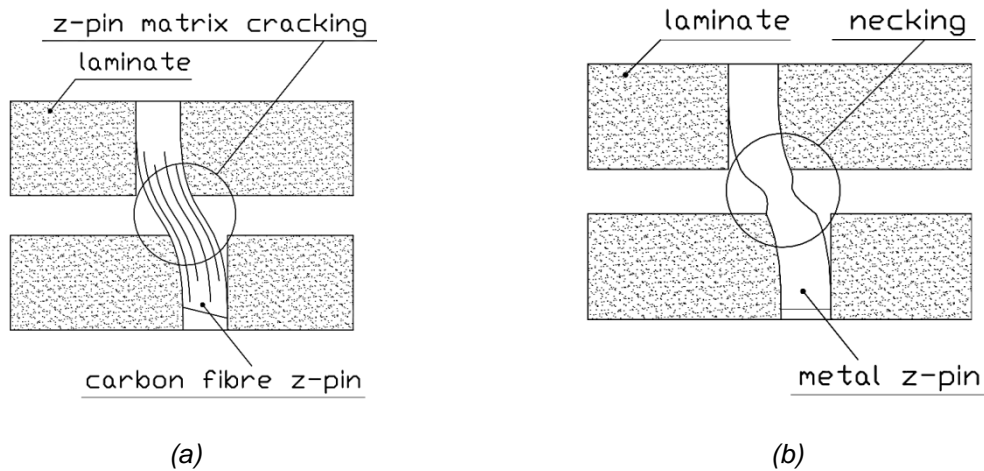
Figure 3.14. Schematic of the (a) longitudinal splitting and (b) plastic deformation on carbon fibre and metal pins.

Table 3.4. Mode II shear traction load and total traction energy of a single z-pin of the different materials. The scatter is one standard deviation of the measured traction property values.

Z-pin Material	Peak Traction Load (N)	Traction Energy (N·mm)
Copper	43 ± 1	23 ± 1
Stainless steel	99 ± 3	43 ± 4
Titanium	132 ± 11	52 ± 1
Carbon	127 ± 4	55 ± 8

3.4.2 Mode II delamination fatigue properties

Paris curves showing plots of the mode II cyclic strain energy release rate (ΔG_{II}) against the delamination crack growth rate (da/dN) for the unpinned laminate and the composites reinforced with the different z-pin materials are presented in Figure 3.15. Z-pinning was effective at increasing the mode II delamination fatigue resistance. The mode II fatigue parameters measured from these curves are given in Table 3.5. The linear portion of the $da/dN - \Delta G_{II}$ curves can be expressed by the Paris law:

$$\frac{da}{dN} = C\Delta G_{II}^{m_{II}}$$

(3.6)

where C and m_{II} are material constants. m_{II} defines the sensitivity of the fatigue crack growth rate to the cyclic stress intensity range; higher value for m_{II} is indicative of greater dependence of da/dN to changes in ΔG_{II}.
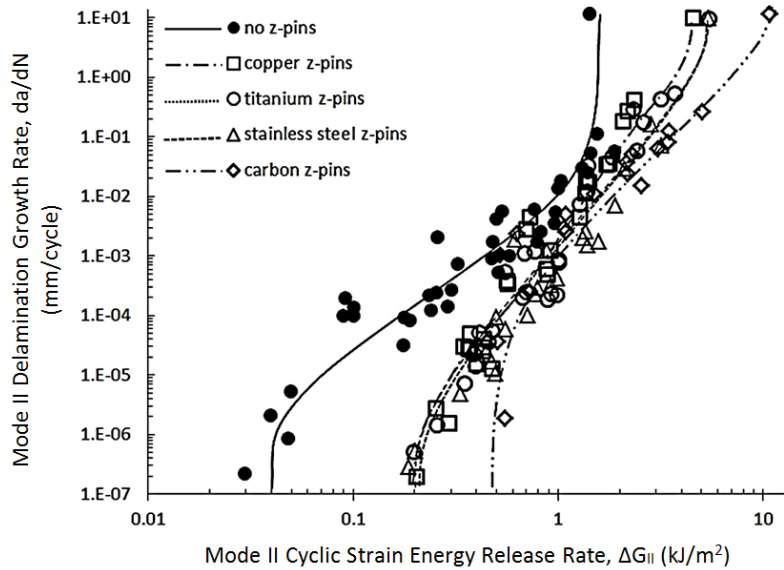
Figure 3.15. Effect of z-pin material on the mode II Paris curve for the carbon-epoxy laminate.

Scatter in the mode II delamination growth rates of the unpinned and z-pinned laminates in the Paris curves is attributed to several factors including stick-slip behaviour of the fatigue cracking process, difficulty in precisely locating the crack tip using optical microscopy, the high sensitivity of the crack growth rate to ΔG, and the discrete spacing of the z-pins causing variations in the growth rate. The measured increase to the mode II fatigue properties due to z-pinning was less pronounced than for mode I [55], particularly at intermediate cyclic intensity values (ΔG_{II}

between ~0.4 and 3 kJ/m²) when there was only a marginal improvement. Z-pins were more effective at increasing the mode II fatigue resistance at relatively low and high cyclic strain energy release rate values when the crack growth rates were slow and fast, respectively.

Table 3.5. ΔG_{II} values for the initiation crack growth (ΔG_{IIi}), fast delamination crack growth (ΔG_{IIc}) and Paris curve parameter 'm$_{II}$' for the unpinned and z-pinned laminates. The last column gives the linear correlation coefficient for the m$_{II}$ value. The numbers in brackets give the times improvement of the z-pin composites compared to the unpinned laminate.

Z-Pin	ΔG_{IIi} [kJ/m²]	ΔG_{IIc} [kJ/m²]	m$_{II}$	Linear Correlation Coefficient (R)
None	0.03	1.05	2.7	0.87
Copper	0.19 (6.8x)	4.4 (4.2x)	5.0	0.94
Stainless steel	0.20 (7.1x)	6.1 (5.8x)	4.8	0.92
Titanium	0.19 (6.8x)	5.0 (4.8x)	4.7	0.93
Carbon fibre	0.52 (17.6x)	10.6 (10.1x)	3.3	0.91

The mode II crack growth rates for the laminate reinforced with copper z-pins were on average slightly higher than the other types of z-pins, although there is a large amount of scatter. The ΔG_{IIi} value to initiate fatigue cracking was increased by about five times with the metal z-pins and more than ten times with the carbon fibre z-pins. The z-pins were also effective at mode II fatigue strengthening at high cyclic stress intensity values when the crack growth rate was fast (above 0.1-1 mm/cycle), particularly the carbon fibre z-pins. The results in Table 3.5 show that the sensitivity of the parameter m_{II} to the type of z-pin material was not significant, considering the low values of linear correlation coefficient (in the range of 0.91 to 0.94).

The mode II fatigue properties (like the mode I properties [55]) were improved by the z-pins forming a large-scale bridging zone along the delamination fatigue crack. The mode II shear traction load-crack sliding displacement curves described in the previous section show that the mode II bridging traction properties are dependent on the type of z-pin, although these differences are not reflected in large differences in the mode II fatigue properties of the different types of z-pinned laminates.

Shown in Figure 3.16 are examples of z-pins made of metal or carbon fibre composite bridging a mode II fatigue crack, and there are substantial differences in the deformation and failure modes. The metal z-pins always plastically deformed under cyclic shear displacement in a region localised to the delamination crack plane (Figure 3.16a). The shear strain deformation of the metal z-pins increased with the amount of crack sliding displacement applied in a single load

cyclic. The metal z-pins would have cyclically strain hardened under repeated loading, causing their yield stress to increase. However, the cyclic shear strains were too low to cause the metal z-pins to completely fail. The carbon z-pins bridging the mode II fatigue crack failed progressively by shear rupture close to the delamination crack (Figure 3.16b). The carbon fibre z-pins failed by longitudinal splitting cracking between the fibres and transverse shear rupture of the individual fibres until eventually the entire pin failed at the delamination crack plane. Despite these differences in the fatigue responses of the ductile metal and brittle carbon fibre z-pins, this did not cause significant differences in their mode II fatigue strengthening efficiency except at low and high ΔG_{II} values when the carbon fibre z-pins were slightly better.

(a)   (b)
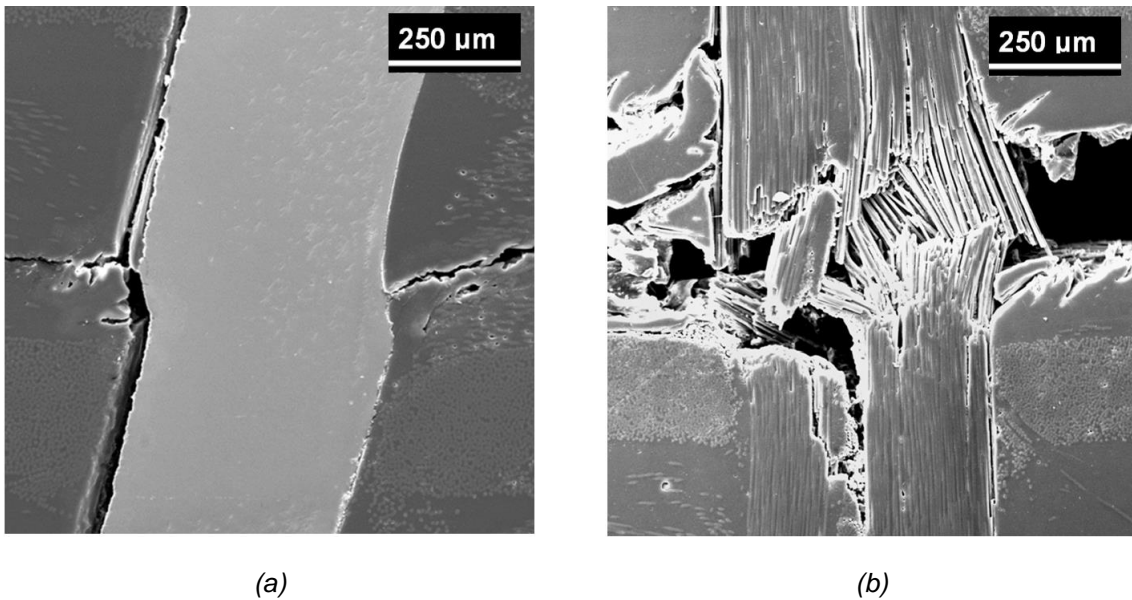
Figure 3.16. Photographs showing mode II fatigue-induced shear deformation of a (a) stainless steel z-pin and (b) shear fracture of a carbon fibre z-pin bridging a fatigue crack.

3.5   Conclusions

This experimental study has proven that an important parameter controlling the mode II delamination fracture toughness and fatigue properties of z-pinned carbon-epoxy laminates is the material used for the pins. The mode II fracture toughness was increased for the laminates reinforced with metal or composite z-pins due to the formation of a large-scale bridging zone along the delamination crack, although the carbon fibre z-pins were the most effective. Because of small lateral displacement induced during ENF testing, the metal z-pins do not fail and show

partial debonding from the laminate and localized plastic deformation whereas the carbon fibre pins show partial debonding and localized splitting damage.

The mode II fatigue resistance was also increased by the metal and carbon fibre z-pins. Irrespective of the z-pin material used, the fatigue strength was improved and especially at the low (ΔG_{II} <0.5 kJ/m^2) and high (ΔG_{II}>1 kJ/m^2) cyclic strain energy release rate values. The metal z-pins plastically deformed close to the delamination crack plane by localised cyclic shear flow, but did not fail. The carbon fibre z-pins also permanently deformed close to the crack plane, and they eventually fractured under cyclic shear loading. Despite these differences in the fatigue responses between the metal and carbon fibre z-pins, this did not change significantly their capacity to increase the mode II delamination fatigue resistance (except at very low and high ΔG_{II} values when the carbon fibre z-pins were slightly better).

Chapter 4:   Mode II Delamination Fracture and Fatigue Properties of Z-pinned Composites: Effect of Volume Content, Diameter and Length of Z-pins

4.1   Abstract

The effects of the volume content, diameter and length of z-pins on the mode II fracture toughness and fatigue resistance of carbon-epoxy laminates is experimentally investigated in this chapter. Z-pins are effective in increasing the mode II delamination toughness (up to 12 times); and the volume content, diameter and length of the pins are all important parameters. Paris curves show that increasing the volume content and diameter and reducing the length of z-pins has a beneficial effect on the mode II fatigue resistance. Z-pins are effective in slowing down the crack growth rate all over the cyclic strain energy release rate intensity range (ΔG_{II}), although they are particularly effective for low *($\Delta G_{II}<0.5 \; kJ/m^2$)* and high *($\Delta G_{II}>1 \; kJ/m^2$)* ranges for which the fatigue crack growth rate is slowed by about one order of magnitude. The mode II interlaminar mechanical properties are improved by the z-pins forming a large-scale bridging traction zone along the delamination.

4.2   Introduction

There is a large body of research work that has investigated the effect of z-pins on the delamination properties of composites, as reported in Chapter 2. Numerous experimental and numerical studies have shown that z-pins can significantly improve the mode I interlaminar fracture toughness [23-26, 28, 31, 34, 44, 47, 101-104] and mode I fatigue resistance of composites [28, 35, 55, 105]. The improvements are influenced by several parameters such as volume content [28, 34], length [28], diameter [28] and material properties of the z-pins [55]. For example, Cartié et al. [34] showed that the mode I fracture toughness and fatigue resistance of carbon-epoxy laminate increases with the volume content of z-pins, and this is due to increasing number of z-pins generating bridging traction loads that oppose crack opening and growth. Increasing the z-pin diameter has a detrimental effect on the mode I delamination resistance [28, 34], and this is due to a reduction in the pin/composite interface area at a fixed volume content. Varying the z-pin length also affects the mode I toughness [28]. When crack opening displacement is applied, z-pins (that were initially bonded to the laminate) experience interface cracking because of their high tensile strength (greater than interfacial strength). The larger is their embedded length the greater is the axial load necessary to crack the z-pin/laminate interface and the longer the pull-out length, and this is reflected in higher mode I fracture toughness. Pingkarawat and Mouritz [28] recently reported that the mode I fatigue resistance is also dependent on the volume content, diameter and length of the z-pins.

This chapter presents an experimental investigation to determine the effects of the volume content, diameter and length of z-pins on the mode II delamination toughness and fatigue resistance of a carbon-epoxy laminate. Improvement in the delamination toughness are measured using crack growth resistance curves (R-curves) whereas fatigue resistance is quantified using Paris curves, from which the effect of z-pinning on the threshold cyclic strain energy release rate value to initiate fatigue cracking, the fatigue crack growth rate, and the cyclic strain energy release rate to cause unstable, fast fatigue cracking are determined. The study also aims to identify the fatigue toughening mechanisms generated by the z-pins that increase both the mode II interlaminar toughness and fatigue resistance, and how the mechanism are affected by the volume content, diameter and length of the z-pins. The z-pins used in this study were unidirectional carbon-fibre composite. The metal z-pins studied in the previous chapter are not used for the research described in this chapter.

4.3   Composite Material

The composite material used in this study was made with unidirectional T700 carbon fibre-epoxy prepreg tape (VTM264), which was supplied by Advanced Composites. This is the same composite material used in the work presented in Chapter 3. The carbon-epoxy prepreg was stacked in a $[0_6/[90/0]_2]_s$ ply pattern. The z-pins were inserted through the uncured prepreg stack using the ultrasonically-assisted pinning (UAZ) process, which was described in the previous chapter. The z-pins used in this work were made of unidirectional carbon fibre-bismaleimide composite supplied by Albany Engineered Composites.

In order to determine experimentally the effect of z-pin diameter, the laminate was reinforced using 280 μm (thin pins) or 510 μm (thick pins) diameter z-pins at a volume content of 2% and embedded length of 4 mm. Laminates were also reinforced with different z-pin contents of 0.5, 2 and 4 vol% whereas diameter and length of the z-pins was kept constant at 280 μm or 4 mm respectively. To investigate the effect of z-pin length, laminates were stacked with the ply orientations of $[0/[90/0]_2]_s$, $[0_6/[90/0]_2]_s$ or $[0_{16}/[90/0]_2]_s$ to obtain a thickness of 2, 4 or 8 mm, respectively. The 2, 4 and 8 mm thick laminates were reinforced with z-pins to a volume content of 2% and diameter of 280 μm. In this way, laminates were made with z-pins having different lengths, which in this chapter are referred to as short (2 mm), intermediate (4 mm) and long (8 mm) pins. The only difference between the composites was the embedded length of the z-pins; all other z-pin parameters such as diameter (280 μm) and volume content (2%) and total thickness of the laminate (13 mm) were the same. For comparison, unpinned laminate samples were also manufactured and, as for the z-pinned samples they were reinforced with additional tabs and cured in autoclave as described in Chapter 3. The different types of unpinned and z-pinned laminates are listed in Table 4.1.

Table 4.1. Mode II fatigue tests matrix.

Effect of Z-Pin Volume Content		
Z-Pin Volume Content	Z-Pin Diameter	Z-Pin Length
low content (0.5%)	thin z-pin (280 μm diameter)	4 mm
Intermediate content (2.0%)	thin z-pin (280 μm diameter)	4 mm
high content (4.0%)	thin z-pin (280 μm diameter)	4 mm
Effect of Z-Pin Diameter		
Z-Pin Diameter	Z-Pin Volume Content	Z-Pin Length
thin z-pin (280 μm diameter)	intermediate content (2.0%)	4 mm
thick z-pin (510 μm diameter)	intermediate content (2.0%)	4 mm
Effect of Z-Pin Length		
Z-Pin Length	Z-Pin Diameter	Z-Pin Volume Content
2 mm	thin z-pin (280 μm diameter)	intermediate content (2.0%)
4 mm	thin z-pin (280 μm diameter)	intermediate content (2.0%)
8 mm	thin z-pin (280 μm diameter)	intermediate content (2.0%)

4.4 Mode II Interlaminar Fracture Toughness and Fatigue Interlaminar Testing

The mode II delamination fracture toughness and delamination fatigue resistance of the unpinned and z-pinned laminates were measured using the end notched flexure (ENF) test procedure that was described in the previous chapter.

4.5 Results and Discussion

4.5.1 Mode II delamination fracture toughness

Effect of z-pin volume content on mode II interlaminar fracture toughness

Presented in Figure 4.1 are the mode II delamination crack growth resistance (R) curves for the unpinned laminate and composites reinforced with different volume contents of z-pins (0.5%, 2% and 4%). The R-curves show plots of the mode II strain energy release rate (G_{II}) against delamination crack extension (Δa), which is the distance the crack has grown from the pre-crack tip. The R-curve for the unpinned laminate is low and flat, revealing that its mode II interlaminar fracture toughness (G_{IIc}) is not dependent on the delamination crack length. However, the fracture process was unstable in the unpinned ENF samples with the crack advancing rapidly from the pre-crack tip. Fractographic examination of the unpinned composite revealed the absence of a large-scale fibre bridging zone behind the delamination front, and this accounts for the flat R-curve and relatively low toughness. The z-pins increased the mode II fracture toughness and altered the crack growth resistance curves. The fracture process was stabilised by the z-pins, and rapid and large-scale crack extension did not occur in the z-pinned ENF samples. The mode II

fracture toughness increased rapidly with the volume content of z-pins (Figure 4.2). The fracture toughness increased by 200–300% for every 1% increase in the volume content of z-pins, and at the highest z-pin content (4%) the delamination resistance was about 12 times higher than the unpinned material.
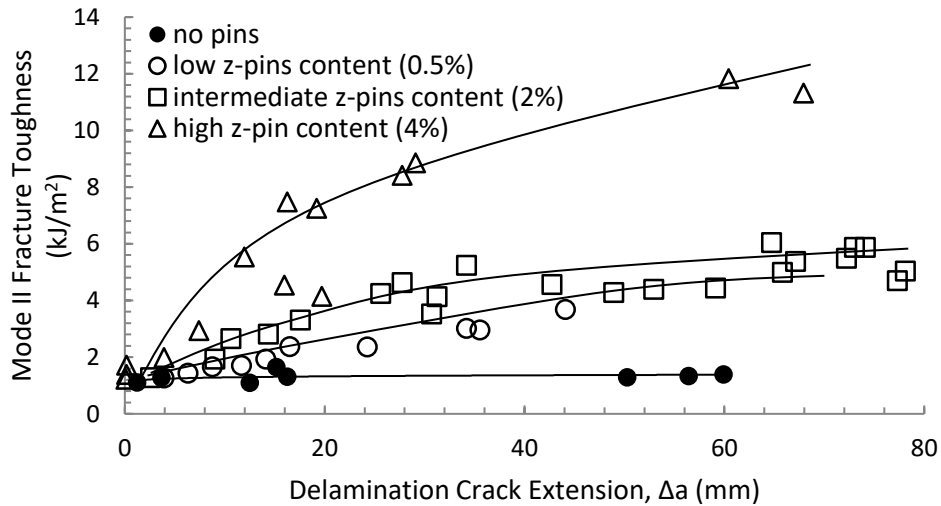
Figure 4.1. R-curves showing the effect of volume content of z-pins on the mode II interlaminar fracture toughness of the carbon-epoxy laminate.
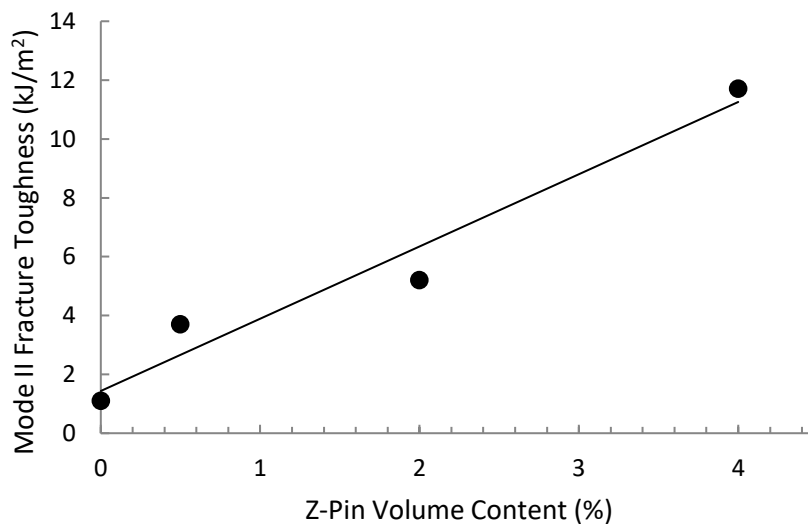
Figure 4.2. Effect of the volume content of z-pins on the average mode II interlaminar fracture toughness of the carbon-epoxy laminate. The average values were calculated by averaging the delamination toughness values which were measured for Δa > 50 mm.

Delamination fracture studies by Cartié et al. [34] and Yan et al. [22] also report an increase to the mode II fracture toughness of carbon–epoxy composites with increasing z-pin content. However, these studies involved mode II fracture toughness (ENF) tests in which the delamination crack length was relatively short (less than 25 mm) and therefore the condition of steady-state toughness (which occurs at long crack lengths) was not attained. The results in Figure 4.1 are the first reported complete mode II *R*-curves for z-pinned composites. The *R*-curves show that the toughening effect induced by the z-pins increase with delamination crack extension until it reached about 40–50 mm, when the fracture toughness reached a steady-state value.

The increase in the *R*-curves was due to the progressive formation of an extrinsic crack bridging process zone by the z-pins behind the delamination front. As the delamination grew in length an increasing number of z-pins joined the bridging zone, and this increased the fracture toughness. As new z-pins joined the bridging zone at the advancing crack front there was a corresponding number of z-pins towards the rear of the bridging zone (where the crack sliding displacement was largest) which failed. Under these conditions the mode II fracture toughness reached a steady-state value. The mode II fracture toughness of a z-pinned composite with the geometry of the ENF specimen (as in Figure 3.4) can be described using [22]:

$$G_{IIR} = G_{IIC}^* + G_{IIP}(\Delta a) \tag{4.1}$$

G_{IIc}^* is the mode II fracture toughness of the unpinned laminate. G_{IIp} is mode II toughness due to the z-pins, and toughening is induced by elastic and permanent shear deformation of the z-pins within the crack bridging zone. The higher the volume content of z-pins is the larger will be the $G_{IIP}(\Delta a)$ value in Equation (4.1), and this will be reflected in a higher mode II interlaminar fracture toughness.

Effect of the z-pin diameter on mode II interlaminar fracture toughness

The mode II interlaminar fracture toughness and *R*-curve behaviour was also dependent on the z-pin diameter. Figure 4.3 presents *R*-curves for the unpinned laminate and the composites reinforced with z-pins having a diameter of 280 or 510 μm. At relatively short crack lengths (under ~40 mm), the toughening effect induced by the thin and thick z-pins was approximately the same. At longer crack lengths, however, the fracture toughness reached a steady-state value for the thin z-pins but continued to rise for the thick z-pins. The rising *R*-curve for the composite

containing the thick z-pins indicates that the crack bridging zone never fully developed, and is longer than the maximum crack length attained in the ENF fracture tests (Δa = 80 mm).
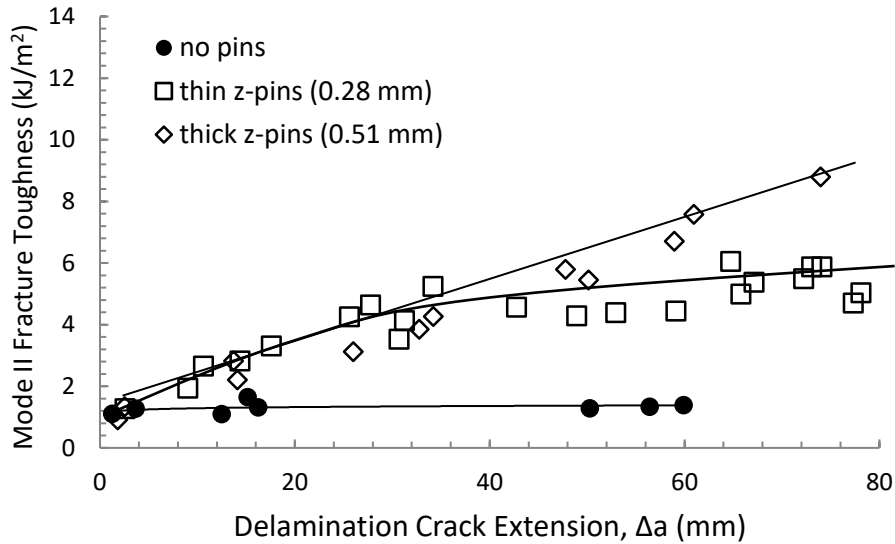
Figure 4.3. R-curves showing the effect of z-pin diameter on the mode II interlaminar fracture toughness of the carbon-epoxy laminate.

Effect of z-pin length on mode II interlaminar fracture toughness

The mode II R-curves showing the effect of the z-pin length are given in Figure 4.4. While the z-pins increased the delamination resistance, regardless of the z-pin length, the toughness was highest for the shortest pins (2 mm) and lower toughness values were measured for the intermediate (4 mm) and longest pins (8 mm). This is different to the mode I toughness, which increased progressively with the z-pin length [28].

The carbon fibre z-pins bridging the mode II crack experienced irreversible shear deformation due to the sliding displacement between the opposing surfaces of the delamination. Regardless of their volume content, diameter or length, the z-pins along the bridging zone were forced to rotate in the direction of interlaminar shear loading along the delamination crack plane as shown in Figure 4.5.
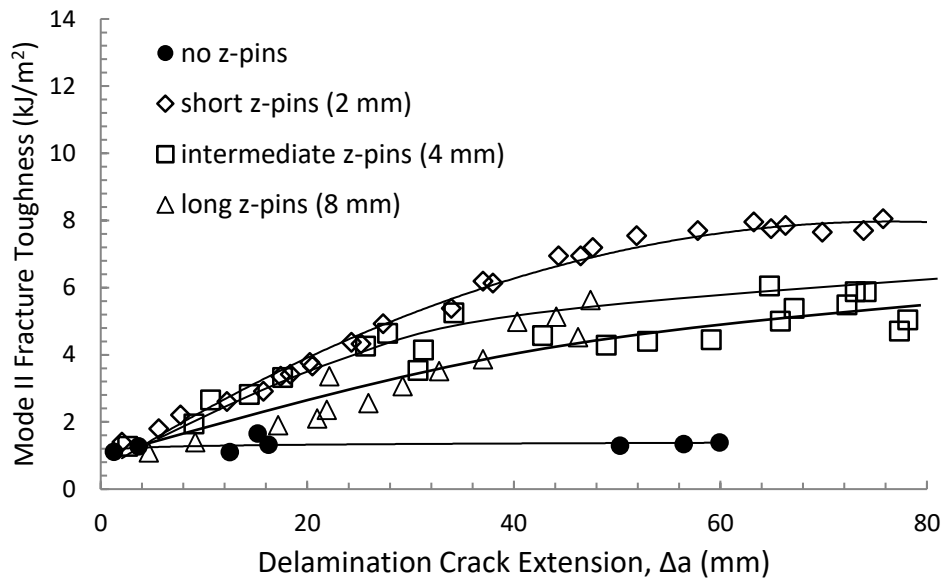
Figure 4.4. R-curves showing the effect of z-pin length on the mode II delamination toughness of the carbon-epoxy laminate.

(a)   (b)
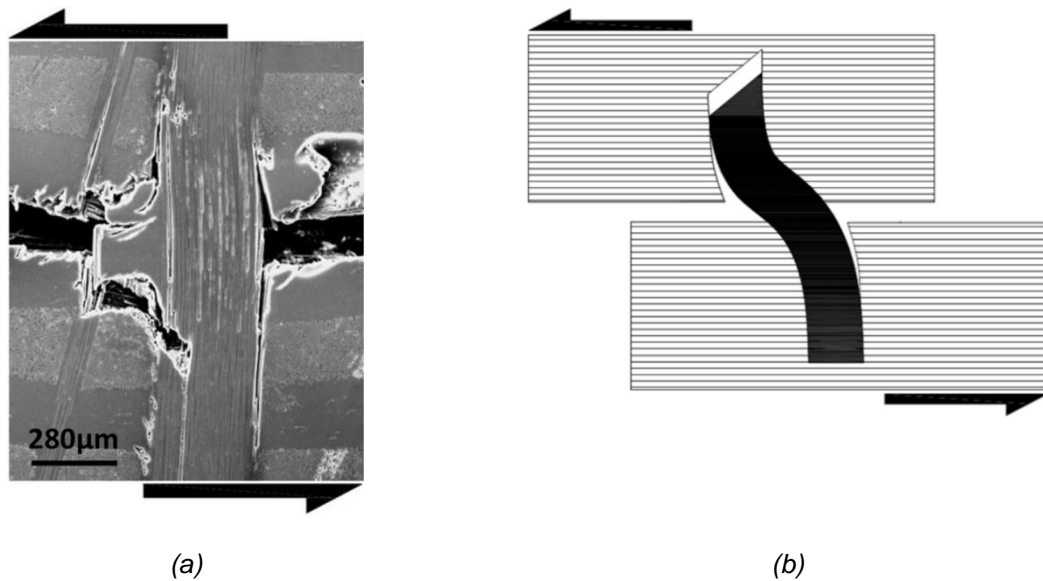
Figure 4.5. (a) Scanning electron micrograph showing shear-induced deformation and damage to a bridging z-pin under mode II interlaminar loading. (b) Schematic diagram of shear-induced deformation of a z-pin. The arrows indicate the direction of the sliding.

Fractographic examination of the delamination crack surfaces revealed that the final shear fracture mode of the z-pins was determined by their length, as shown in Figure 4.6. The shortest z-pin failed by partial shear-induced rotation and then pull-out. The intermediate length z-pins

experienced a small amount of pull-out before failing by shear rupture. The longest z-pins fractured in shear at the delamination crack surface without experiencing any pull-out.

The z-pins closest to the mode II delamination front elastically deform in shear, irrespective of their volume content, diameter or length. The shear traction load generated by localised elastic shear deformation of a single z-pin is:

$$P_{IIe} = \frac{\tau_{IIe}\pi d_p^2}{4} \tag{4.2}$$

τ_{IIe} is the shear stress exerted on the z-pin and d_p is the pin diameter. This equation shows that the elastic traction load generated by the z-pin is not dependent on its length. For longer z-pins there is significant resistance to rotation and shear failure occurs prior to pull-out. As shown in Figure 4.6, z-pin pull-out from the laminate is a complex process. The mode II bridging law is assumed to have a similar form to that of mode I failure whereby pull-out begins to occur after debonding at a critical load. Depending on the materials and geometry of the ENF test the z-pins may break before being completely pulled out, as in the cases shown in Figure 4.6b and c. The shear traction force generated by these processes is determined using:

$$P_{IIf} = \tau_{IIf}\pi d_p(l_p - \delta_p) \tag{4.3}$$

τ_{IIf} is the interfacial shear stress generated by a sliding z-pin under mode II interlaminar loading. l_p and δ_p are the embedded length prior to pull-out and the amount of pull-out experienced by the z-pin, respectively. The equation shows that the shear traction force opposing slip and pull-out increases linearly with the z-pin length. However, longer z-pins cannot rotate as easily along the mode II delamination crack plane and fail in shear. Therefore, increasing the z-pin length can reduce the amount of crack sliding displacement that can occur before the z-pin fails. The reduction to the mode II fracture toughness with increasing z-pin length is therefore attributed to the increasing resistance imposed against pin rotation along the crack plane. The shortest z-pins induced the lowest shear resistance against pull-out, and therefore these pins were pulled completely from the composite.

(a)

(b)
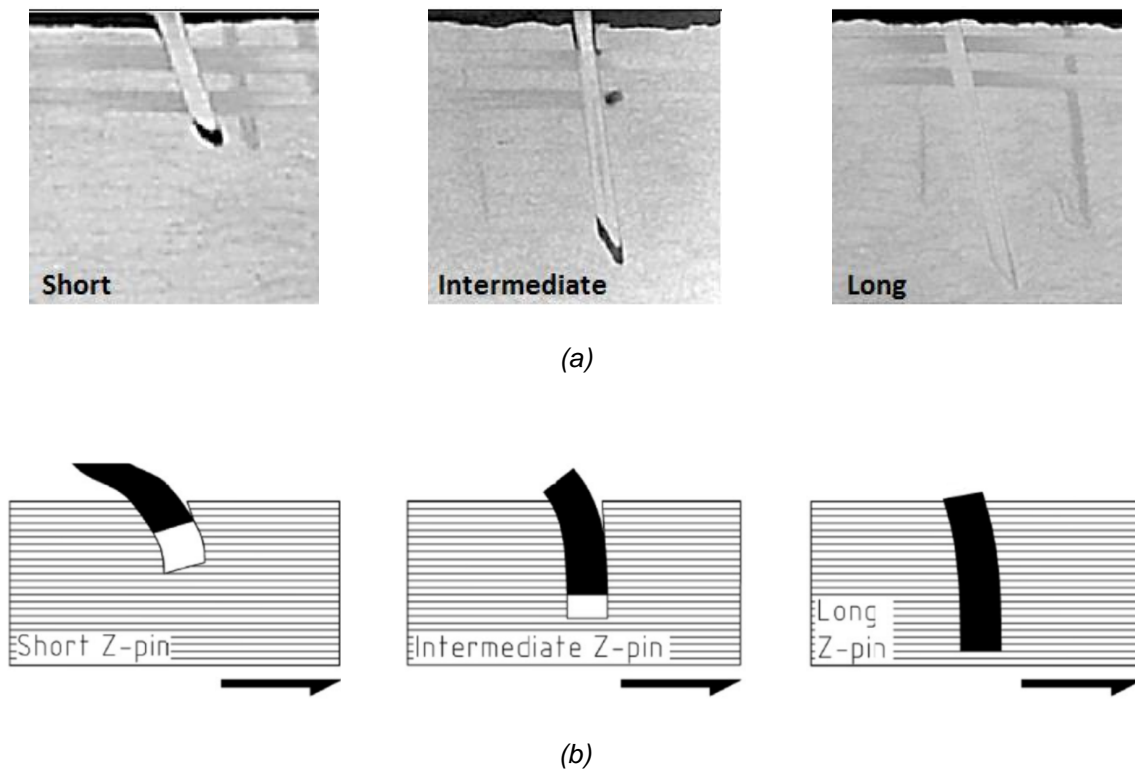
Figure 4.6. (a) X-ray CT photographs and (b) schematic diagrams showing the effect of increasing z-pin length on the pin failure event under mode II interlaminar loading.

4.5.2 Mode II delamination fatigue resistance

Effect of z-pin volume content on mode II interlaminar fatigue resistance

Figure 4.7 shows the effect of the volume content of z-pins on the mode II interlaminar fatigue properties of the carbon–epoxy laminate. The figure presents Paris-like curves of the measured relationship between mode II cyclic strain energy release rate range (ΔG_{II}) and delamination crack growth rate (da/dN) for the composites. The curves in Figure 4.7 are lines-of-best fit through the experimental data. There is a large amount scatter in the crack growth rates for both the unpinned and z-pinned laminates. As described in Chapter 3, some of the scatter is attributed to experimental difficulties in accurately measuring the crack front. Also, the fatigue cracks slowed when approaching the z-pins (crack arrest) and accelerated when z-pins at the rear of the bridging zone failed (crack advance), and this stick-slip behaviour also contributed to the scatter.

Despite scatter in the fatigue data, the Paris-like curves presented in Figure 4.7 show that z-pinning increased (in most instances) the mode II delamination fatigue resistance. At the lowest z-pin content (0.5%), the fatigue resistance was improved at low and high cyclic strain energy release rate values, although over the intermediate range (ΔG_{II} between $\sim 0.2 - 1 \ kJ/m^2$) there

was no significant improvement. Any small increase in the fatigue resistance due to the z-pins may be masked by the large amount of scatter in the crack growth rates. Similarly, the laminate reinforced at the intermediate z-pin content (2%) displayed superior fatigue resistance at low and high cyclic strain energy release rates, but the improvement was marginal over the intermediate range. The laminate with the highest z-pin content (4%) had the highest fatigue resistance, but also the greatest amount of scatter. These findings reveal that fatigue strengthening is dependent on the cyclic range of strain energy release rates (as reported in Chapter 3) as well as the z-pin content. Z-pinning is most effective at resisting fatigue cracking under low and high cyclic shear stress conditions. Table 4.2 gives the values for m_{II} (crack growth rate exponent) for the unpinned and z-pinned composites. All the values for m_{II} are relatively low, and there is no clear correlation with the volume content of z-pins. Also, the linear correlation coefficient values are relatively low further supporting that no statistical trend exist between the m_{II} value and z-pin content.
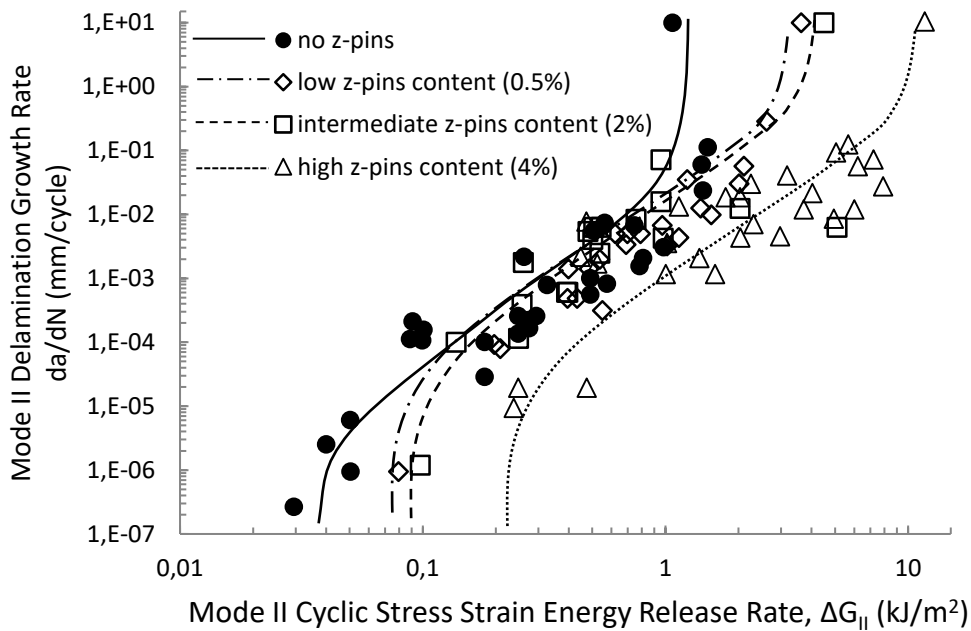
Figure 4.7. Effect of volume content of z-pins on the Paris-like curve for the carbon-epoxy laminate. The curves are fitted to the data. The z-pins were 280 μm in diameter and 4 mm in length.

Table 4.2. Values for the Paris curve parameter 'm' for the unpinned and z-pinned composites.

Z-Pin Volume Content	Z-Pin Diameter	Z-Pin Length	m_{II}	Linear Correlation Coefficient (R)
None	-	-	2.7	0.87
0.5%	280 μm	4 mm	3.3	0.95
2%	280 μm	4 mm	4.9	0.91
4%	280 μm	4 mm	2.0	0.81

The Paris curves presented in Figure 4.7 also show that the threshold cyclic strain energy release rate value ($\Delta G_{II(t)}$) needed to initiate fatigue crack growth increased with the volume content of z-pins. It was not possible to determine the precise value of $\Delta G_{II(t)}$ due to the large amount of scatter in the crack growth rate data. Instead, $\Delta G_{II(t)}$ was taken to be value at the fatigue crack growth rate of 1×10^{-7} mm per load cycle, which is slightly above when measurable delamination cracking starts to occur. Figure 4.8 shows the effect of increasing volume content of z-pins on the threshold cyclic strain energy release rate value. There is a linear correlation between the z-pin content and the cyclic value needed to initiate mode II crack growth. $\Delta G_{II(t)}$ increases by ~ 170% for every 1% increase to the volume content of z-pins, and at the highest z-pin content that value is nearly 8 times higher than the unpinned laminate. This clearly shows that z-pinning is effective at resisting the initiation of mode II fatigue cracking.
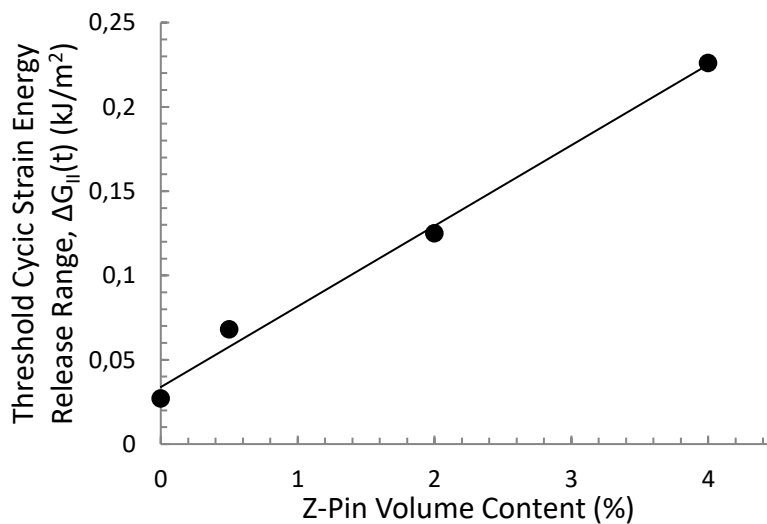
Figure 4.8. Effect of volume content of z-pins on the threshold cyclic strain energy release rate value needed to initiate delamination fatigue cracking in the carbon–epoxy composite. Note that due to the large amount of scatter, these values are approximate. $\Delta G_{II(t)}$ was defined at the da/dN value of 10^{-7} mm/cycle.

Z-pins were also effective at resisting rapid fatigue cracking at high cyclic strain energy release rate values, as shown in Figure 4.7. The fatigue crack growth rate for the unpinned composite accelerated rapidly when the cyclic strain energy range approached the mode II interlaminar fracture toughness ($\Delta G_{II} \rightarrow \Delta G_{II(c)}$ of 1.1 kJ/m^2), which defines the onset of unstable (rapid) delamination cracking.

The improvement to the mode II delamination fatigue resistance was due to the increasing number of z-pins forming a large-scale extrinsic bridging zone behind the delamination crack front. It is well known that large-scale crack bridging promotes high mode II interlaminar fracture toughness in z-pinned composites under monotonically increasing crack sliding displacements [25, 36], and a similar strengthening process is operative for fatigue cracks. Figure 4.9 presents a cross-sectional view of a z-pinned composite showing the different stages of z-pin bridging along the mode II fatigue crack. The bridging process is complex with the physical condition of the carbon fibre z-pin changing continuously along the bridging process zone. Nearest the delamination front, where the amount of shear sliding displacement between the opposing crack faces is very low, the z-pins bridge the fatigue crack without being damaged (Region A). Inside Region A the bridging z-pins respond elastically to the small crack sliding displacement, and there is no damage to the pins themselves. Further behind the delamination front the z-pins debond from the surrounding composite material (Region B). Debonding initiates at or near the delamination crack plane, and then propagates along the z-pin/composite interfacial region with increasing cyclic loading. Following complete debonding, the bridging z-pins begin to undergo transverse shear failure localised to the fatigue crack plane (Region C). Cyclic shear displacement of the bridging z-pins causes progressive cracking and fibre fracture with an increasing number of loading cycles until eventually the z-pins completely failed in shear (Region D).
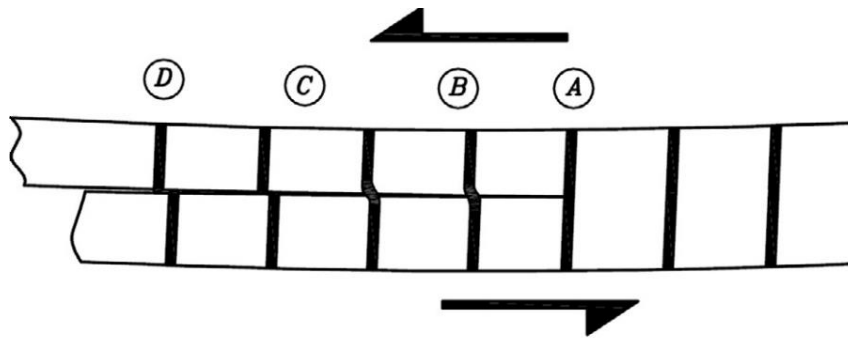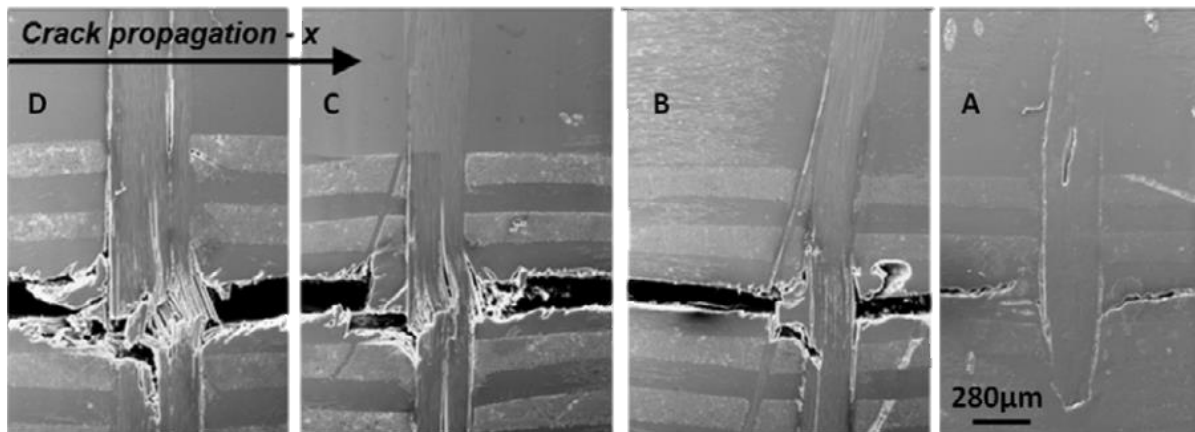
Figure 4.9. Photographs showing the bridging z-pins at different locations (as indicated in the schematic of the ENF specimen) along a mode II delamination fatigue crack.

Shear displacement of the z-pins causes them to press laterally into the composite material close to the crack plane in a toughening process known as snubbing [33]. Snubbing opposes shear deformation of the z-pins, resulting in an enhanced bridging force. Figure 4.10 shows a magnified view of a single z-pin within Region C of the bridging zone, and the composite material adjacent to the pin is severely deformed and cracked. This damage occurred by the z-pin pressing laterally into the composite under cyclic shear loading, and this snubbing process contributed to the fatigue strengthening process. The z-pins also experience a very small amount of pull-out in Region C, and this is caused by debonding followed by shear-induced rotation of the debonded z-pins along the crack plane. The pull-out increases with the amount of z-pin rotation.

At the rear of the bridging zone, where the crack sliding displacement is large, the z-pins completely fractured along the delamination crack plane (Region D). Even though the z-pins in Region D were broken, a traction load is still generated by friction between the opposing surfaces of broken pins. Despite the progressive damage to the z-pins with increasing crack sliding

displacement along the bridging zone, they retain sufficient shear strength to generate fatigue traction loads between the opposing delamination surfaces and thereby lower the magnitude of the cyclic shear stress applied to the crack tip. As a result, the mode II fatigue resistance is increased by z-pinning. Figure 4.11 shows a broken z-pin at the surface of a delamination fatigue crack. This is a z-pin that has completely failed under mode II cyclic loading (Region D). The composite material surrounding the fractured z-pin is also damaged due to snubbing. Even though the z-pins in region D are broken, it is feasible that they still contributed to fatigue strengthening by mechanical interlocking as shown schematically in Figure 4.12. During testing it was observed that the opposing fractured portions of the z-pins mechanically interlocked at the minimum crack sliding point in each load cycle, thereby creating an opposing friction traction stress. When the crack sliding within a single load cycle was increased this forced the two portions of the fractured z-pin to separate. Therefore, fractured z-pins retained the capacity to generate bridging traction loads which contributed to the improved mode II fatigue resistance.
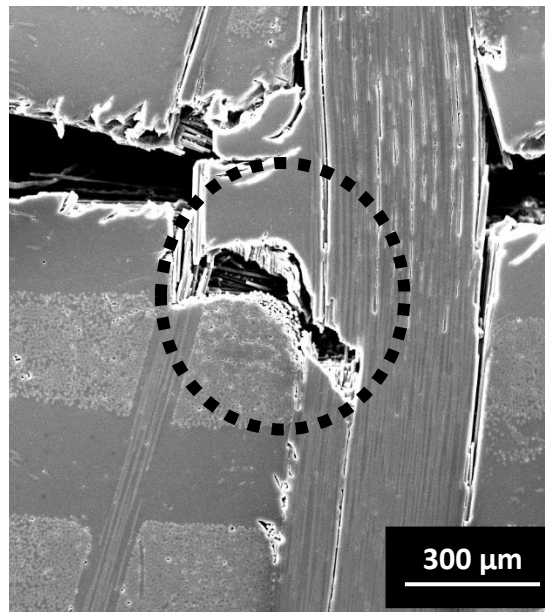
Figure 4.10. SEM photograph showing a cross-sectional view of a bridging z-pin showing snubbing-induced damage (circled) to the composite under mode II interlaminar fatigue loading.

The fatigue resistance improved when the z-pin content was increased from the low (0.5%) to intermediate (2.0%) level because a greater number of pins were involved in the bridging zone. This reduced the cyclic shear stress applied to each z-pin within the bridging zone, which thereby increased the number of loading cycles needed to induce debonding, shear deformation and shear rupture of the pins. Raising the z-pin content from the intermediate to highest (4%) level did not

improve the apparent fatigue resistance further because the fatigue mechanism transitioned from a single fatigue crack to multiple cracks. Examination of the ENF samples during testing revealed that the fatigue crack growth process was influenced by the volume content of z-pins. Fatigue occurred as a single delamination along the mid-plane of the unpinned laminates as well as the composites with the low and intermediate volume content of z-pins. At the highest z-pin content, however, the fatigue process involved multiple delamination cracks growing in parallel along neighbouring ply interfaces. This transition in the fatigue crack process is illustrated in Figure 4.13, whereby multiple delaminations propagated along the 0/90 ply interfaces in the composite with the highest z-pin content. It appears that when the z-pin content exceeds a critical level (which in the composite studied here is between 2% and 4%) it is energetically more favourable for multiple fatigue cracks to grow concurrently rather than as a single crack. This transition in the cracking process is indicative of the high fatigue strengthening attained by reinforcing the composite at the highest z-pin content.
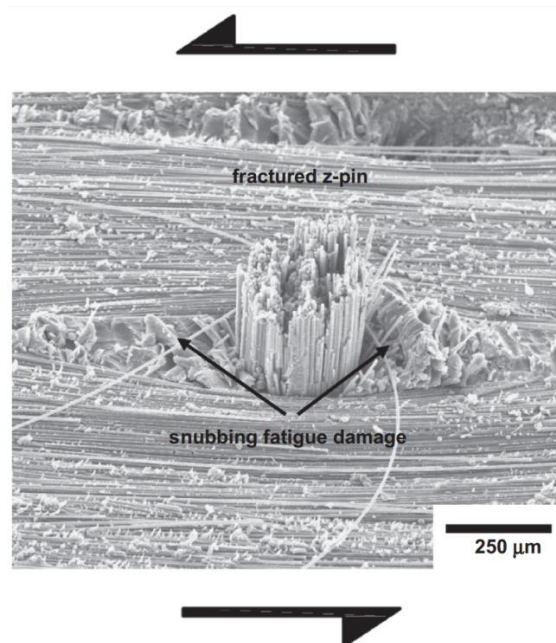
Figure 4.11. Fractured z-pin caused by mode II interlaminar fatigue loading. Note the fatigue-induced snubbing damage adjacent to the z-pin.
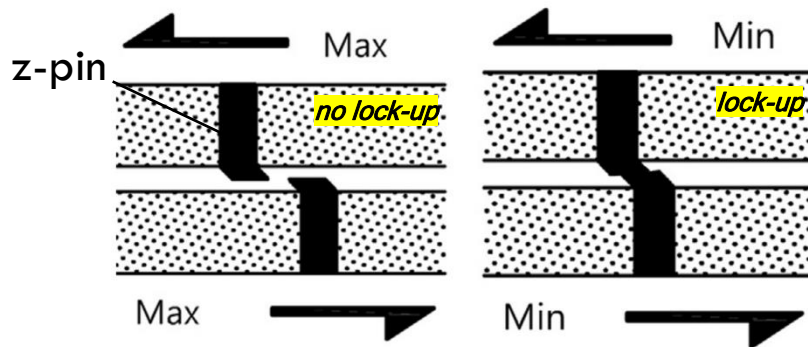
Figure 4.12. Schematic representation of bridging traction stress generated by a broken z-pin along a delamination fatigue crack whereby it lock-ups when the fatigue stress is relaxed to a minimum value.
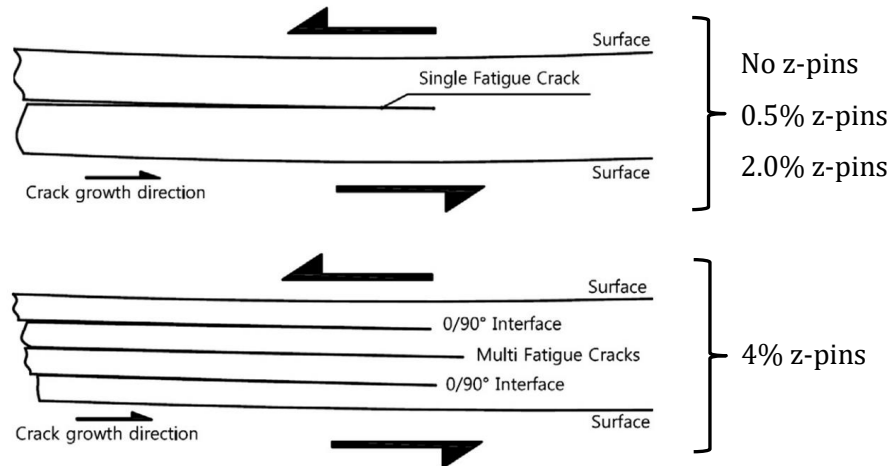
Figure 4.13. Schematic representation of the transition of the fatigue cracking process from a single to multiple delaminations in the ENF sample with increasing volume content of z-pins.

Effect of z-pin diameter on mode II fatigue resistance

Mode II Paris curves showing the effect of z-pin diameter on the fatigue properties are presented in Figure 4.14. Curves are shown for composites reinforced with thin or thick z-pins at the same volume content (2%) and 4 mm embedded length. For comparison, the Paris curve for the unpinned laminate is shown. The curves are lines-of-best fit through the data, and the Paris curve values for m_{II} are given in Table 4.3. There is no clear trend between z-pin diameter and the m_{II} parameter due to the large amount of scatter as defined by the linear correlation coefficient.

Figure 4.14 shows that both the thin and thick z-pins improved the mode II interlaminar fatigue resistance of the composite, particularly in the lower and higher ranges of ΔG_{II}. It appears that the threshold cyclic strain energy release rate needed to initiate the fatigue crack increased with the z-pin diameter. Both the thin and thick z-pins also increased the maximum cyclic strain energy release rate value under which rapid fatigue cracking occurred. However, the thick z-pins were more effective, with the onset of fast fatigue cracking occurring at a higher ΔG_{II} value than for the thin z-pins. This improvement is attributed to the higher toughening effect of the thick z-pins at long delamination cracks, as indicated by the R-curves shown in Figure 4.1.
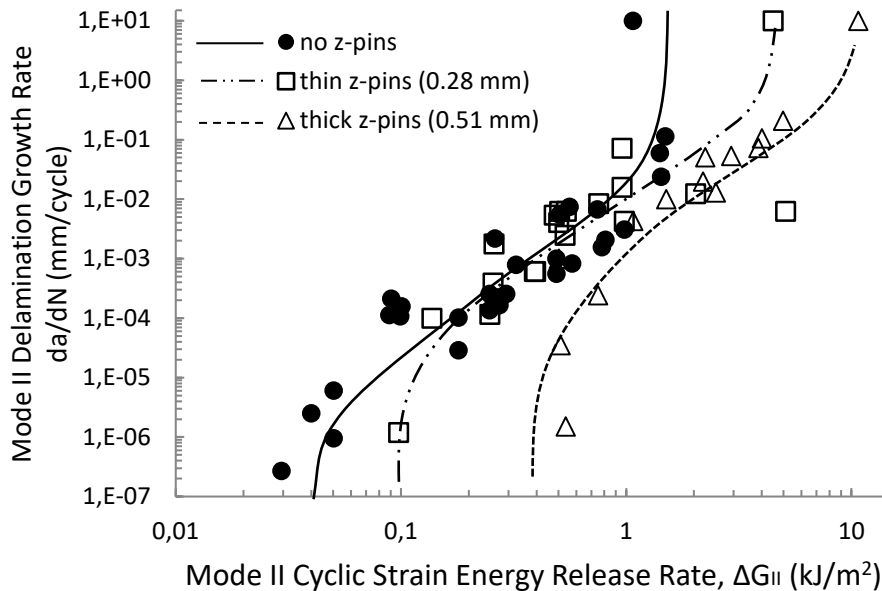
Figure 4.14. Effect of the z-pin diameter on the Paris curve for the carbon-epoxy composite. The curves are fitted to the data. The volume content and length of z-pins were 2% and 4 mm, respectively, in both z-pinned composites.

Table 4.3. Values for the Paris curve parameter 'm$_{II}$' for the unpinned and z-pinned composites.

Z-Pin Diameter	Z-Pin Volume Content	Z-Pin Length	m$_{II}$	Linear Correlation Coefficient (R)
no pins	0%		2.7	0.89
280 μm	2.0%	4 mm	4.9	0.91
510 μm	2.0%	4 mm	3.3	0.91

The fatigue-induced strengthening mechanisms and failure mode of the composites reinforced with the thin and thick z-pins were found to be similar. Fractographic examination of the ENF test

specimens revealed that the fatigue resistance was increased by the z-pins forming a large-scale bridging zone along the delamination crack, irrespective of the z-pin diameter. The failure mode of the thin and thick z-pins was also similar, and involved debonding, shear deformation and fracture close to the fatigue crack plane (the same as that shown in Figure 4.9).

Effect of z-pin length on the mode II delamination fatigue resistance

Figure 4.15 shows the improvement to the delamination fatigue resistance for the composites reinforced with the short (2 mm), intermediate (4 mm) or long (8 mm) z-pins. Irrespective of the z-pin length, the delamination fatigue resistance was improved compared to the unpinned laminate. The fatigue curves for the composites reinforced with the short, intermediate and long z-pins were similar, revealing that the mode II fatigue properties are not sensitive to pin length. The z-pins provided the largest improvements to the mode II fatigue resistance at low ($\Delta G_{II} <$ $0.5 \ kJ/m^2$) and high ($\Delta G_{II} > 1 \ kJ/m^2$) cyclic shear conditions. However, over most of the range ($0.5 \ kJ/m^2 < \Delta G_{II} < 1 \ kJ/m^2$), there was only a small improvement in the fatigue resistance with z-pinning. Table 4.4 presents the m_{II} values for the different laminates and there is no clear trend making it difficult to conclude that it was influenced by the z-pin length.

However, the final failure mode of the z-pins was dependent on their length. Figure 4.16 shows the mode II fatigue crack surfaces of the composites reinforced with different z-pin lengths. Fatigue-induced failure of the shortest z-pins occurred mostly by pull-out, with a small proportion of the pins failing by shear rupture. At the intermediate length, most of the z-pins were partially pulled from the composite before failing by shear rupture. At the longest length the z-pins failed by shear rupture along the crack plane, with no pull-out preceding final failure. This transition in the mode II fatigue failure mechanism is attributed to competition that exists between pull-out and rupture of the z-pins. When the z-pins are short, the bonded contact area with the composite is relatively small and therefore interfacial shear stresses generated under cyclic mode II loading high enough to cause debonding followed by pull-out. When the z-pins are long, the large bonded area reduces the magnitude of the interfacial shear stress to a sufficiently low value that pull-out does not occur. Instead, the segment of z-pin bridging the mode II fatigue crack fails by shear rupture. At the intermediate z-pin length, a mixture of pull-out and shear rupture occurs because the fatigue stress to cause debonding and pull-out is similar to the fatigue stress to cause rupture.
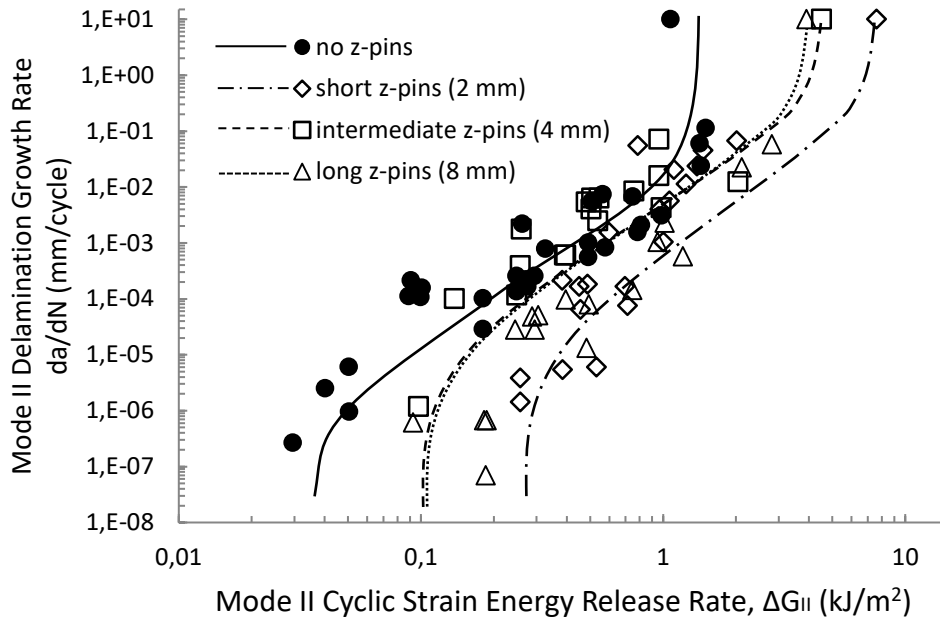
Figure 4.15. Effect of z-pin length on the mode II delamination fatigue resistance. The curves are fitted to the data. The volume content and diameter of z-pins were 2% and 280 μm, respectively, in the z-pinned composites.

Table 4.4 Values for the Paris curve parameter 'm_{II}' for the unpinned and z-pinned composites.

Z-Pin Length	Z-Pin Diameter	Z-Pin Volume Content	m_{II}	Linear Correlation Coefficient (R)
No pins			2.7	0.89
2 mm	280 μm	2.0%	4.3	0.68
4 mm	280 μm	2.0%	4.9	0.91
8 mm	280 μm	2.0%	3.3	0.88
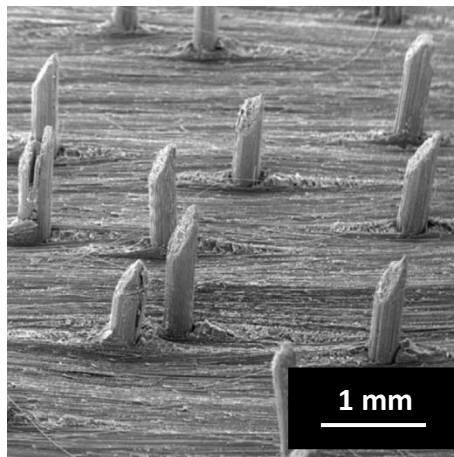
(a)
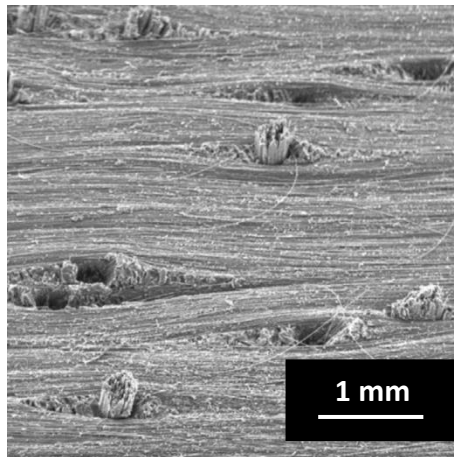
(b)
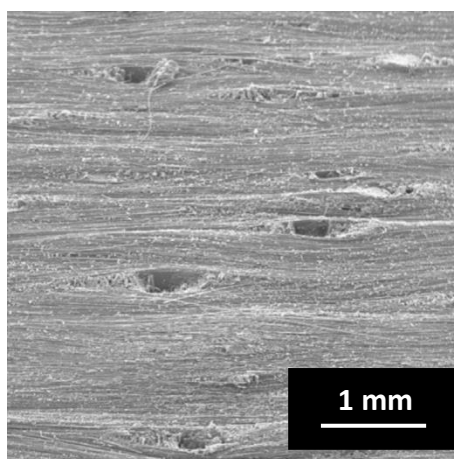
(c)

Figure 4.16. Scanning electron micrographs showing the fatigue crack surface of the composites containing (a) short, (b) intermediate and (c) long z-pins under mode II interlaminar fatigue loading.

4.6   Conclusion

Z-pinning is an effective method for increasing the mode II interlaminar fracture toughness and fatigue resistance of composite materials. The mode II fracture toughness increases with the volume content up to a limiting value. The fracture toughness also increase with the z-pin diameter and when the z-pin length is reduced because of a transition in the fracture mechanisms.

The threshold mode II cyclic strain energy release rate $\Delta G_{II(t)}$ value to initiate the growth of mode II delamination cracks was increased by z-pins. $\Delta G_{II(t)}$ increased with the volume content, diameter and decreasing length of z-pins. Z-pinning also slowed the growth rate of mode II fatigue cracking, particularly at low and high cyclic strain energy release rate values. The maximum mode II interlaminar cyclic stress needed to cause the onset of unstable (rapid) fatigue cracking also increased when the volume content and diameter of z-pins were increased. Z-pins increase the mode II fatigue resistance by generating a large-scale extrinsic bridging zone along the fatigue crack. The carbon fibre z-pins within the bridging zone fail via complex fatigue processes which, in order of increasing crack sliding displacement, involve interfacial debonding, splitting and shear fracture. Z-pins which have completely fractured are still capable of generating shear traction loads via mechanical interlocking.

Chapter 5: Mixed-Mode I/II Delamination Fracture and Fatigue Properties of Z-pinned Composites

5.1 Abstract

This chapter presents an experimental investigation into the mixed-mode I/II interlaminar fracture toughness and fatigue resistant properties of carbon fibre–epoxy laminate reinforced with z-pins. The effects of the G_I-to-G_{II} ratio on the delamination fracture toughening and fatigue strengthening mechanisms of z-pins are also investigated. Previous studies (including this PhD project) have showed that the fracture toughness and fatigue resistance are increased by z-pins under mode I and mode II static and cyclic loadings, although z-pins are more effective under mode I. The research presented in this chapter proves that the fracture toughness and fatigue resistance of z-pinned laminates both increase with increasing mode I component of mixed-mode loading, and this is due to a transition in the toughening mechanisms from shear deformation (typical of mode II loading) to pull-out (typical of mode I loading) of the z-pins.

5.2 Introduction

This PhD project and other studies have shown that there are a large number of parameters that affect the capacity of z-pins to improve the delamination toughness and fatigue strength of composite laminates. The effect of parameters such as the volume content, length and diameter of z-pins on the fracture toughness have been experimentally and analytically investigated under mode I and II loads [22-24, 26, 28, 30, 31, 34, 36, 44]. The results in chapters 3 and 4 have proven that the mode II fracture toughness, fatigue properties and interlaminar strengthening mechanisms are controlled by volume content, diameter, length and material properties of the z-pins. However, the percentage of improvement is usually less for mode II compared to mode I loading [15, 34], and this is due to z-pins generating higher traction loads in mode I.

As reported in Chapter 2, z-pins increase the fracture toughness of composites under mixed-mode I/II interlaminar loads [25, 32, 49, 106, 107]. Rugg et al. [25] investigated the mixed-mode delamination behaviour of carbon-epoxy laminates reinforced with z-pins made of titanium or composite. They showed that a low z-pin content (1.5 vol%) was sufficient to increase the toughness by up to a factor of three. Rugg and colleagues also showed that z-pins improved the ultimate failure load of T-joints by up to 40% when subjected to mixed-mode loading, although the percentage improvement depends on the test configuration.

There is a transition in the crack toughening and failure mechanisms of z-pins depending on the interlaminar loading mode. Yasaee et al. [106] experimentally determined the effect of load angle on the fracture load for composite blocks reinforced with a single carbon fibre z-pin. They observed a change in the z-pin failure mechanism when transitioning from pure mode I (which involved debonding and pull-out) to mode II (which involved shear failure). Due to experimental difficulties however, it was not possible to measure the amount of absorbed strain energy for the different loading modes. Allegri et al. [108] extended the experimental study by Yasaee et al. [106] by modelling the deformation and failure mode of z-pins when analysed as single beams undergoing small and finite rotations by elastic deformation. Zhang et al. [107] developed a three-dimensional finite element model to analyse the mixed-mode I/II response of a z-pin embedded in a laminate. The model takes into account the microstructure of z-pinned composites, and is able to compute the bridging forces of a z-pin during debonding, pull-out and shear fracture. Apart from these studies, the interlaminar fracture toughness properties and toughening mechanisms of z-pinned laminates under mixed-mode interlaminar loads have not been extensively studied. Also, there has been no study into the delamination fatigue properties of z-pinned laminates under mixed-mode loading.

Presented in this chapter is an experimental study that aims to determine the effect of the mixed-mode I/II loading on the fracture toughness, fatigue properties and delamination strengthening mechanisms of z-pinned laminates. The effect of progressively increasing the percentage of mode I loading from 0% (pure mode II), 25%, 50%, 75% and 100% (pure mode I) on the fracture and fatigue properties of a laminate reinforced with carbon fibre z-pins is determined, and compared to the mixed-mode properties of an unpinned composite.

5.3   Materials

The unpinned and z-pinned laminates used in this study were manufactured using unidirectional T700 carbon fibre-epoxy resin prepreg tape (VTM264 supplied by Advanced Composites). The plies were stacked in a $[0_6/[90/0]_2]_s$ configuration to a thickness of 4 mm. The prepreg plies were then z-pinned in the through-thickness direction using the ultrasonically-assisted pinning (UAZ) process, which is described in Chapter 3. The laminate was z-pinned using the thin (0.28 mm diameter) carbon fibre rods to a volume content of 2%. The unpinned and z-pinned laminates were cured and consolidated under the conditions described in section 3.3.1. The composites were made into delamination test coupons with the dimensions given in Figure 5.1.
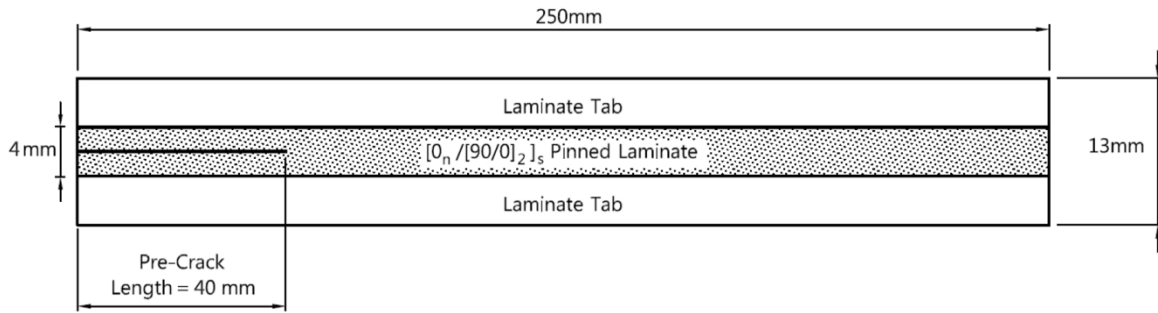
Figure 5.1. Schematic of the mixed mode-bending (MMB) z-pinned sample. The sample was 25 mm wide.

5.4   Mixed-Mode I/II Interlaminar Fracture Toughness and Fatigue Testing

The unpinned and z-pinned laminates were tested using the Mixed Mode Bending (MMB) fixture shown in Figure 5.2. Tests were conducted using the experimental procedure specified in ASTM standard D6671/D6671M–06 [109]. The base of the MMB fixture supports the test specimen while the upper lever is loaded. The lever pin acts as a fulcrum which applies a downward force at the mid-length of the MMB sample, and this induces a mode II-like interlaminar stress at the crack tip while the rotation of the lever induces a mode I opening displacement at the pre-cracked end of the MMB sample. The length of the lever arm (c) was varied to achieve different mixed $G_I - G_{II}$ mode ratios, which in this study were 0 (pure mode II), 0.25, 0.5, 0.75 and 1 (pure mode I).

(a)
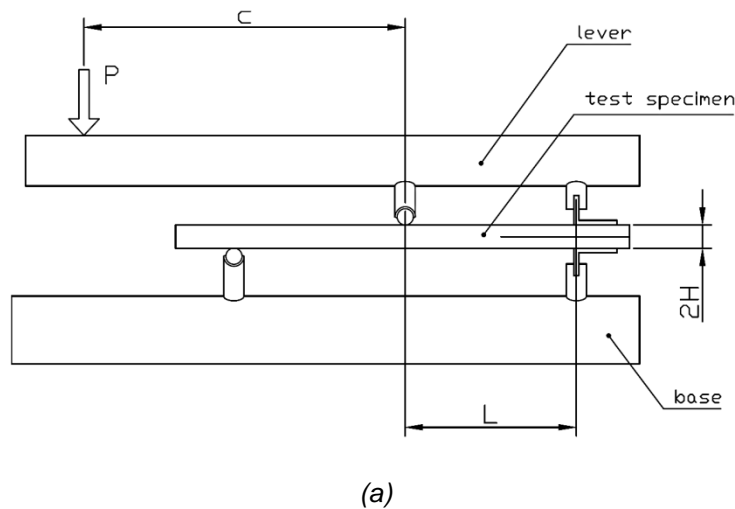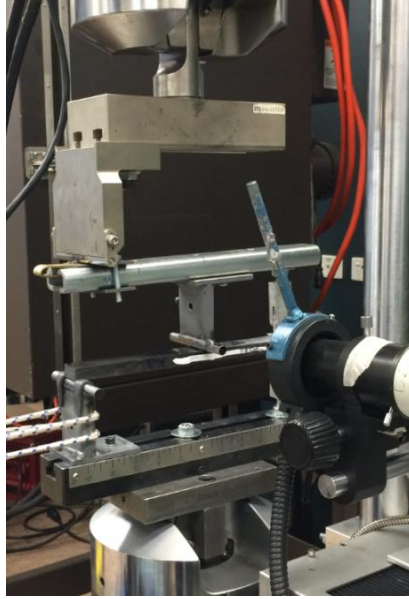
(b)

Figure 5.2. (a) Schematic and (b) photograph of the mixed mode I/II bending test apparatus.

The interlaminar strain energy release rate was measured by applying a monotonically increasing displacement at the lever at a constant rate of 2 mm/min to the MMB sample. The delamination crack was allowed to propagate at short intervals (3 to 5 mm) from the pre-crack along the sample mid-plane, and at each increment the values for crack length and load were recorded. These values were used to calculate the total mixed-mode strain energy release rate using:

$$G_{tot} = G_I + G_{II} \tag{5.1}$$

where G_I is the mode I component of strain energy release rate:

$$G_I = \frac{12P^2(3c-L)^2}{16b^2h^3L^2E_{11}} \tag{5.2}$$

and G_{II} is the mode II component of strain energy release rate:

$$G_{II} = \frac{9P^2(c+L)^2}{16b^2h^3L^2E_{11}} \tag{5.3}$$

P is the applied load. b, h and L are width, half-thickness and half-span length of the MMB sample, respectively. c is the distance between the mid-length of the sample and the loading point of the lever.

The mixed-mode interlaminar fatigue resistance was determined by applying cyclic loads to the MMB sample at a frequency of 10 Hz and R ratio of 0.1, which is the ratio between the minimum and maximum displacements in one load cycle. The fatigue crack was allowed to propagate for short intervals, and at each increment the test was stopped and the load and crack length were measured. The total cyclic strain energy release rate was calculated using:

$$\Delta G_{tot} = G_{tot\ max} - G_{tot\ min} \tag{5.4}$$

where

$$G_{tot\ max} = G_{I\ max} + G_{II\ max} \tag{5.5}$$

and

$$G_{tot\ min} = G_{I\ min} + G_{II\ min} \tag{5.6}$$

Values for the cyclic range of the strain energy release rate were increased from a very low value for which there was no crack growth (below the threshold strain energy release rate for crack growth) up to values for which fast (unstable) crack growth was observed. da/dN values were measured over about 8 orders of magnitude (from 10^{-7} to 10 mm of crack growth per cycle), and plotted as a Paris-like curve.

5.5   Failure Analysis Inspection

Scanning electron microscope (described in section 3.3.4) and X-ray computed tomography (Figure 5.3) were used to analyse the delamination and strengthening mechanisms of the z-pinned laminate following mixed-mode delamination testing. X-ray CT analysis was performed by digitally processing 2000 cross-section images per round angle. Each of the 2000 photographs (333 ms of time exposure) were obtained from a set of five images in total; two of which were discarded. The three remaining images were digitally averaged and used to generate a three-dimensional reconstruction of the MMB coupon. To obtain penetration of the X-rays through the

laminate to the detector, the machine was operated at 40 kV and 140 µA for the beam voltage and current, respectively. The resolution of the CT digital images was about 15 µm.

Figure 5.3. GE Phoenix v/tome/x X-ray CT machine.

5.6   Results and Discussion

Figure 5.4 shows the effect of the mixed-mode I/II ratio on the *R*-curves for the unpinned and z-pinned laminates tested at 100% mode I or mode II loading. Irrespective of whether the unpinned laminate was loaded in mode I or II, the R-curves were flat and within a short crack length (<10 mm) reached the steady-state fracture toughness value. This occurs because there was no significant fibre bridging along the mode I or II delamination cracks. There was only a small difference between the fracture toughness values for the unpinned laminate loaded under mode I and mode II. Because the mode II *R*-curve was only slightly higher than the mode I curve, mixed-mode I/II loading is expected to result in *R*-curves between the pure mode I and II curves with very little difference in the fracture toughness values. For this reason, the unpinned laminate was not tested under mixed-mode loading.

Figure 5.4 shows that the *R*-curve for the z-pinned laminate increased rapidly with an increasing component of mode I loading. Figure 5.5 shows a plot of the mode I/II ratio on the steady-state interlaminar fracture toughness (G_c) of the z-pinned laminate. The delamination resistance increases with the proportion of mode I loading up to $\sim$ 50%, above which there is no significant further increases in toughness.
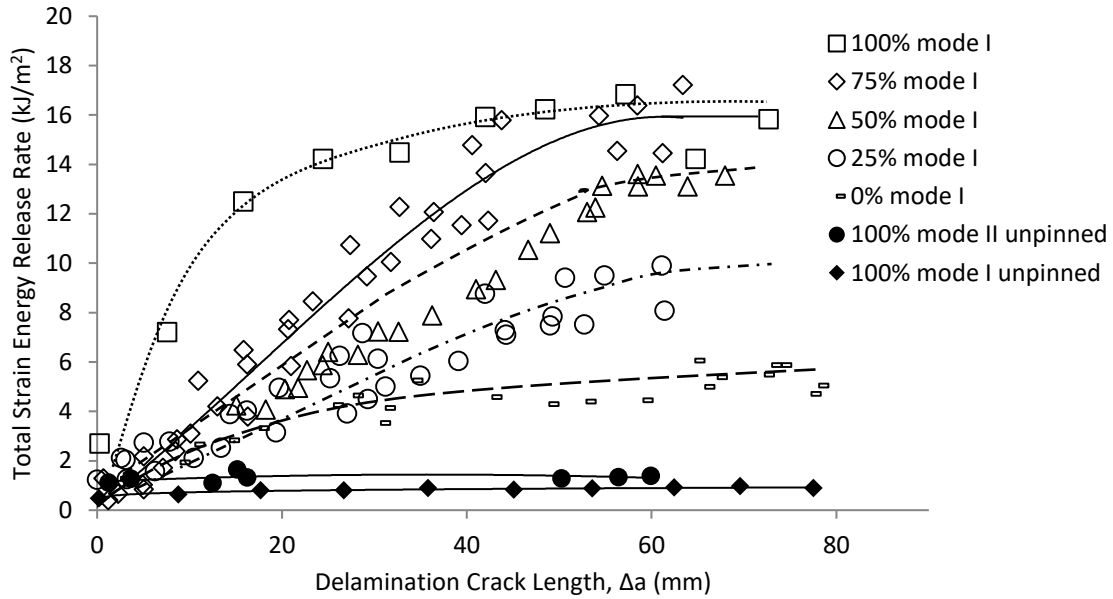
Figure 5.4. Effect of mixed-mode I/II ratio on the R-curves for the z-pinned (open data points) laminate and 100% mode I and mode II of the unpinned laminate.
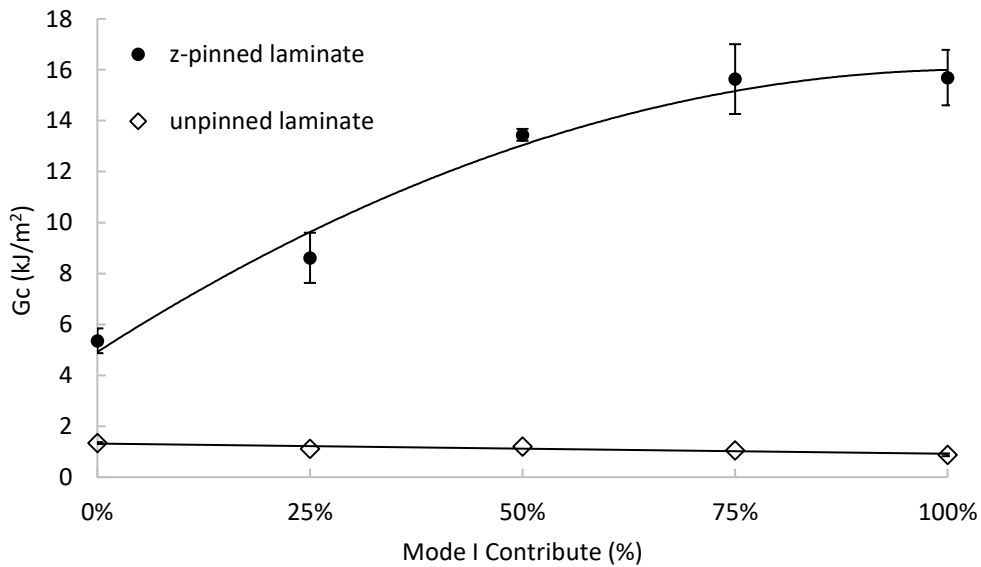
Figure 5.5. Effect of the mixed-mode I/II ratio on the steady-state interlaminar fracture toughness for the z-pinned laminate.The error bars indicate one standard deviation.

There is a change in the z-pin toughening mechanism when transitioning from pure mode I to mode II loading, as shown in Figure 5.6. Previous studies have shown that z-pins, when subjected to mode I loading, debond and then pull-out from the laminate [28]. This PhD project and other studies have shown that z-pins experience shear failure under pure mode II loading, with no pull-

out (unless the pin is very short). A combination of the mode I and mode II failure mechanisms was observed when applying mixed loading conditions. The MMB samples loaded with a mode I contribution of 50% and 75% experienced partial pull-out and shear failure of the z-pins (Figure 5.6). When loaded with 25% mode I the z-pins mostly failed by shear fracture.
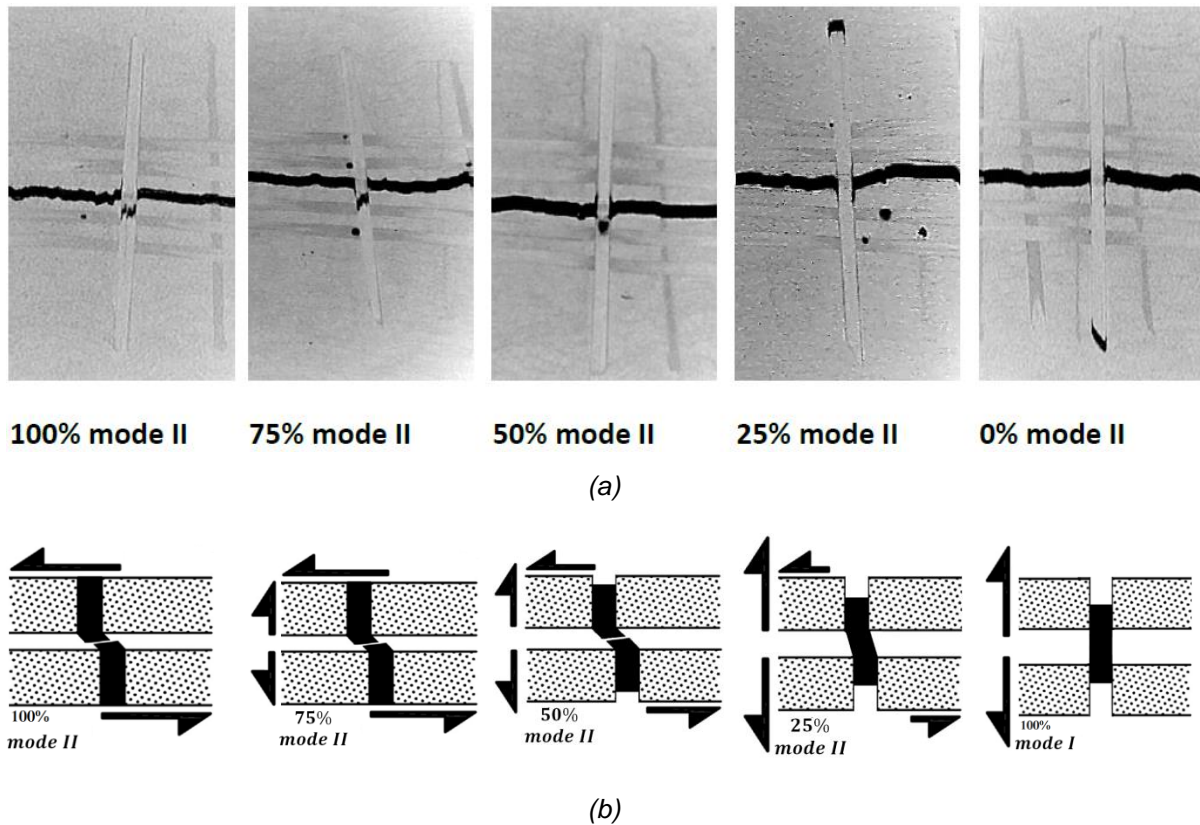
Figure 5.6. (a) Cross-section X-ray CT photographs and (b) schematic representations of the failure of a z-pin under different mixed mode ratios.

The Paris curves for the unpinned and z-pinned laminates for different mixed-mode I/II loads are presented in Figure 5.7. The crack growth rate per cycle (da/dN) is plotted against the cyclic strain energy release rate range (ΔG). As reported earlier, there is large scatter in the curves for both the z-pinned and unpinned laminates, and this is due to the stick-slip nature of the fatigue cracking process as well as difficulties in identifying the exact location of the crack tip. Despite the large scatter, Figure 5.7 shows that increasing the mode I component increases the fatigue resistance of the unpinned laminate over the entire range of stress intensity values. However, for high ΔG values the difference is negligible for the unpinned laminate, and this is consistent with the fracture toughness properties which are similar for mode I and mode II.

Due to large scatter the crack initiation strain energy release rate value (ΔG_i) was taken at a cyclic growth rate of 10^{-7} mm/cycle. Using this value to define the crack initiation, then the threshold value to initiate fatigue crack growth in the pinned laminate was increased about five times from 0% to 100% mode I component. Table 5.1 gives the values for the Paris curve parameter $m_{I/II}$, for the unpinned laminate. Although the $m_{I/II}$ values are generally lower for the pure mode II compared to the pure mode I, there is no clear trend when transitioning through different mixed-mode I/II ratios.
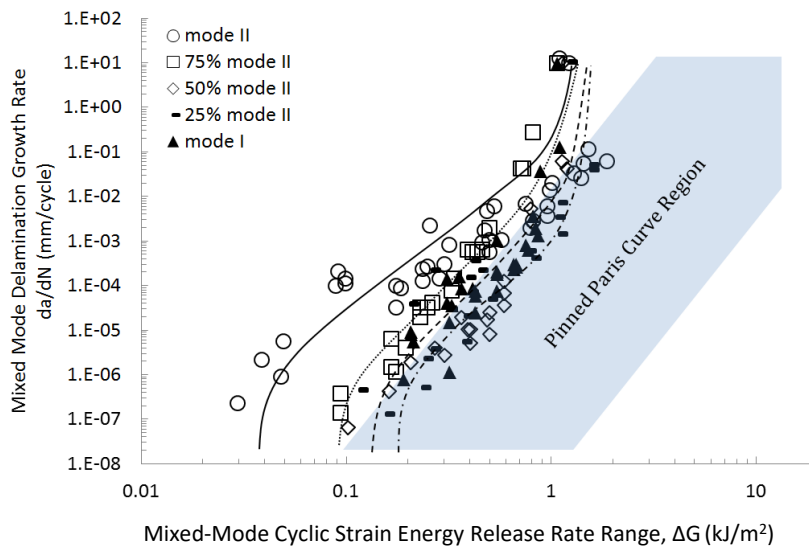
(a)
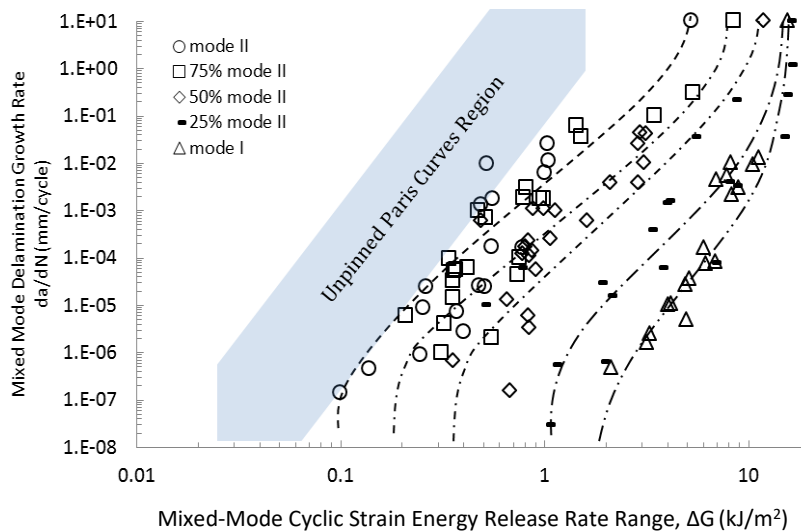
(b)

Figure 5.7. Paris curves showing the effect of the mixed-mode ratio on the delamination fatigue resistance for the (a) unpinned and (b) z-pinned composites.

Table 5.1. Values for the cyclic strain energy release rate to initiate crack growth (ΔG), and Paris curve parameter $m_{I/II}$ for the unpinned and z-pinned laminates. The linear correlation coefficient (R) for the $m_{I/II}$ value is also given.

Mode I Portion	Unpinned Laminate			Z-Pinned Laminate		
	ΔG_i $[kJ/m^2]$	$m_{I/II}$	Linear Correlation Coefficient (R)	ΔG_i $[kJ/m^2]$	$m_{I/II}$	Linear Correlation Coefficient (R)
0%	0.03	2.7	0.89	0.52	4.9	0.91
25%	0.1	5.9	0.97	0.42	4.7	0.68
50%	0.13	5.5	0.87	0.49	4.3	0.66
75%	0.16	4.4	0.84	1.03	5.1	0.81
100%	0.15	6.7	0.81	2.5	8.4	0.88

Z-pins are highly effective at improving the delamination fatigue resistance under the different mixed-mode loading conditions. Z-pins increase the threshold cyclic strain energy release rate range to initiate crack growth (Table 5.1). The fatigue resistance increased with increasing mode I loading component, and this is due to a transition in the fatigue strengthening mechanisms. Figure 5.8 shows cross sectional views of a z-pin bridging the fatigue delamination crack for 100% mode II, 50% mode I-50% mode and 100% mode I. The z-pins experienced shear failure for pure mode II loading. Under mode I, the pins debonded and pulled-out from the laminate. Under mixed-mode fatigue loading (G$_I$/G$_{II}$ = 50%), the pins experienced debonding and fracture. The transition in the bridging traction properties due to changes in the bridging mechanism of the z-pins accounts for the increasing efficiency of the z-pins to improve the fatigue resistance when the mode I cyclic load component becomes larger.

(a)   (b)   (c)
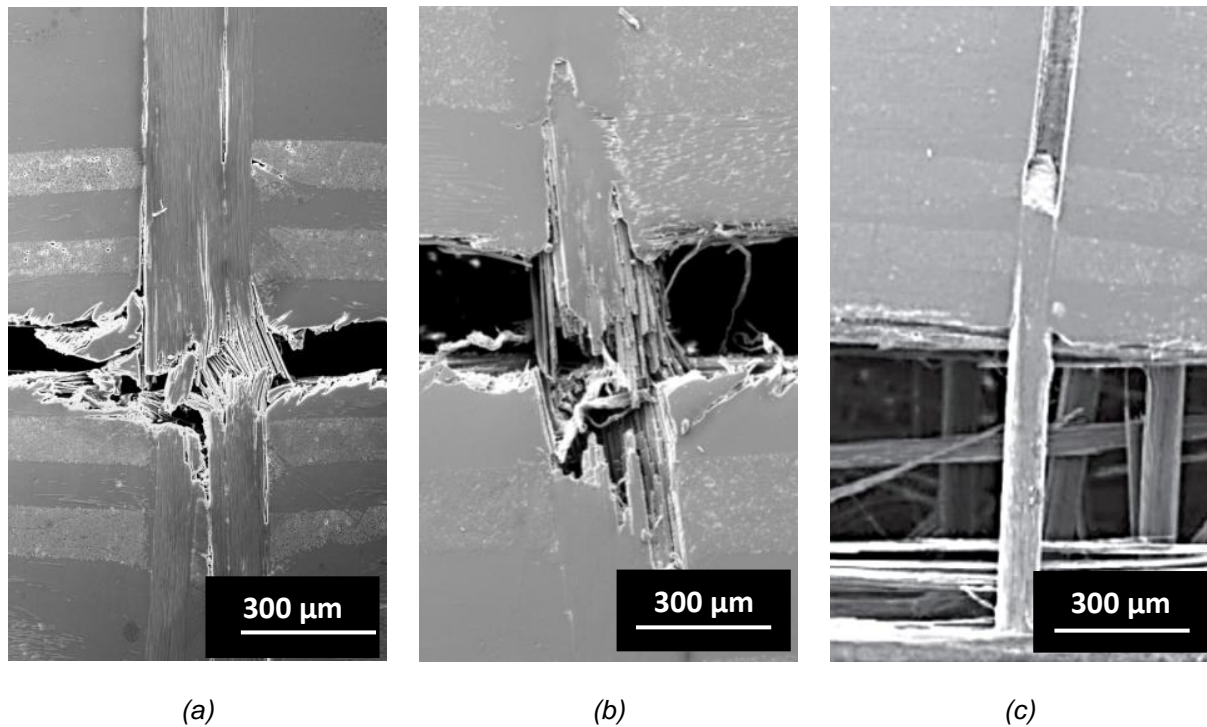
Figure 5.8. Cross-sectional views of a z-pin bridgning the delamination fatigue crack under (a) 100% mode II, (b) mixed mode I/II = 0.5 and (c) 100% mode I cyclic loading conditions.

5.7   Conclusion

Previous research has shown that z-pins improve the mode I and mode II delamination toughness and delamination fatigue resistance of laminates. The amount of improvement is controlled from several parameters such as volume content, length, diameter and material properties of z-pins. The study reported in this chapter has proven that the interlaminar fracture toughness and fatigue resistant properties of z-pinned laminates also depend on the mixed-mode I/II ratio. Z-pins are more effective under mode I than mode II because of their ability to generate higher traction energy associated with pull-out, caused by high friction forces as the pin slides against the laminate. When increasing the mode I component, both the delamination toughness and fatigue resistance were improved, and this was due to a transition in the toughening mechanisms.

Chapter 6:   Impact Damage Tolerance of Z-pinned Laminates

6.1   Abstract

This chapter presents an experimental investigation into the impact damage resistance and compressive properties of carbon fibre reinforced epoxy laminates reinforced with z-pins. The effects of z-pin material and length on the barely visible impact damage response and compressive properties (pre- and post-impact) of a cross-ply carbon-epoxy laminate was evaluated. Impact tests were performed on composite coupons at different incident energy levels (10 to 60 J), depending on the laminate thickness. C-scan ultrasonic and X-ray computed tomography revealed that the impact loading resulted in barely visible damage consisting of multiple delamination and matrix cracks together with back-face splitting to the unpinned laminate and different types of z-pinned composites. The amount of impact-induced delamination damage to the composite was reduced by z-pinning. The percentage reduction to the impact damage due to z-pins increases with the impact energy due to the development of a larger-scale crack bridging zone. The impact damage resistance was similar (within 10%) for the different metals used for the z-pins, although the carbon fibre z-pins were the most effective.

Pre-impact compression testing revealed the z-pins did not change significantly the compressive modulus, although the strength is reduced by about 5 to 15% because of fibre waviness induced by the z-pins. The post-impact compressive strength of the z-pinned laminates was higher (about 20%) than the unpinned material, and this was due to the z-pins reducing the impact damage area. Pre- and post-impact compressive properties were similar for the different materials used for the z-pins.

6.2   Introduction

A large body of experimental and numerical research has led to a thorough understanding of the delamination properties and interlaminar toughening mechanisms of z-pinned laminates for the modes I, II and mixed I/II loading conditions, and this was reviewed and described in the previous chapters. As a consequence, z-pins can reduce the amount of delamination damage caused by impact events from low energy objects, ballistic projectiles and large hailstones [27, 43, 56, 110, 111]. The improved impact damage resistance gained with z-pins results in higher post-impact in-plane compressive properties compared to unpinned laminates [27, 58, 110]. For these

reasons, z-pinning is a promising technology for increasing the impact damage resistance and damage tolerance of aircraft composite structures. Zhang et al [54] found that the damage area caused by an impact event was reduced up to 64% by z-pins, depending on the impact energy and laminate thickness. A similar improvement (up to 50%) was measured by Childress and Freitas [112]. The improvements to the impact damage resistance is due to z-pins forming a large-scale bridging zone which increases the delamination toughness. However, z-pins are ineffective at increasing the threshold energy necessary to initiate the damage because of their inability to impede short delamination crack growth (below 5-to-10 mm) [113, 114].

Due to fibre waviness caused by z-pin insertion, z-pinned laminates have reduced in-plane compression modulus and strength (although the loss is usually below 10%) [44, 64-66]. The post-impact compressive strength is usually higher for z-pinned laminates, and this is due to the reduced impact damage area compared to the unpinned laminate and higher buckling resistance due to z-pins resisting opening displacement between plies [58, 110].

This research chapter aims to investigate the effects of the material and length of z-pins on the impact resistance and post-impact compression properties of carbon-epoxy laminates.

6.3 Composite Material

Unpinned and z-pinned composite specimens were manufactured to different thicknesses using unidirectional T700 carbon fibre-epoxy prepreg tape. The laminates were stacked in $[0/90]_{3s}$, $[0/90]_{5s}$ or $[0/90]_{9s}$ ply pattern to obtain a thickness of 2, 4 or 7 mm, respectively. The laminates were then reinforced with carbon fibre z-pins to a volume content of 2% and diameter of 510 µm, as reported in Table 6.1. The only difference between the composites was the embedded length of the z-pins; all other z-pin parameters such as diameter (510 µm) and volume content (2%) were fixed.

The effect of the z-pin material was investigated for 4 mm thick laminates. The z-pins were made of carbon fibre composite, stainless steel, titanium or copper (see Chapter 3 for the material properties). The z-pins were inserted in a 60 mm x 100 mm sized central region of the laminate coupon (as indicated in Figure 6.1) using the insertion processes described in Section 3.3. By z-pinning completely across the width of the composite coupon, a centre-symmetric loading condition was achieved. Carbon-epoxy laminates without z-pins were also manufactured so that the improvement due to z-pins could be assessed. The unpinned and z-pinned laminates were

cured within an autoclave at 120°C and 620 kPa. Samples were subsequentially cut to the dimensions of 100 mm wide x 150 mm long (Figure 6.1).

Table 6.1. Composite samples used in the experimental work.

Effect of Z-Pin Length		
Z-Pin Length	Z-Pin Diameter	Z-Pin Volume Content
no pins	no pins	no pins
2 mm	510 µm	2.0%
4 mm	510 µm	2.0%
7 mm	510 µm	2.0%
Effect of Z-Pin Material (4 mm length)		
Z-Pin Material	Z-Pin Diameter	Z-Pin Volume Content
no pins	no pins	no pins
carbon fibre	510 µm	2.0%
stainless steel	510 µm	2.0%
titanium	510 µm	2.0%
copper	510 µm	2.0%
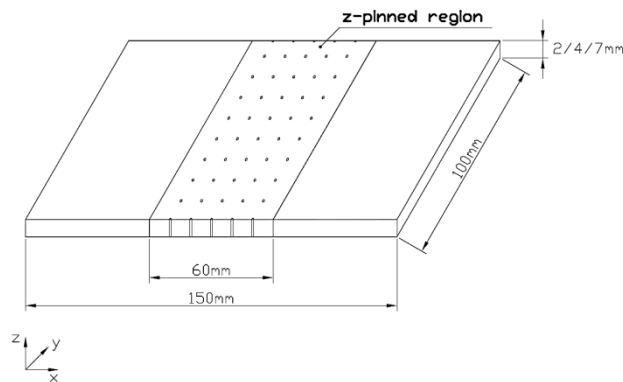
Figure 6.1. Schematic of the z-pinned samples used for impact testing.

6.4 Research Methodology

Barely visible impact tests were performed on the unpinned and z-pinned laminates using the instrument shown in Figure 6.2 and under the conditions illustrated in Figure 6.3. The samples were supported along their edges using clamps. All tests were performed using a 12 mm hemispherical hardened steel impactor which weighed 3.8 kg. The impactor was dropped (free-fall) from different heights on to the center of the coupon (Figure 6.3). The impactor was instrumented with a dynamic force transducer to measure the impulse force-time response

during contact with the coupon. The impulse force was measured at a sampling rate of 19.2 kHz. Three samples for each combination of material and impact energy were tested.

Following impact, the laminates were visually and ultrasonically inspected to determine the type and measure the damaged area caused by the impact. The unpinned and z-pinned laminate coupons were inspected before and after impact testing with through-thickness (C-scan) ultrasonics using a Omniscan MXU-M instrument (Figure 6.4). A 5 MHz ultrasonic transducer (Model 5L-64-NW1) was used. All inspections were performed on the impacted surface of the coupon using a gain of 5, 10 and 12 dB for the 2, 4 and 7 mm thick samples, respectively.

The pre- and post-impact compressive strengths of the unpinned and z-pinned laminates were measured using the Airbus compression test method (AITM1-0100). The coupons were compressed along the 0° fibre direction at an end-shortening rate of 0.5 mm/min until failure. The ends of the coupon were clamped whereas the sides were laterally supported using anti-buckling guides, as shown in Figure 6.5. Three samples of the unpinned laminate and the different types of z-pinned composites were compression tested.
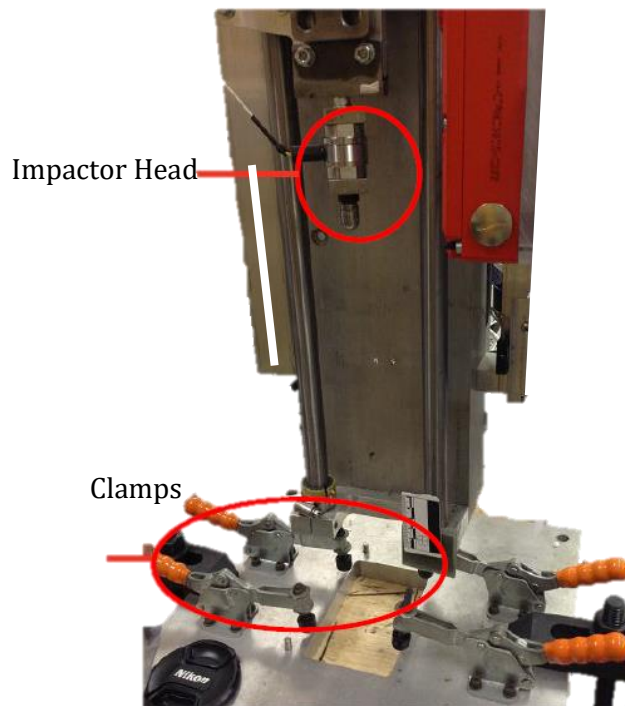
Figure 6.2. Facility used for impact testing the unpinned and z-pinned laminate coupons.
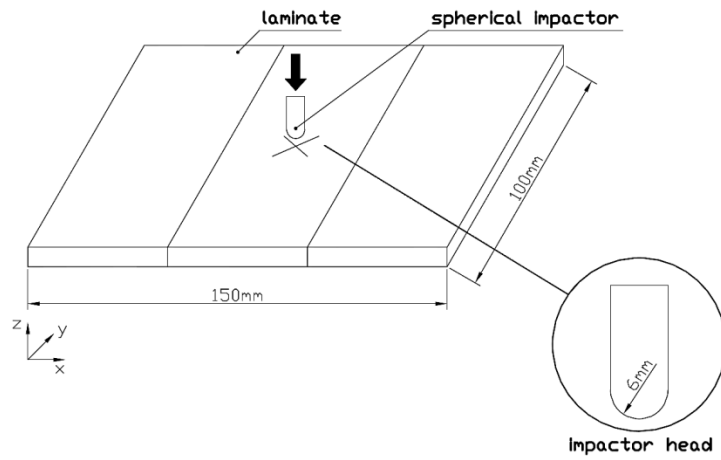
Figure 6.3. Schematic representation of the impact test.
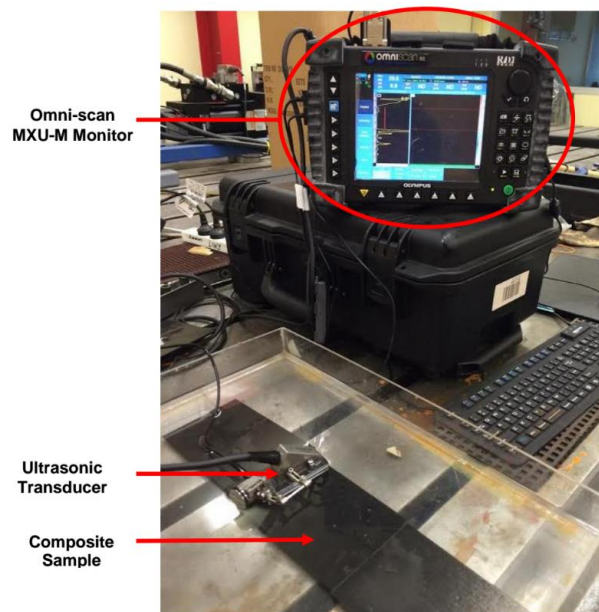
Figure 6.4. Omniscan MXU-M instrument used for C-scan ultrasonic inspections of composite coupons.
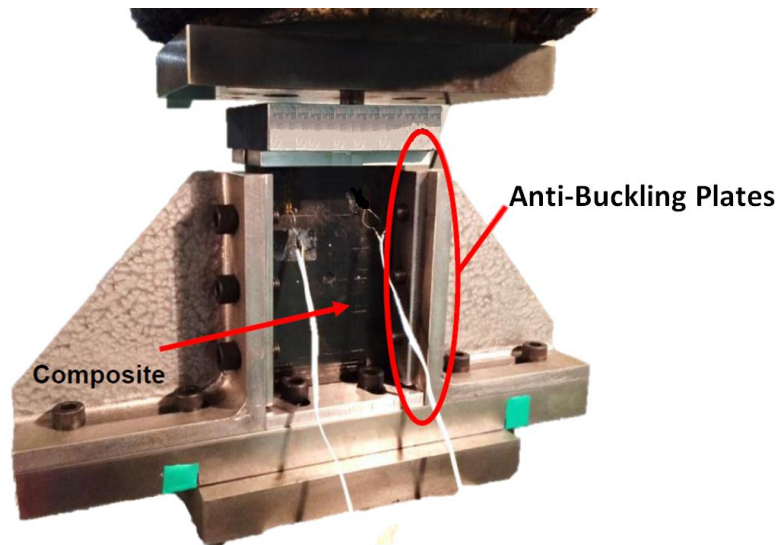
Figure 6.5. Compression test set-up for the laminate coupons.

6.5   Results and Discussion

6.5.1 Impact damage resistance

Figure 6.6 compares the impulse force-time curves measured for the unpinned and different types of z-pinned composites with different thicknesses. The curves were similar in profile for the different z-pin materials, and so only profiles for the carbon fibre pins are shown. The oscillations in the curves are due to a combination of load drops caused by damage within the composite and vibrations (dynamic stress waves) within the impactor. The amplitude of the oscillations was significantly larger for the unpinned laminates and this possibly indicates more damage growth. It was found that the maximum load recorded was slightly higher for the z-pinned laminates. This is possibly because of the reduced impact damage which limited the loss in compliance.
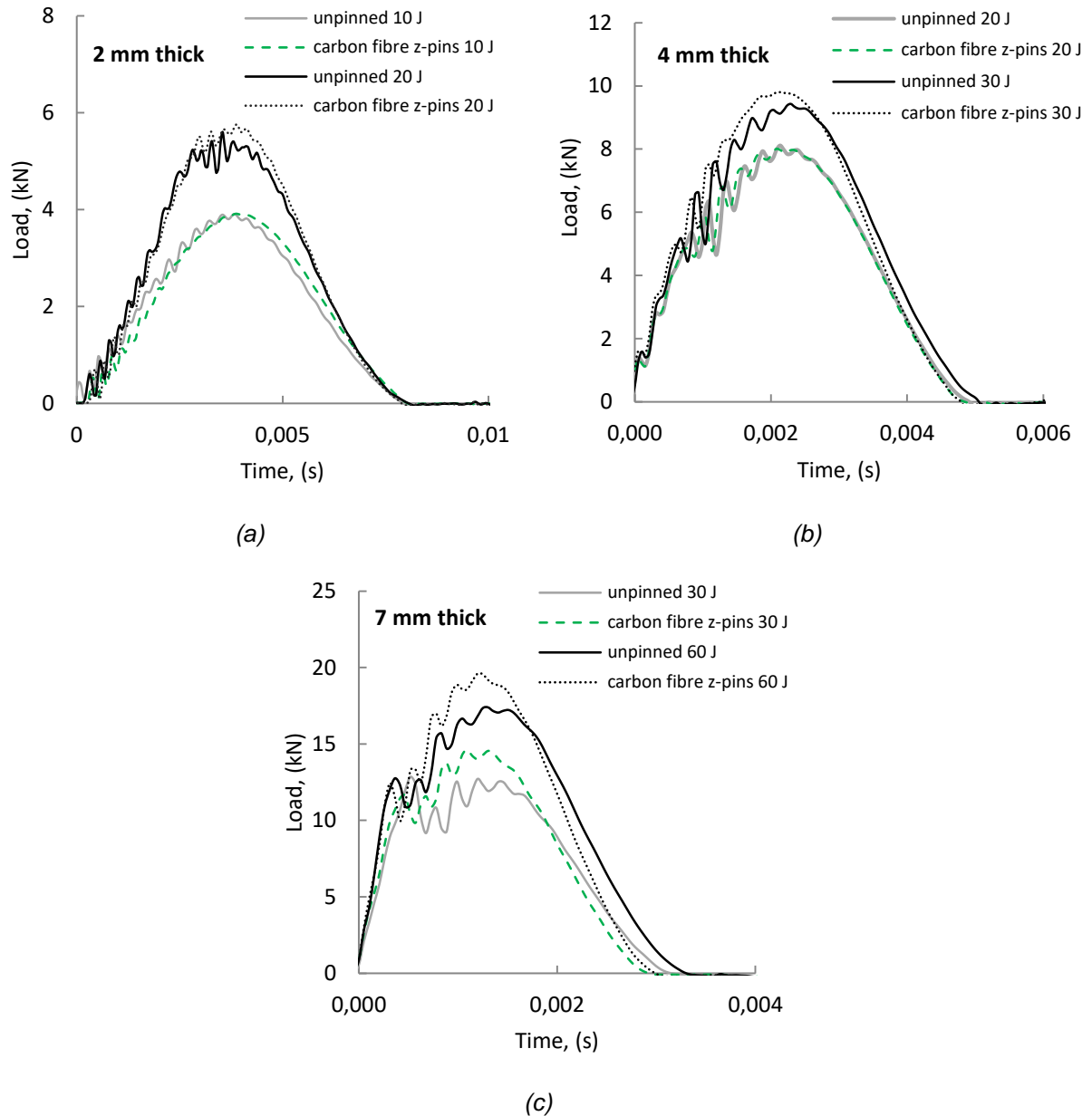
Figure 6.6. Effect of impact energy on the impulse load-time response of the (a) 2 mm, (b) 4 mm, and (c) 7 mm thick unpinned and z-pinned laminates.

6.5.2 Impact damage resistance of z-pinned laminates

Following impact testing, the unpinned and z-pinned laminate coupons were inspected visually as well as using through-transmission ultrasonics and X-ray computed tomography. Visually, the front of the composites (impacted side) had a shallow dent where the impactor locally crushed the surface. The back surface showed longitudinal splitting cracks which was aligned in the 0° fibre direction. These damage features were observed for the unpinned and different types of z-pinned composites. C-scan images of the unpinned laminate and one of the z-pinned composites

are presented in Figure 6.7. The delamination damage is characterised by a quatrefoil shape with the four lobs oriented along the 0° and 90° fibre directions. This shape is attributed to the cross-ply (0°/90°) fibre orientation of the laminates. Figure 6.8 shows the typical damage propagation in the 2, 4 and 7 mm thick z-pinned laminates. Thin samples, which experience large bending deflection during impact, experienced matrix cracking and laminate splitting near the back (opposite the impact side). With the thicker samples (above 4 mm), the impact induces higher localised shear stresses which cause fibre failure surrounding the impact location.

(a)   *(b)*
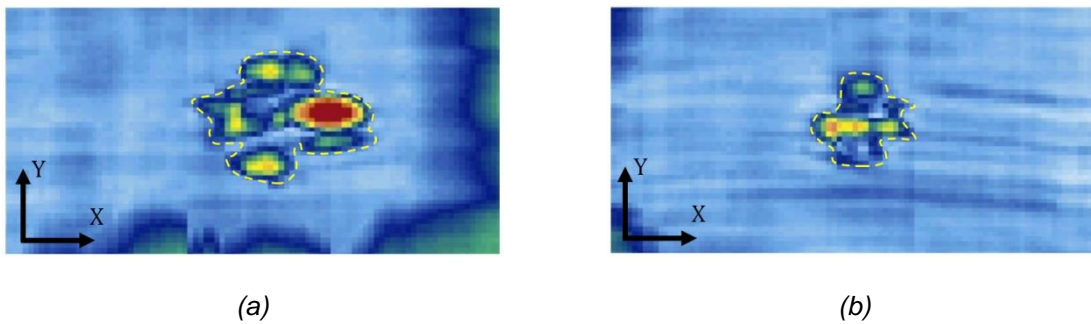
Figure 6.7. C-scan ultrasound images of impacted (a) unpinned and (b) z-pinned laminates. The z-pinned sample was reinforced with the carbon fibre pins. Both samples were 4 mm thick and impacted at an incident energy of 30 J.

(a)

(b)

118
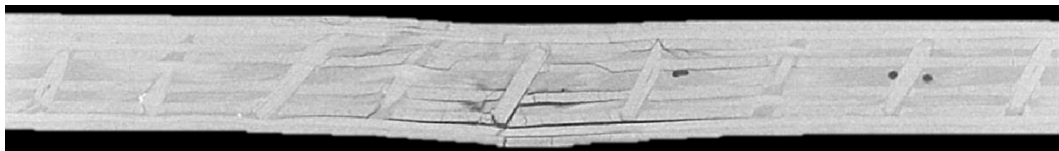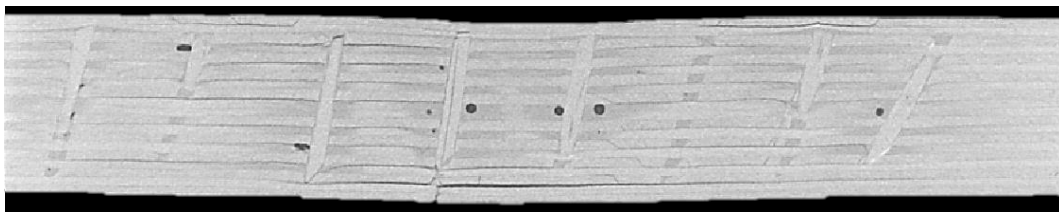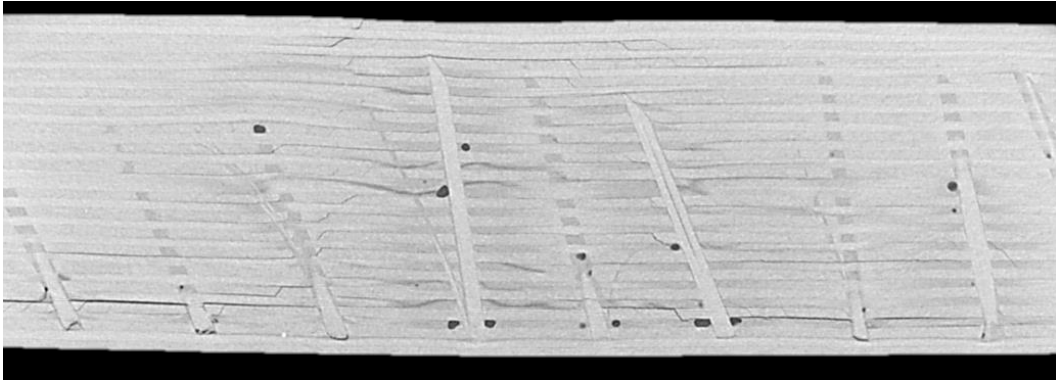
(c)

Figure 6.8. Cross-sectional X-ray CT images showing the effect of the laminate thickness on damage to the (a) 2 mm, (b) 4 mm and (c) 7 mm thick z-pinned laminates. 2, 4 and 7 mm thick coupons were impacted at an incident energy of 20, 30 and 60 J, respectively.

Figure 6.9 show the effect of incident impact energy on the delamination damage area for the unpinned and z-pinned laminates. The area was measured from C-scan ultrasound images using raster graphics editor software. The z-pins reduced significantly the impact damage area, irrespective of their material properties and length. It was found that the percentage reduction in the damage size due to z-pinning increases with the impact energy. This is due to the development of a large-scale bridging zone by the z-pins which increases the delamination fracture toughness. As observed by Isa et al. [110], z-pins do not provide benefits at low impact energies because the delamination cracks are too short for the pins to form a large-scale bridging zone. Indeed, the 2 mm thick laminate reinforced with carbon fibre z-pins and impacted at 10 J showed a similar amount of damage to the 2 mm thick unpinned laminate. However, higher damage resistance occurred with the z-pinned laminate at the higher impact energy (20 J). The largest improvement in damage resistance was achieved using 4 mm long z-pins (Figure 6.9b), with a reduction of ~55% to the damage area. The results in Figure 6.9b also show that, z-pin influenced the impact damage resistance. The improvement to the impact damage resistance correlated with the increase in the interlaminar toughening effect of the z-pins, which was lowest for copper, similar for stainless steel and titanium, and best for carbon fibre.

During impact loading the z-pins are elastically deformed, partially or completed debonded from the surrounding composite material, and may experience partial pull-out and deform in shear during delamination cracking (Figure 6.8). Numerous studies have shown that these crack

bridging processes of the z-pins generate high traction loads and absorb a large amount of energy [29, 33, 36, 41].

(a)

(b)

(c)
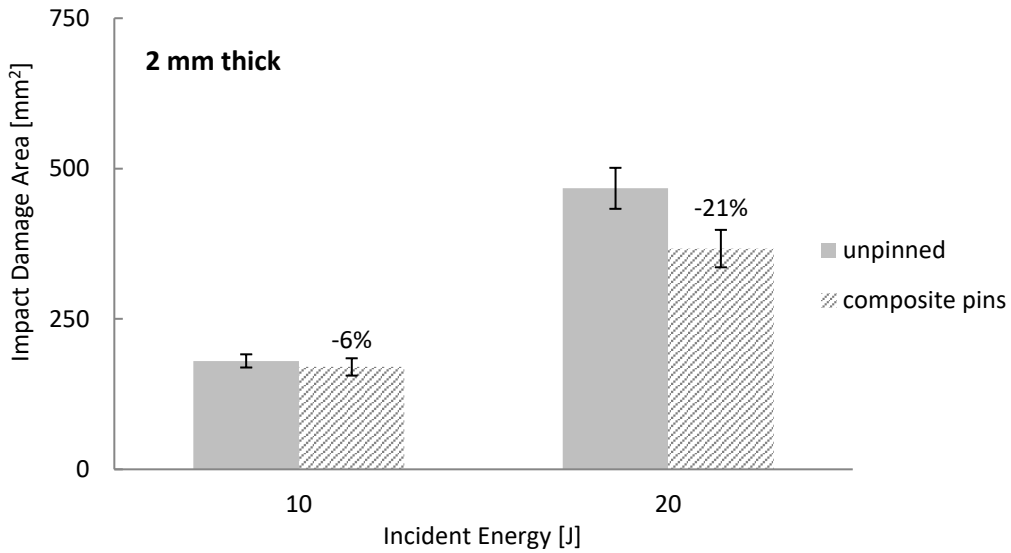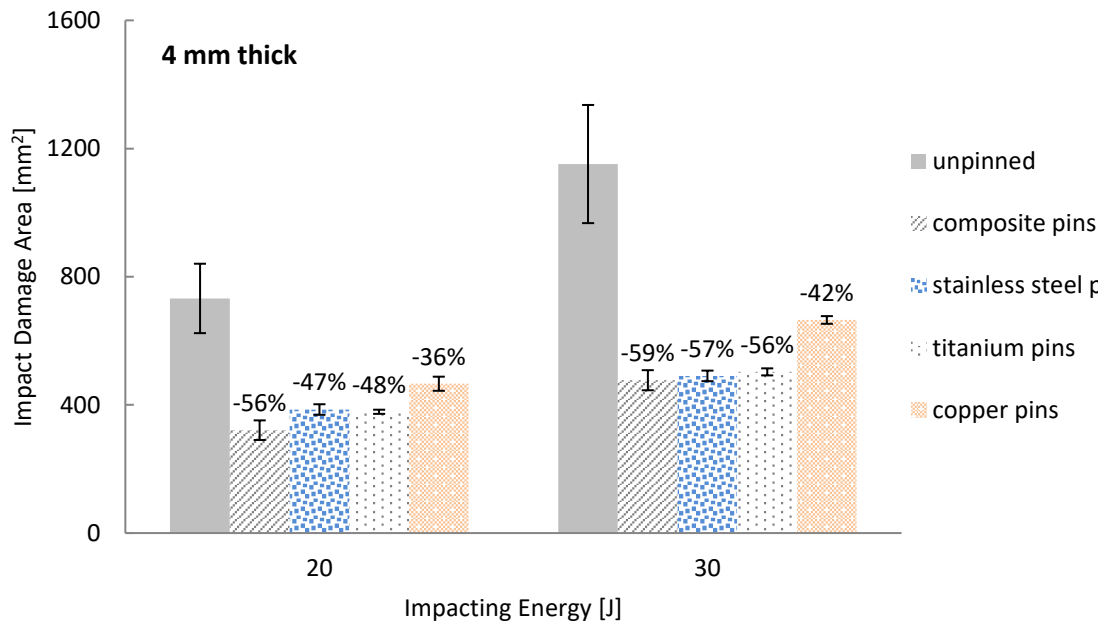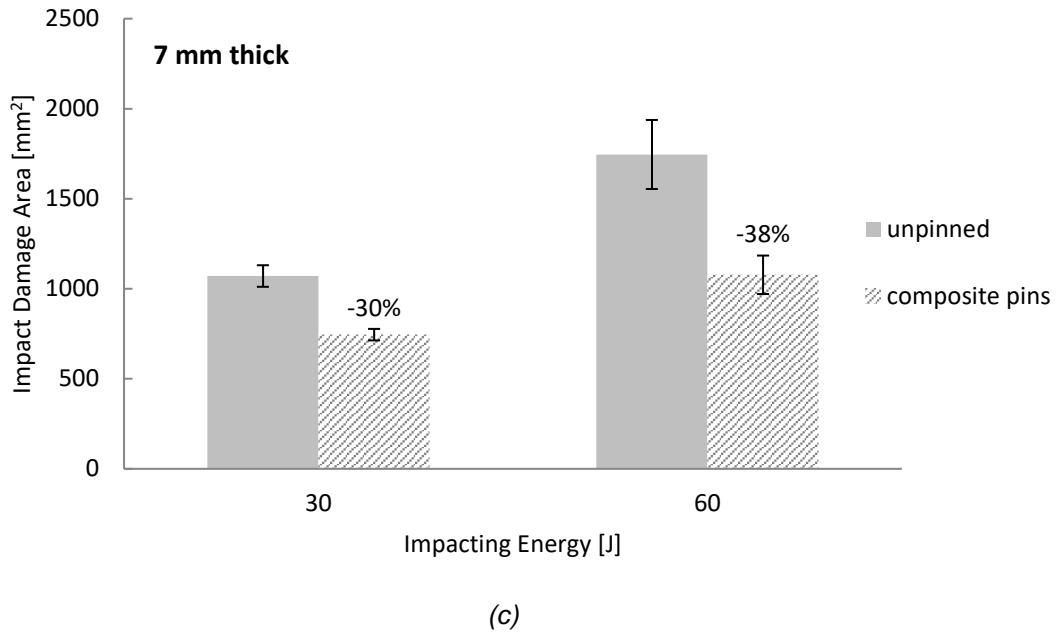
Figure 6.9. Effect of impact energy on the damage area for the (a) 2 mm, (b) 4 mm and (c) 7 mm thick unpinned and z-pinned laminates. The numbers above the bar charts indicate the percentage reduction in the damage area compared to the unpinned material.

6.5.3 In-plane compressive properties

Compressive stress-strain curves measured for the unpinned laminate and a z-pinned composite without and with impact damage are presented in Figure 6.10. The unpinned material exhibited a linear stress-compression displacement relationship to final failure, and there was no evidence of inelastic deformation before failure. With the z-pinned laminate, the catastrophic failure was announced by forming of micro-cracks around the pin locations which can be seen in the stress-displacement curve in small load oscillations (~ ±5 N). Irrespective of the presence of z-pins, impacted laminates all failed by damage propagating from the impact point. The results show that the z-pins caused a small variation to the elastic compressive response of the composite material; furthermore, the z-pinned composites always failed within the centre z-pinned region by microbuckling/kinking, as shown in Figure 6.12, which leads to the finding that the pins did not change the compressive failure mode.
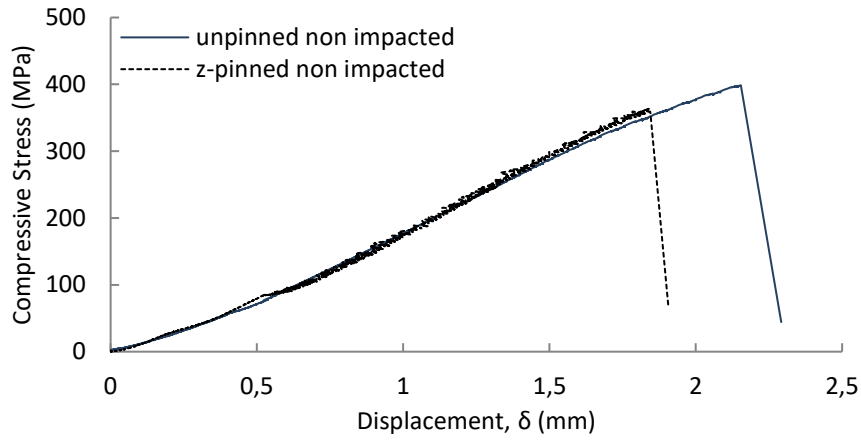
(a)
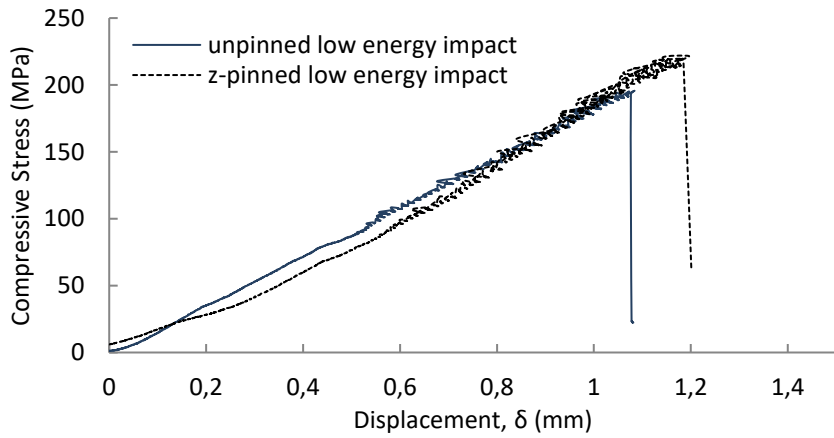
(b)
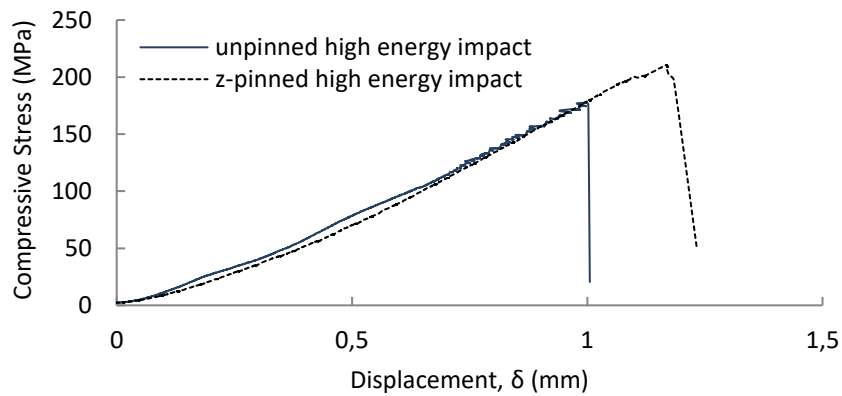
(c)

Figure 6.10. Effect of z-pin reinforcement on compressive stress-displacement curves for the unpinned and z-pinned composites when (a) non impacted, (b) impacted with low (20 J) and (c) with high (30 J) energy. Samples were 4 mm thick and reinforced with carbon fibre z-pins.

The pre- and post-compressive strengths of the unpinned laminate and different types of z-pinned composites are shown in Figure 6.11. The average pre-impact strengths for the z-pinned laminates are similar or slightly lower (up to 10%) than the unpinned laminate having the same thickness. As reported in Chapter 2, published research into the compressive properties of z-pinned composites show that z-pins can reduce the pre-impact compressive modulus and strength [65, 66, 110], and this is due to in-plane fibre waviness and out-of-plane fibre crimping caused by the pins [65, 110]. Numerical (finite element analysis) and experimental testing shows that fibre waviness and crimping lowers the compressive strength needed to initiate kinking of the load-bearing fibres in z-pinned composites [65, 66, 110]. Other studies report reductions to the compressive strength of quasi-isotropic carbon-epoxy composites up to about 14% due to z-pinning [115]. Therefore, the measured changes to the compressive strength of the composites studied here are within the range reported by other studies.

Figure 6.11b shows the effect of the z-pin material on the pre-impact strength. Irrespective of the z-pin material used, the pre-impact compressive strengths are similar and this is expected due to the same geometry of the different z-pins which thereby causes the same amount of in-plane fibre waviness and out-of-plane fibre crimping.
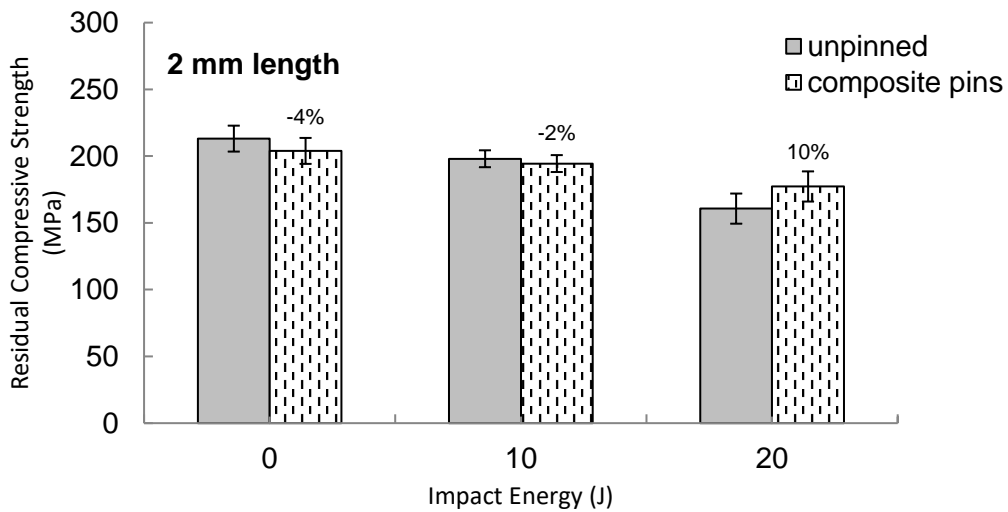
(a)
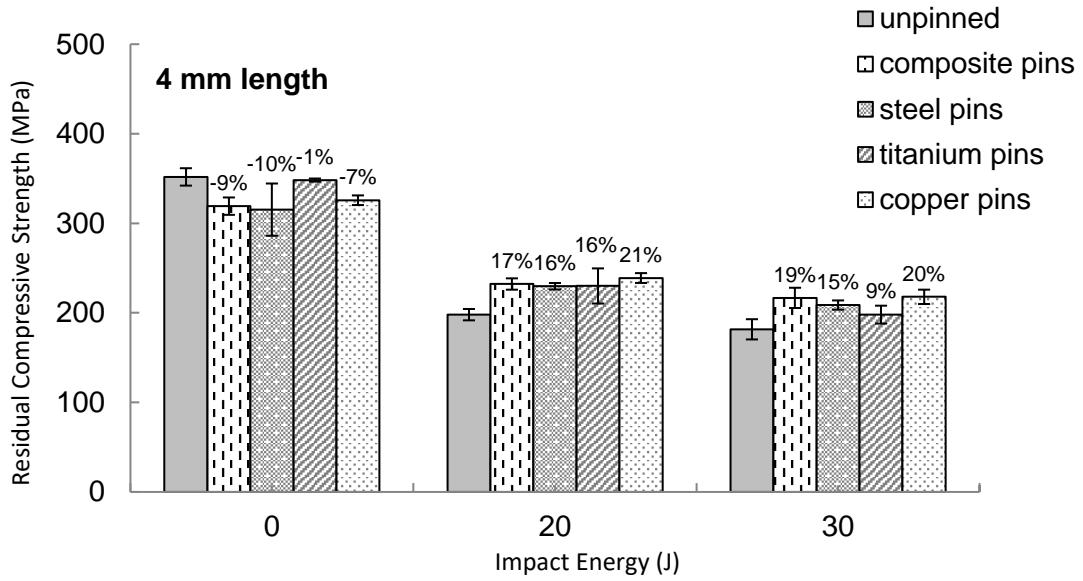
(b)
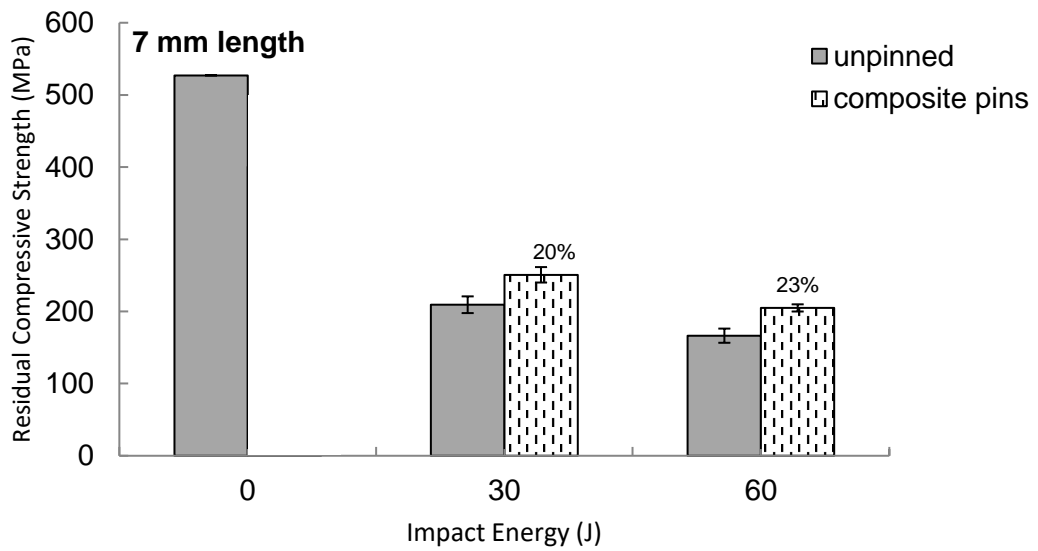
(c)

Figure 6.11. The pre- and post-impact compressive strengths for the (a) 2 mm, (b) 4 mm and (c) 7 mm thick laminates. The error bars indicate one standard deviation.

Figure 6.12 shows the failure modes of the unpinned laminate and z-pinned composites with different thicknesses. The failure mechanism was not affected significantly by z-pins, and both the unpinned and z-pinned laminates failed by kinking and microbuckling. As expected, the post-impact compressive strengths for the unpinned laminate and different types of z-pinned composites were lower than the pre-impact strength (Figure 6.11). The percentage reduction in compressive strengths caused by the impacts for the unpinned laminate was greater than for the z-pinned materials. That is, z-pinning minimized the percentage loss in post-impact compressive strength of the composite material, and are typically ~20% higher. Furthermore, the post-impact strength of the z-pinned composites was not affected significantly by the type of z-pin material.

(a)

(b)

(c)
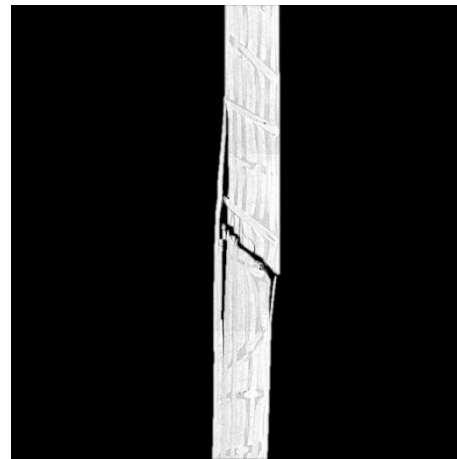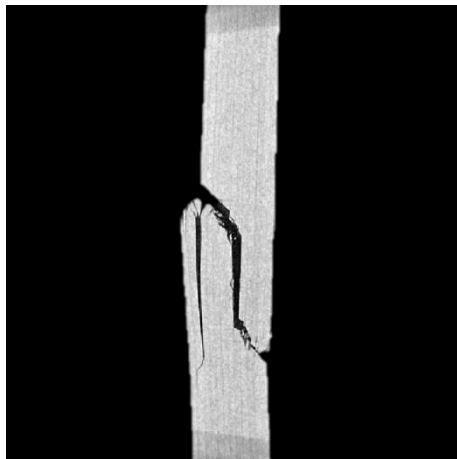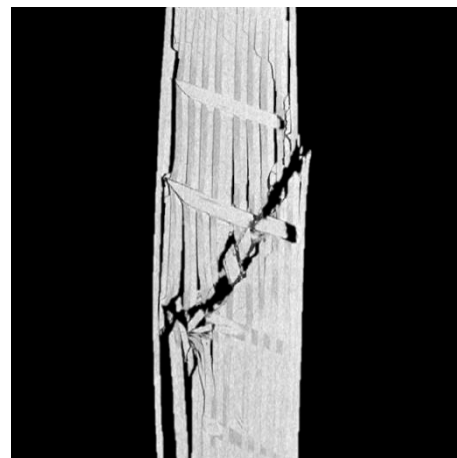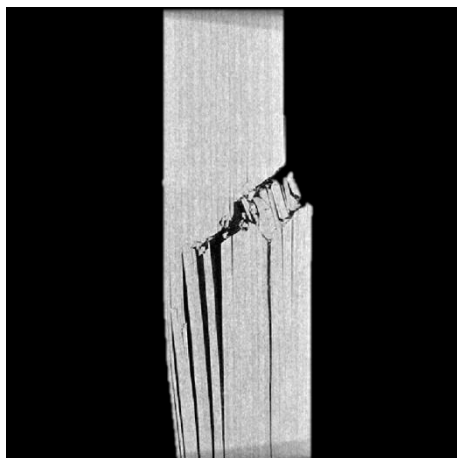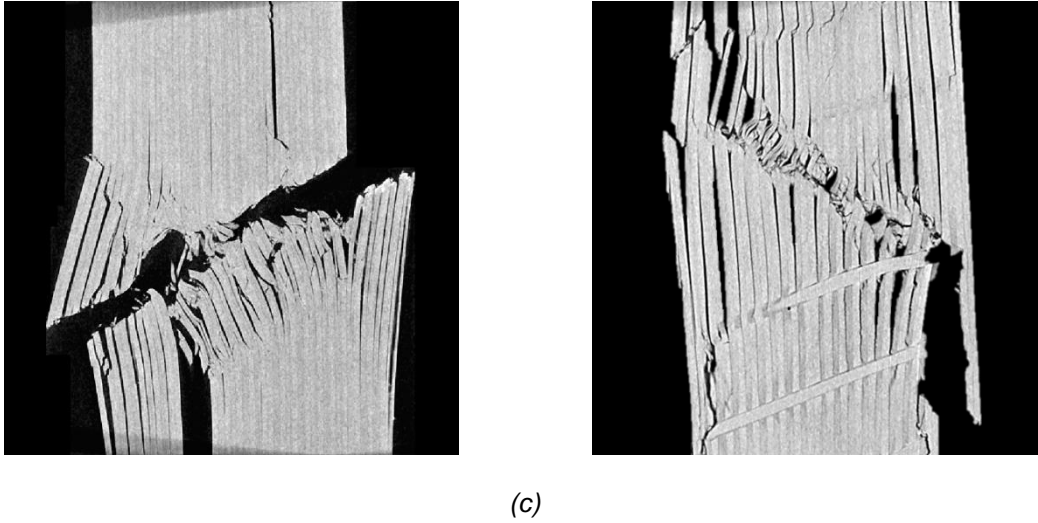
Figure 6.12. X-ray images showing compressive failure of the unpinned (left) and z-pinned (right) laminates for the (a) 2 mm, (b) 4 mm and (c) 7 mm thickness.

6.6   Conclusion

This and other studies have proven that z-pinning is an effective technique to reduce the amount of impact damage and increase the compression-after-impact properties of carbon fibre epoxy laminates. The effect of the length and mechanical properties of z-pins were investigated, and it was found that the z-pins reduced the impact damage area by up to 50% and improved the post-impact compressive strength by about 20%. Z-pins are effective in reducing the impact damage because of the greater amount of energy absorbed by the elastic deformation, debonding and partial pull-out. Increasing the impact energy increases the percentage reduction to the impact damage due to the development of a large-scale bridging zone. The material properties of the z-pins do not affect significantly the impact damage resistance of the laminates.

Chapter 7: Electrical Conductivity and Damage Detection of Z-Pinned Composites

7.1 Abstract

Presented in this chapter is an experimental study into the effects of the volume content and electrical properties of z-pins on the through-thickness and in-plane electrical conductivity of carbon-epoxy laminates. The laminates were reinforced with z-pins made of carbon fibre, stainless steel, titanium or copper, which have different electrical properties. It was found that the through-thickness conductivity is increased (up to 6 orders of magnitude with copper pins) due to z-pins being highly conductive and creating preferential paths for current flow. However, varying the volume content or electrical properties of the z-pins did not change significantly the in-plane conductivity of the laminates. A simple model based on rule-of-mixture can predict the electrical conductivity properties of z-pinned laminates.

In the second part of the work, the use of z-pins to detect delamination cracking due to changes to the through-thickness electrical resistance of carbon-epoxy laminates was investigated. Double cantilever beam (DCB) z-pinned samples were loaded under increasing crack opening displacement. The through-thickness electrical resistance was found to increase with increasing delamination length. The higher the volume content of z-pins then the larger was the effect of the variation of the through-thickness resistance. This reveals that z-pins can be used for delamination crack detection.

7.2 Introduction

A problem with using carbon fibre composites in aircraft structures is their low planar and through-thickness electrical conductivity, which is due mostly to the low conductivity of the epoxy matrix and resistance of the fibre-matrix interface. The Federal Aviation Authority (FAA) regulations [90] specify that lightning strike protection must provide a continuous conductive path over the entire aircraft surface. Even stricter conditions apply to components at high risk of lightning strikes, such as the radome or nose which are required to withstand currents up to 200 kA without being severely damaged. Other regions (e.g. wings and fuselage) are only required to act as a conductive path for the current. Aircraft designers are forced to insert fine copper mesh into composites to protect the aircraft from lightning strike, although the meshes are expensive and add weight.

The electrical conductivity of composites can be improved by the addition of conductive nanofillers to the polymer matrix such as carbon nanotubes (CNTs) [85-88], carbon nanofibres (CNFs) [89, 90] and graphene [91, 92]. Research reveals that a small addition of carbon nanofillers (1-2 wt%) can increase the electrical conductivity by many orders of magnitude. Ladani et al. [85] have shown that by electro-magnetically orienting the nanofillers prior to resin curing can further increase the electrical conductivity in the through-thickness direction, particularly for low weight contents of CNFs.

Zhang et al. [116] recently reported the only research work that aims to provide z-pinned composite of damage sensing properties via the measurement of through-thickness electrical resistance. This technique was able to detect the location and length of mode I delamination cracks in carbon-epoxy laminate. The technique works by monitoring the electrical conductivity of the z-pins. When they fail by pull-out there is a large increase to the resistance, indicating cracking. However, only one type of z-pinned laminate was studied, and the method has practical limitations.

This research chapter presents an experimental investigation into the electrical properties of carbon-epoxy laminates in the through-thickness, longitudinal and transverse directions. The effects of the electrical properties of the z-pins and their volume content were determined. The research also investigates the suitability of z-pins to detect delamination cracks in carbon-epoxy laminates.

7.3   Materials and Experimental Methodology

7.3.1 Electrical conductivity tests

Z-pinned composite blocks were manufactured using carbon fibre-epoxy prepreg tape (VTM 264). The geometry and dimensions are shown in Figure 7.1. The uncured plies were stacked in a $[0]_{25}$ ply sequence to a total thickness of 5 mm. The uncured laminate was reinforced in the through-thickness direction with z-pins made of unidirectional carbon fibre-bismaleimide (BMI), copper (99.9% purity), titanium (grade 1; 99.5% purity) or stainless steel (316L). The length (5 mm) and diameter (510 μm) of the z-pins was the same for the different laminates. The carbon fibre z-pins were inserted into the uncured laminate using the UAZ process whereas the metal z-pins were manually inserted, as described in Section 3.3.1. The electrical conductivity properties of the unpinned laminate and the different types of materials used for the z-pins are shown in Figure 7.2. The z-pins were inserted at different volume contents (between 0.25% and 4%).

(a)   (b)
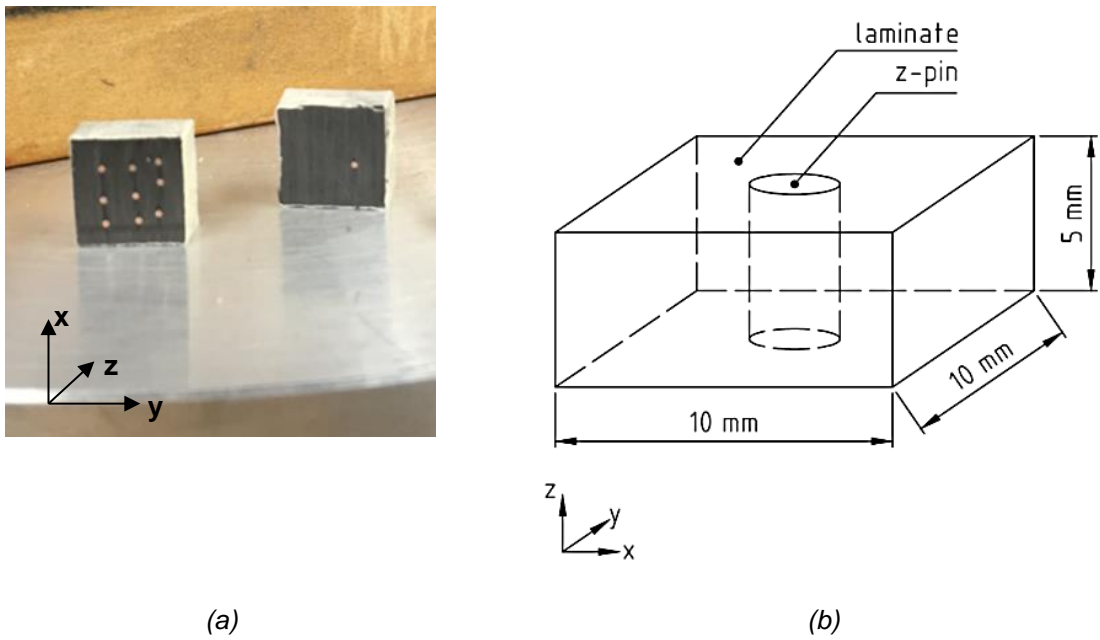
Figure 7.1. (a) Photograph and (b) dimensions of the composite samples for electrical conductivity testing. The z-pin in (b) is not to scale.

Electrical Conductivity [S/m]
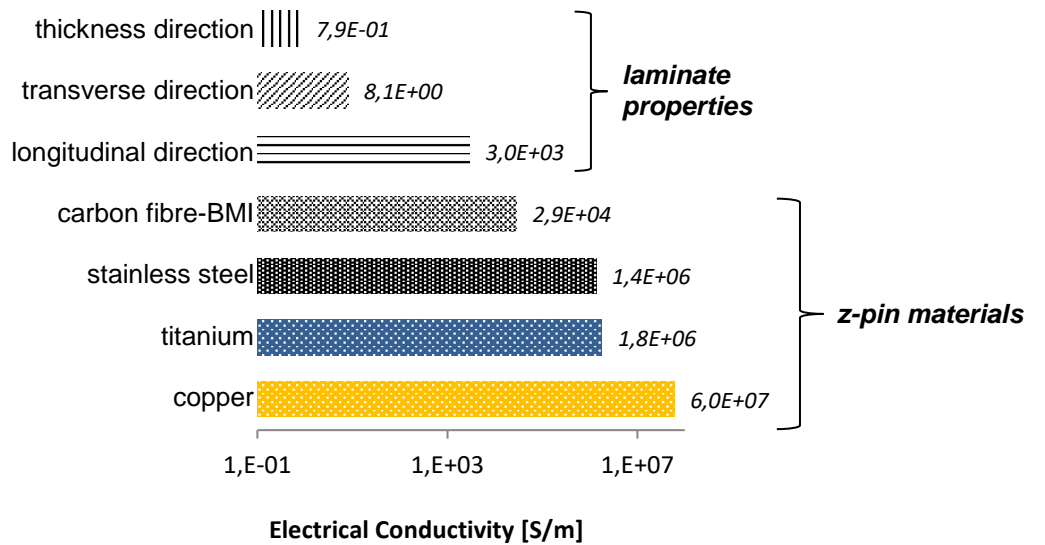
Figure 7.2. Electrical conductivity values for the unpinned laminate and the materials used for the z-pins [117]. The values for the laminates and the carbon BMI z-pins were measured.

The surfaces of the unpinned and z-pinned laminates were machined flat and then polished using diamond paste (0.5 μm). The surfaces where then coated with silver electrical conductive paste (60% silver). A light through-thickness pressure was applied to the sample to ensure contact

between the copper plates (used as probes) and the laminate surfaces (Figure 7.3). The electrical measurements were performed using the 4-wires method and using a Keysight micro Ohm meter (type 3442OA).
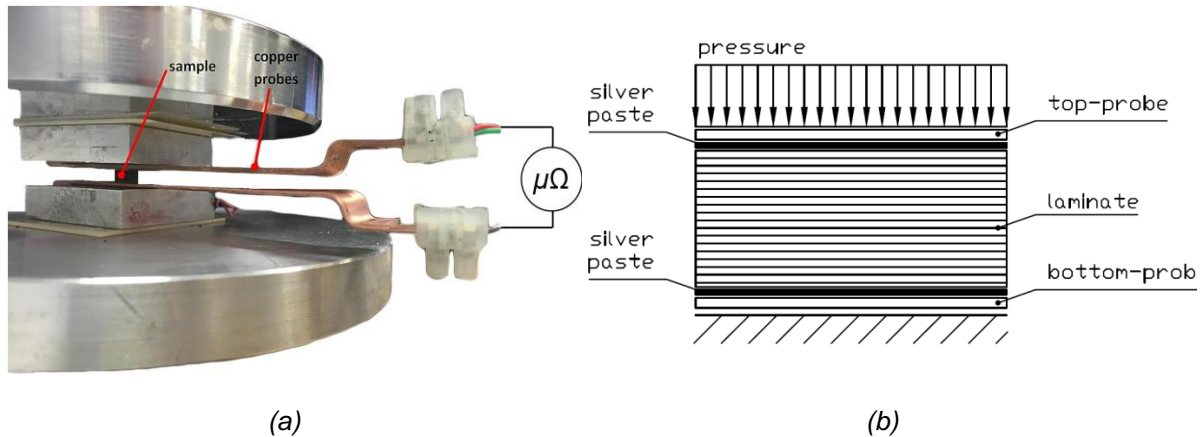
Figure 7.3. (a) Photograph and (b) schematic of the test set-up.

7.3.2 Delamination length detection

Unpinned and z-pinned DCB laminates were made using unidirectional T700 carbon fibre–epoxy prepreg for the delamination crack detection testing. The prepreg was reinforced with 280 μm diameter carbon fibre z-pins at the volume contents of 0.5%, 2% or 4%. In addition, laminates containing carbon fibre, titanium, stainless steel or copper z-pins were produced. These laminates contained 510 μm diameter z-pins at the volume content of 2%. Both the unpinned and z-pinned laminates were sandwiched between 2 mm-thick laminates tabs which were co-cured in an autoclave.

The DCB samples were loaded at the pre-cracked end at a constant displacement rate of 2 mm/min. The crack was forced to propagate at short intervals (1 to 2 mm). For each interval the test was stopped, and the electrical resistance of the delaminated composite (R_C) in the through-thickness direction (e.g. 90° to the crack plane) was measured and compared against the original resistance value (R_O). This process was repeated multiple times as the delamination grew to a final length of ~130 mm.

(a)   *(b)*
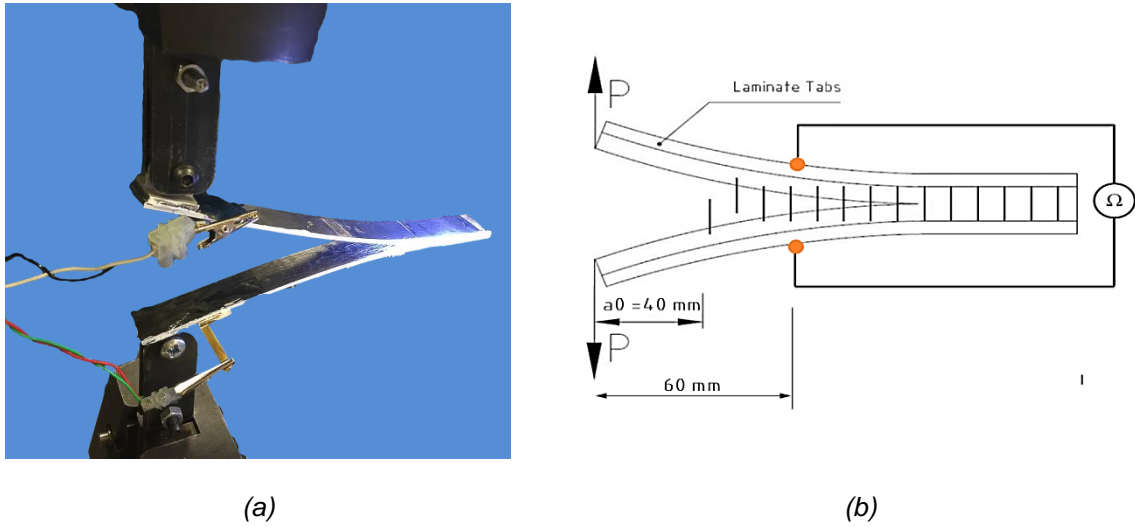
Figure 7.4. (a) Photograph and (b) schematic showing the electrical resistance measurement of a z-pinned DCB specimen.

7.4 Results and Discussion

7.4.1 Electrical conductivity

Figure 7.5 shown the effects of the volume content and material properties of z-pins on the through-thickness electrical conductivity of the carbon-epoxy laminate. The electrical conductivity was increased by the z-pins in the order: carbon fibre (least effective), stainless steel, titanium and copper (most effective). This order correlates with the electrical conductivity of the z-pin material (see Figure 7.2). The conductivity also increased at an almost linear rate with the volume content of z-pins.

A simple analytical model based on rule-of-mixture can be used to closely calculate the through-thickness electrical conductivity (σ_z) of the z-pinned laminates:

$$\sigma_z = \sigma_{pin} \cdot \left(V_{pin}\right) + \sigma_o \cdot (1 - V_{pin}) \tag{7.1}$$

where V_{pin} and σ_{pin} are the volume content and axial electrical conductivity of the z-pins, respectively. σ_o is the through-thickness conductivity of the unpinned laminate. The solid curves in Figure 7.5 show the calculated electrical conductivities for the different z-pinned laminates, and there is excellent agreement with the experimental conductivity values.
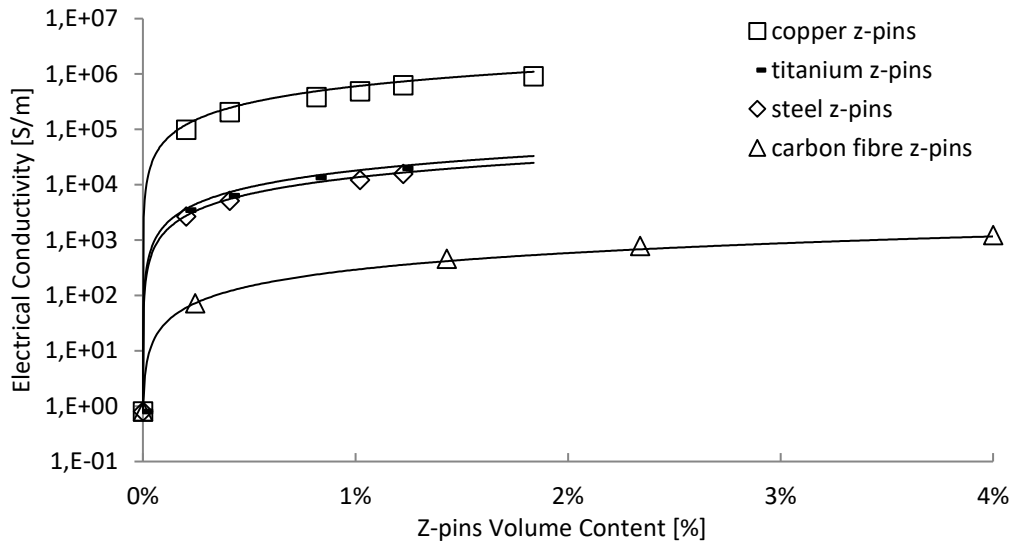
Figure 7.5. Effect of volume content and material of the z-pins on the through-thickness electrical conductivity of the carbon-epoxy laminate.

Figure 7.6 shows the effects of volume content and material of the z-pins on the electrical conductivity measured in the longitudinal (0° fibre) and transverse (90°) directions for the laminate. It was found that the in-plane electrical conductivity was not affected significantly by the z-pins whereas the transverse conductivity was reduced slightly. The longitudinal conductivity was not affected by z-pins because the carbon fibres, which conduct most of the electric current, are not disturbed significantly by the z-pins (Figure 7.7a). There is a small reduction to the transverse conductivity, and this is attributed to the resin-rich regions (Figure 7.7b) (described in section 2.3.2) containing epoxy resin which is a dielectric material disrupting the current flow near the z-pins. The electrical conductivity may also be reduced by interfacial cracking between the z-pins and laminate, which disrupts the current flow. As mentioned in Chapter 2, this cracking is caused by differences in the thermal expansion coefficients of the z-pins and composite material. Z-pin insertion, however, creates a high density fibre region (Figure 7.7b) which increases the fibre-to-fibre contact near the pins resulting in an improved localised electrical conductivity. Figure 7.6b show that the detrimental effect on the transverse conductivity is higher for the metal pins (although is small), which also (as reported in section 3.3.1) have a larger thermal expansion coefficient which is reflected in more extensive interface cracking.

(a) *(b)*
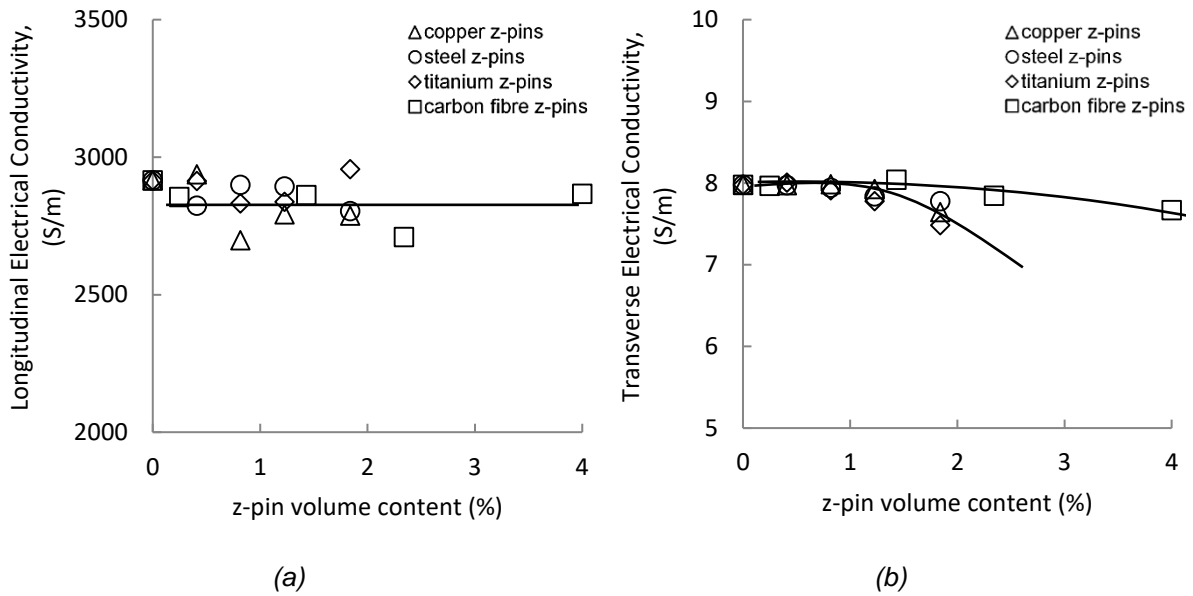
Figure 7.6. Effects of the volume content and material of z-pins on the (a) longitudinal and (b) transverse elecrical conductivity of the carbon-epoxy laminates.

(a) *(b)*
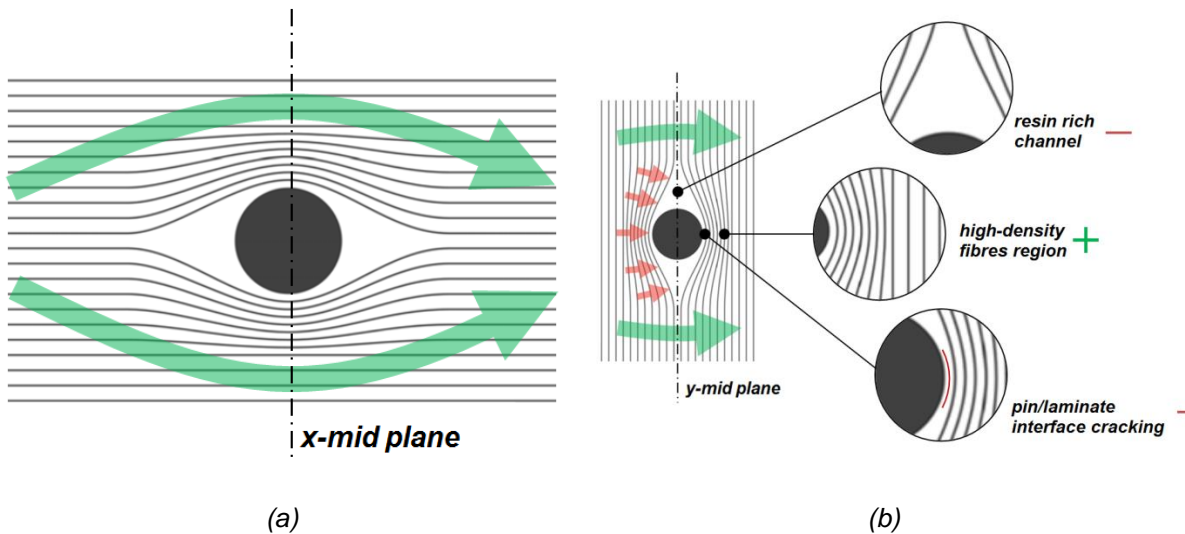
Figure 7.7. Schematic of a z-pinned laminate showing the effect of a z-pin on the (a) longitudinal and (b) transverse electrical conductivity.

7.4.2 Delamination crack detection

Figure 7.8 shows the effect of the delamination crack length on the through-thickness electrical resistance for the unpinned laminate and composites reinforced with the carbon fibre z-pins at different volume contents. In all cases the resistivity increases with crack length due to the delamination disrupting current flow in the through-thickness direction. The curve for the unpinned laminate, compared to the z-pinned composites, shows less sensitivity to delamination

crack growth. It is believed that the larger increase in electrical resistivity for the z-pinned composites is due to pull-out of the z-pins, which represent the only conductive path for current flow across the delaminations (Figure 7.9a). When the delamination crack length further increases the following row of z-pins becomes the new conductive path that still has the same resistance (R_{pin}) which is much smaller compared to the resistance ($R_{in\text{-}plane}$) that connects the probe to the conductive z-pin row. That is, for the z-pinned laminates the change in the measured (resistance measured using the multimeter) resistance is dominated by the change in the in-plane resistance which increases with the delamination crack length. For the z-pinned laminates the change in the measured resistance can be written as:

$$\Delta R_{pinned-tot}(\Delta a) = 2\Delta R_{in-plane}(\Delta a) + \Delta R_{pin} \approx \Delta 2R_{in-plane}(\Delta a) \tag{7.2}$$

The through-thickness resistivity change increases with the volume content of z-pins up to 2%, above which there is no further significant increase.
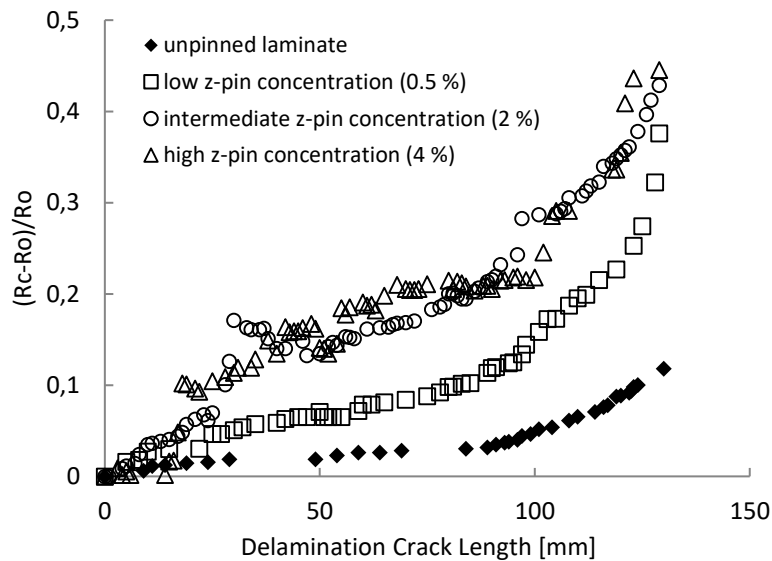
Figure 7.8. Effect of volume content of z-pins on the change to the through-thickness electrical resistance of the unpinned and z-pinned laminates.

For the unpinned laminate, $R_{in\text{-}plane}$ is much lower than the through-thickness resistance (R_o) which is almost constant for increasing delamination lengths. This results in a smaller change in resistance with increasing delamination crack length for the unpinned laminate. For the unpinned laminate the change in the electrical resistance can be written as:

$$\Delta R_{unpinned-tot}(\Delta a) = \Delta 2R_{in-plane}(\Delta a) + \Delta R_{unpinned} \approx \Delta R_{unpinned} \qquad (7.3)$$
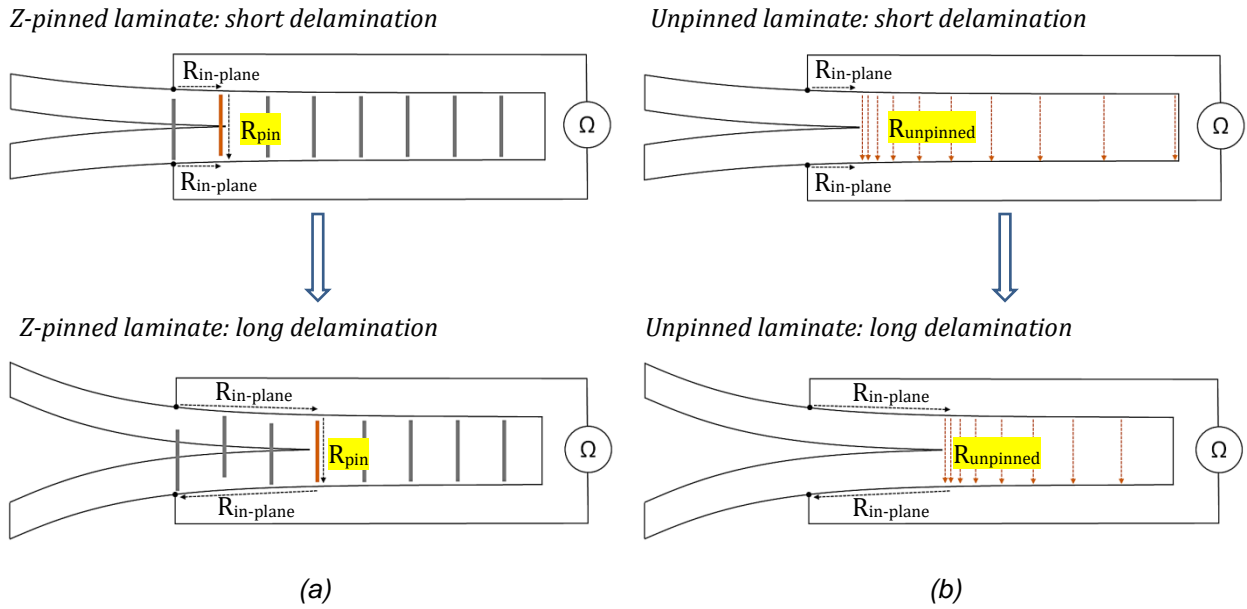
Figure 7.9. Schematic drawings showing the electrical conductive mode for a (a) z-pinned and (b) an unpinned laminate.

Figure 7.10 shows the effect of the delamination crack length on the through-thickness electrical resistance for the unpinned laminate and the composites reinforced with z-pins made of different materials. Irrespective of the electrical conductivity of the z-pins, the measured through-thickness electrical resistance increases with the delamination crack length. The through-thickness resistance change is higher when using carbon fibre composite compared to metals. This difference is attributed to more extensive interfacial cracking around the metal z-pins. Because of the higher thermal expansion coefficient of the metal z-pins they experience more severe interfacial cracking. This is believed to have an insulating effect between the z-pins and the laminate, forcing the current flow into the surrounding laminate. This creates an electrical conductive mode (Figure 7.11c) which is a combination between the two conductive modes schematically displayed in Figure 7.11a and b.
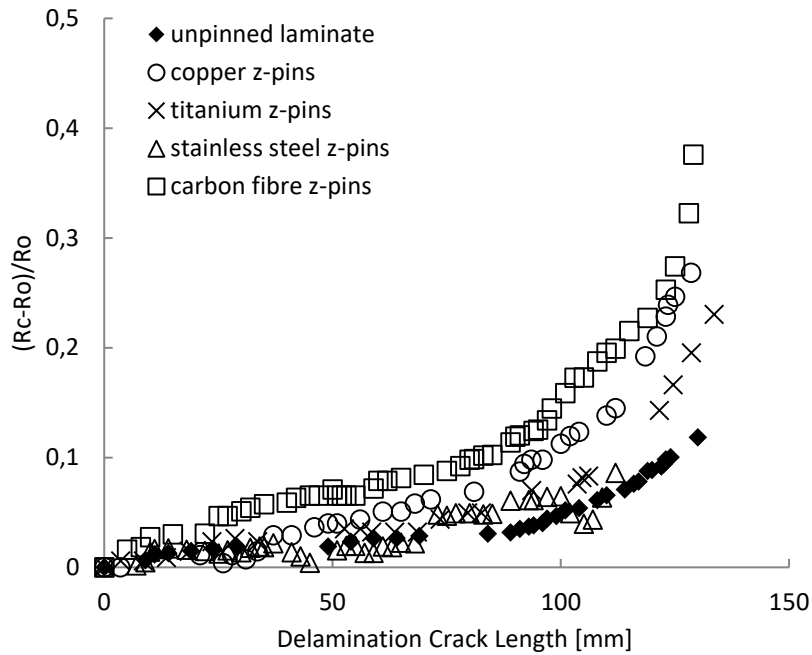
Figure 7.10. Effect of the of z-pin material on the through-thickness electrical resistance measurement for the unpinned and z-pinned laminates.

| (a) | (b) | (c) |
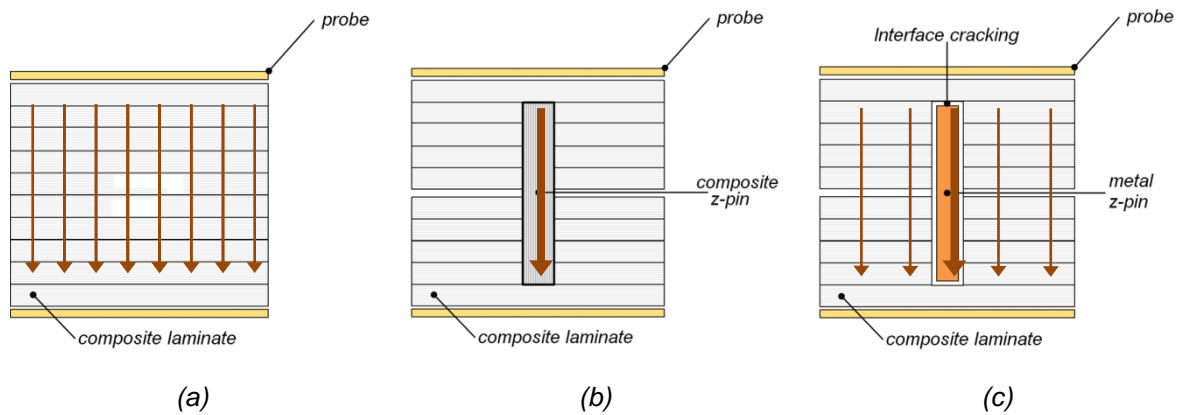
Figure 7.11. Electrical conductive mode for an (a) unpinned laminate and a z-pinned laminate reinforced with (b) carbon fibre composite and (c) metal z-pins. The arrows indicate the current flow paths.

7.5   Conclusion

Z-pinning is an effective technique for increasing the through-thickness electrical conductivity of carbon fibre epoxy laminates. The conductivity increases linearly with the volume content of z-pins due to the creation of conductive paths for the current flow in the through-thickness direction. The conductivity depends on the electrical properties of the z-pin, and it increased in the order: carbon fibre composite (least conductive), stainless steel, titanium and copper (most

conductive). The planar electrical conductivity was not affected significantly by the z-pins. The z-pins had a small detrimental effect on the transverse conductivity due to dielectric resin-rich regions surrounding the pin sites.

Z-pins can be used for delamination damage detection in laminates loaded under mode I. The measured through-thickness resistance increased with the delamination crack length and, due to different conductive modes, the changes in the resistivity were greater for the z-pinned laminates.

Chapter 8: Thermal Diffusivity of Z-Pinned Composites

8.1 Abstract

On aircraft, cooling of components such as leading edges on supersonic aircraft, surrounding areas to the auxiliary power unit (APU), and hydraulic pump enclosures require high heat transfer capacity to efficiently and rapidly dissipate heat. Carbon fibre polymer matrix composites are characterised by low through-thickness thermal conductivity, and this can be a concern when used on aircraft. This chapter presents a finite element (FE) modelling study investigating the thermal properties of z-pinned laminates. The effects of the volume content (from 0 to 5%) and material (carbon fibre, stainless steel, titanium, copper) of z-pins on the through-thickness and in-plane thermal diffusivities was analysed using the laser flash method which was implemented into an FE model. The improvements to the through-thickness thermal diffusivity can also be predicted using a simple model based on the rule-of-mixture. The through-thickness thermal diffusivity can be improved significantly by increasing the volume content and thermal conductivity of z-pins, and it is improved in the order: stainless steel, carbon fibre, titanium and copper (most effective). The through-thickness thermal diffusivity is increased by z-pins (up 10 fold) which create a preferential path for heat transfer in carbon-epoxy laminates. However, varying the volume content and thermal conductivity of z-pins did not significantly affect the in-plane thermal diffusivity.

8.2 Introduction

The through-thickness thermal conductivity of polymer matrix composites is strongly influenced by the thermal properties of the matrix and fibre-matrix interface. There is a large body of experimental and numerical research that have studied the effectiveness of different approaches to improve the thermal conductivity of composites. The most common approach is the inclusion of nanofillers made of highly-thermally conductive materials such as carbon or metals [84, 118-124] or a combination of the two [125]. Once embedded into the matrix, the fillers create a thermal conductive path through the laminate (Figure 8.1). Shape, aspect ratio, distribution, volume content and material of the fillers are all parameters that significantly affect the thermal conductivity properties of the laminate. Han et al. [126] enhanced the through-thickness thermal conductivity of carbon fibre polymer matrix composites using carbon black. Carbon black was

dispersed between the ply layers using ethylene glycol monoethyl ether (EGME). It was experimentally observed by Han and colleagues that the EGME itself is able to increase the thermal conductivity by partially dissolving the uncured resin on the prepreg tape which increases the fibre/fibre contact. The thermal conductivity was increased using this method by about 36%. The small amount of carbon black (0.8 wt%) increased the conductivity by about 210%. Other research has studied the synergetic effect due to the combination of carbon and metal fillers. Kandare et al. [125] combined graphene-nanoplatelets with silver particles or wire, and found a synergetic effect due to the combined fillers which is higher than the sum of the single components resulting in an improvement to the through-thickness thermal conductivity of about 70%. Han et al. [127] measured improvements of ~60% in the through-thickness thermal conductivity by increasing the cure pressure which increases the fibre/fibre contact. Highly conductive nanofillers and surface modified fibres are effective ways to increase the through-thickness thermal conductivity. It has also been proven that these techniques can be effective at improving the delamination resistance of composite laminates [86, 87, 89, 91, 92, 128].
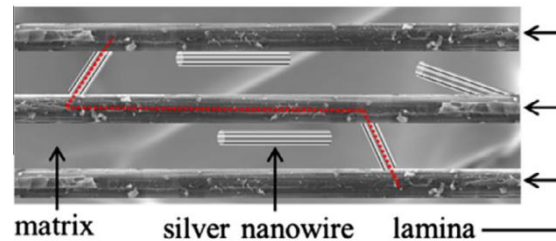
Figure 8.1. Silver nanowires interconnecting carbon fibre laminas within a composite laminate to increase the thermal conductivity [125].

The only reported work to investigate the effect of three-dimensional fibre reinforcement on the through-thickness thermal conductivity of CFRP was performed by Schuster et al. [129]. The insertion of copper wire as the z-binder (6%vol) in 3D woven carbon fibre composite resulted in the through-thickness thermal conductivity being increased up to 8 times over the benchmark composite without z-reinforcement. Although this technique is much more effective than the filler-based approaches at increasing the thermal, conductivity, not considering the higher delamination resistance properties, it is still hard to implement on prepreg materials, which in aerospace structures represents the preferred choice for manufacturing highly-loaded components.

In this chapter, the effects of the volume content and material of z-pins on the thermal diffusivity of carbon fibre-epoxy laminates is numerically investigated using finite element (FE) analysis. The FE model was validated for some common materials properties found in literature review and results were compared with values predicted with a simple model based on the rule-of-mixture.

8.3   FE Model and Test Methodology

Figure 8.2a shows the finite element model used in this study to model the thermal diffusivity of z-pinned laminates. 10 mm wide x 10 mm long, 5 mm thick unit cell blocks were modelled and meshed using 8 node linear heat transfer bricks (DC3D8 type Abaqus®). The effects of the volume content (from 0 to 5 vol%) and material (carbon fibre, stainless steel, titanium and copper) of the z-pins on the thermal diffusivity was numerically investigated. The laser flash analysis was numerically implemented and used to compute the thermal diffusivity in the thickness (z) and planar (x, y) directions of the unpinned and z-pinned laminates. A unit heat-step pulse (1 W/m^2) of short duration (1 ms) was applied on one side of the sample and the temperature rise on the back surface (average nodal temperature) was compared, and then used to calculate the thermal diffusivity of the composites. The thermal diffusivity for the unpinned and z-pinned laminates was calculated using [130]:

$$\alpha = 0.1388 \cdot \frac{d^2}{t_{50\%}} \qquad\qquad (8.1)$$

where d is the thickness of the sample and $t_{50\%}$ is the time for the backside surface (average nodal temperature) to reach the 50% of the maximum temperature rise from the instant of heat pulse application (Figure 8.2b). The back surface was assumed to have a film convection coefficient of $5 \text{ W/(m}^2\text{K)}$ (typical free air convection value) whilst the remaining surfaces were considered as adiabatic.

(a)

(b)
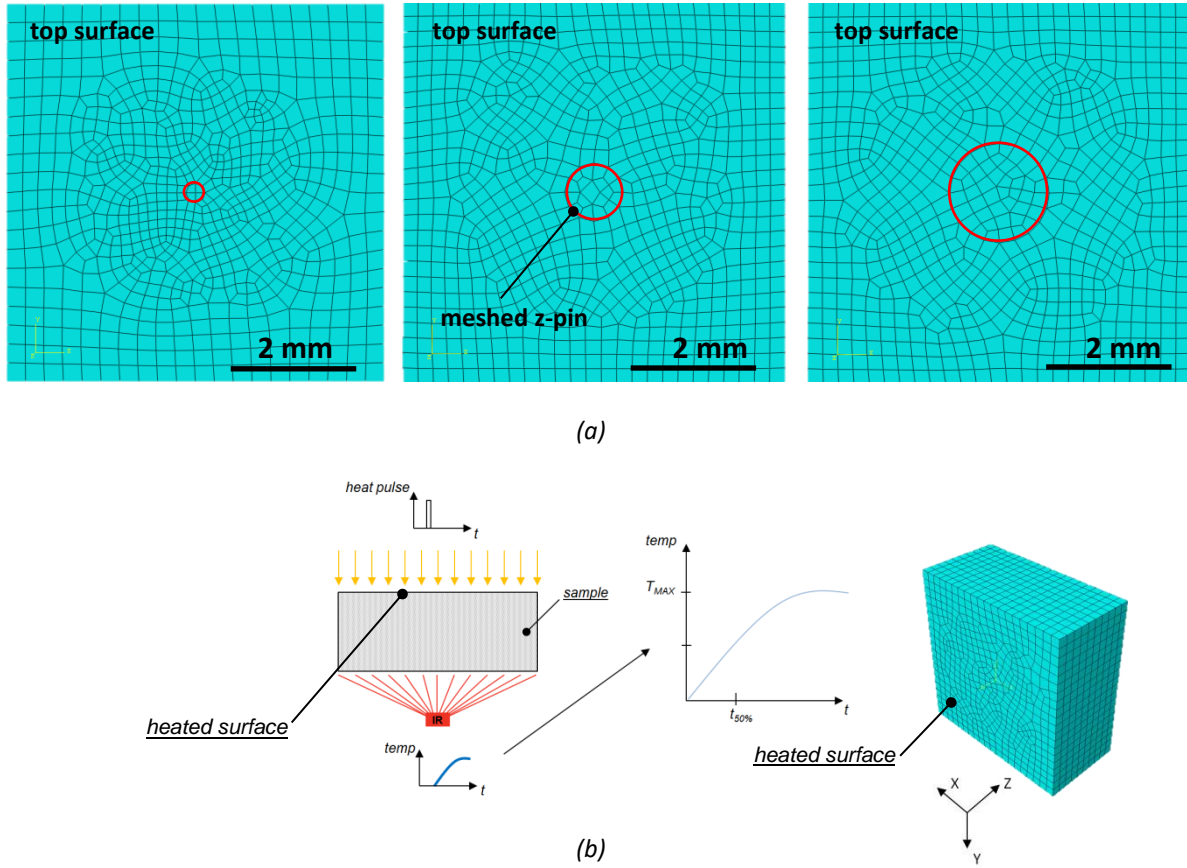
Figure 8.2. (a) FE model and (b) schematic of the test used to compute the thermal diffusivity of the unpinned and z-pinned laminates.

The thermal properties of the materials used in the modelling are given in Table 8.1. The linear curves in Figure 8.4 show the calculated increases in the thermal diffusivity using Equation 8.2.

Table 8.1. Thermal material properties [131-136].

Material	Thermal Conductivity [W/m·K]	Thermal Diffusivity FE Model [mm^2/s]	Thermal Diffusivity Literature [mm^2/s]
CFRP x-direction (55% Vf)	7	9.5	/
CFRP y-direction (55% Vf)	0.8	2.6	/
CFRP z-direction (55% Vf)	0.6	1.3	/
z-pins axial-direction (60% Vf)	10	11.9	/
z-pins transverse-direction (60% Vf)	0.8	/	/
pure copper	385	112	111
stainless steel 316L	16.3	4.7	4.1
titanium (grade 1)	16	6.6	6.8

8.4   Results and Discussion

Figure 8.3 shows the calculated temperature rise at the back surface (x-y plane) for the unpinned laminate and for the composites reinforced with copper z-pins (0.2, 0.8 and 1.8 vol%). As expected, the heating rate increases with the z-pin content, and therefore the time for the temperature to reach the 50% threshold is reduced and this is reflected in higher thermal diffusivity (Equation 8.1). The effects of the volume content and material of z-pins on the through-thickness thermal diffusivity is shown in Figure 8.4. The improvement to the thermal diffusivity depends on the thermal properties of the z-pin, with stainless steel being the least effective, followed by carbon fibre composite and titanium, and then copper being the most effective.

A simple analytical model based on the rule-of-mixture is used to predict the through-thickness thermal diffusivity:

$$\alpha_z = \alpha_{pin} \cdot \left(V_{pin} \right) + \alpha_o \cdot (1 - V_{pin}) \tag{8.2}$$

where V_{pin} and α_{pin} are the volume content and the thermal diffusivity of the z-pins respectively and α_o is the through-thickness diffusivity of the unpinned laminate.
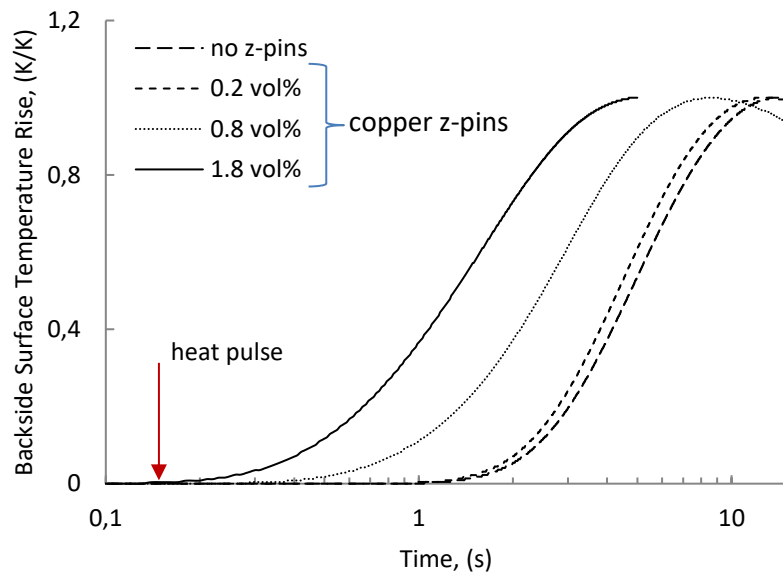
Figure 8.3. Back surface temperature rise for laminates reinforced with copper z-pins at different volume contents. The arrow indicates when the heat pulse was applied.
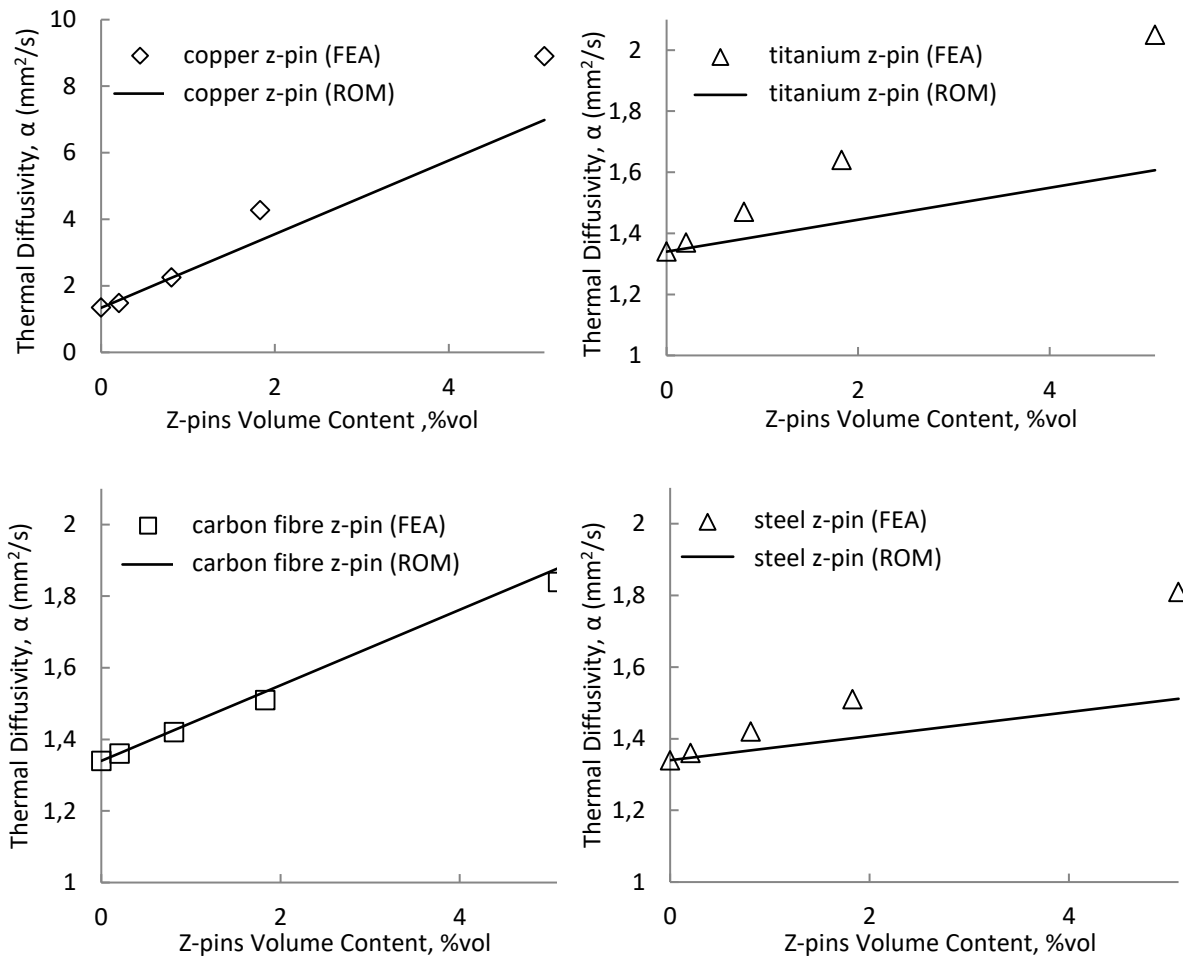
Figure 8.4. Effects of the volume content and material properties of z-pins on the through-thickness thermal diffusivity for the carbon-epoxy laminate using FE analysis and rule-of-mixture.

Z-pins are effective in improving the through-thickness thermal properties of laminates because of their high thermal properties compared to the host laminate. Z-pins thermally connect the two opposing surfaces sides of the composite and generate preferential paths for the heat flux in the through-thickness direction. Figure 8.5 shows a sequence of cross-sectional FE images of the temperature distribution for the unpinned laminate (Figure 8.5a) and for the same laminate reinforced with copper and carbon fibre z-pins (Figure 8.5b) at different time intervals after application of the heat pulse. It is shown that the z-pins significantly altered the heat flow rate and distribution. This is shown schematically in Figure 8.6. The heat being transferred laterally at the z-pin/laminate interface explains the gap between the numerical values and the values predicted via rule-of-mixture (which does not account for z-pin/laminate heat transfer). This behaviour is more significant when using metal z-pins (which have isotropic thermal properties).
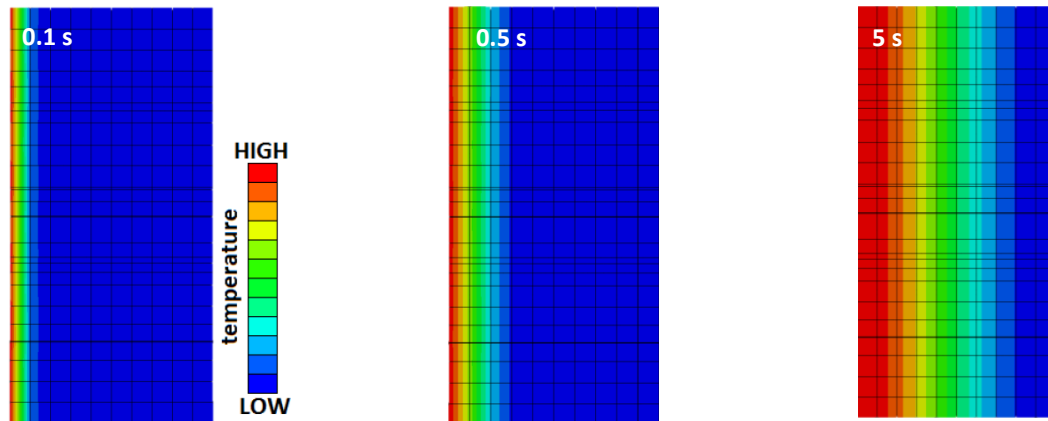
(a)
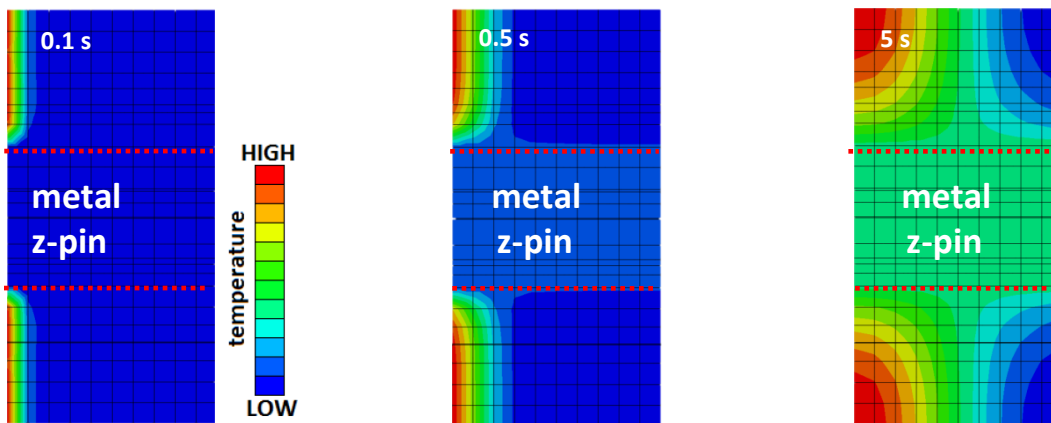
(b)
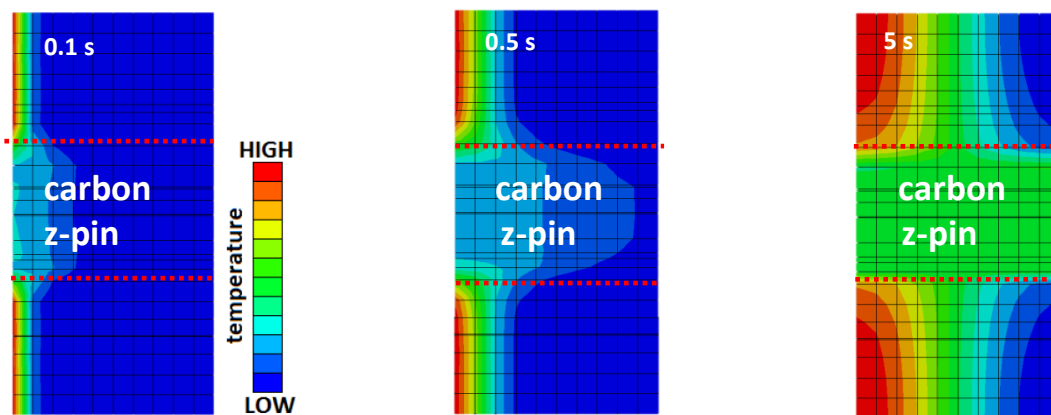
(c)

Figure 8.5. Cross-sectional temperature distribution for the (a) unpinned laminate and z-pinned composites with (b) copper and (c) carbon fibre z-pins. The z-pinned composites were reinforced with copper or carbon fibre z-pins at a volume content of 5%. The heat pulse was applied to the left side of the laminates.
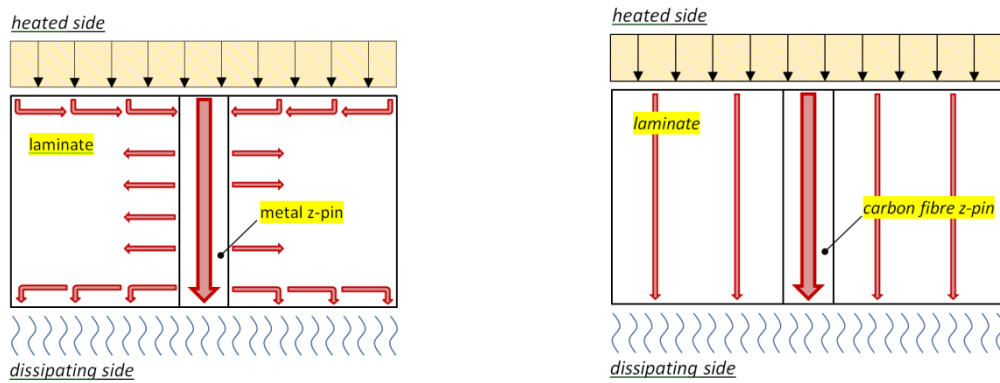
Figure 8.6. Thermal conductivity mechanism for z-pinned laminates reinforced with (a) metal and (b) carbon fibre z-pins. The arrows indicate the heat flow direction.

When using carbon fibre composite z-pins the mismatch between numerical and predicted values becomes almost irrelevant because of the low heat transferred at the pin/laminate interface. This is due to the fact that even though z-pins have good axial thermal properties their low transverse thermal properties do not allow for significant z-pin/laminate interface heat conduction which limits the global through-thickness heat conduction.

The FE model also revealed that z-pins do not significantly alter the in-plane thermal properties of the laminates, as shown in Figure 8.7. This is because the z-pins are discrete and localised in the lateral direction, and consequently there is not significant heat conduction through the unpinned regions.
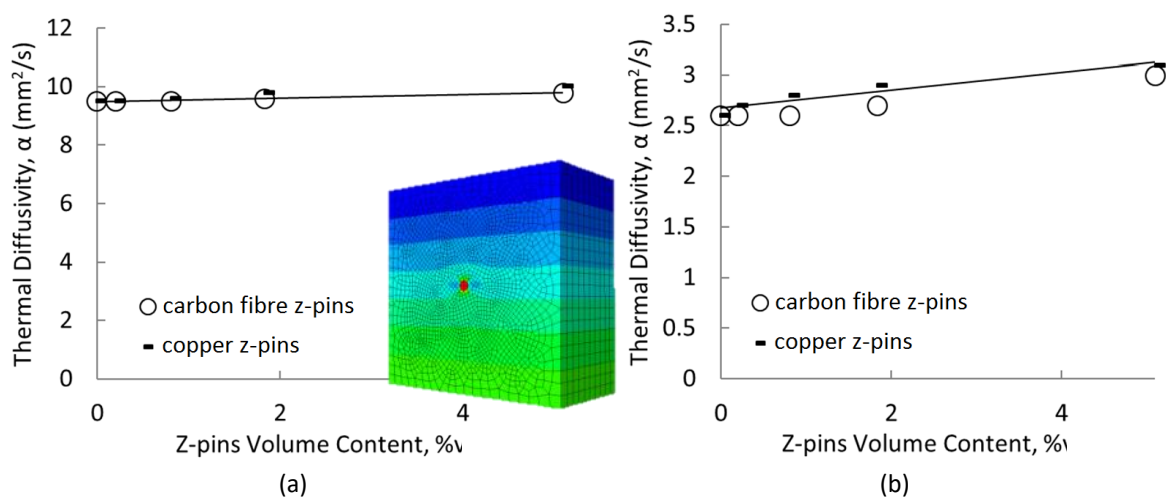
Figure 8.7. Effect of volume content and material properties of z-pins on the (a) longitudinal and (b) transverse thermal diffusivity for the unpinned and z-pinned laminates. The solid curves are lines of best fit. The thermal diffusivity for the laminates reinforced with titanium or stainless steel z-pins was similar to the carbon fibre z-pins.

8.5 Conclusions

The effects of the volume content and thermal properties of z-pins on the through-thickness and in-plane (longitudinal and transverse) thermal diffusivity of carbon-epoxy laminate were numerically investigated. The through-thickness thermal diffusivity increased linearly with the volume content and thermal conductivity of the z-pins because of the creation of highly conductive paths through the material. However, z-pins are ineffective at improving the in-plane thermal properties of laminates. More work is needed in order to investigate the heat exchange at the z-pin/laminate interface and the effect of the z-pin pattern distribution and other parameters such as offset angle of insertion and geometry of the z-pins in order to maximise the thermal conductivity properties whilst retaining satisfactory mechanical and electrical properties.

Chapter 9:   Conclusions and Further Research

9.1   Summary

This PhD thesis has presented an experimental study into carbon-epoxy laminates reinforced in the through-thickness direction with z-pins. Research into the delamination fracture toughness, delamination fatigue resistance and impact damage tolerance was presented, and showed that z-pinning is an effective technique at improving these properties. Through a combination of friction and adhesion, z-pin lock the laminate plies together exercising bridging traction loads across delamination cracks which resist their further propagation. The effectiveness of z-pins at improving the through-thickness electrical conductivity and thermal diffusivity of carbon-epoxy laminates was also assessed through experimental and/or numerical investigations. Compared to the host laminate, z-pins have high electrical and thermal conductivities which create preferential paths for current and heat flow through-the-thickness.

9.2   Conclusions

9.2.1 Damage tolerance of z-pinned composites

The first part of this thesis has presented an experimental study into the improvements to the interlaminar fracture toughness and delamination fatigue resistance of z-pinned composites subjected to mode II static and cyclic loading conditions. The research showed that z-pins are effective at improving the mode II delamination toughness (up to 10 fold) and the fatigue resistance of carbon-epoxy laminates. The effect of the material properties, volume content, length and diameter of the z-pins was investigated. Irrespective of the material used for the z-pins, the mode II fracture toughness was increased due to the formation of a large-scale bridging zone along the delamination crack, although the carbon fibre z-pins were more effective than the metal pins. The mode II fracture toughness also increases with the volume content and diameter of the z-pins up to limiting values. The toughness increases when the z-pin length is reduced because of a transition in the crack bridging toughening mechanism. Irrespective of the volume content and diameter of z-pins, the carbon fibre z-pins within the bridging zone fail via complex processes which, with increasing crack sliding displacement, involve interfacial debonding, splitting and shear fracture. Because of small lateral displacement induced during the ENF test, metal z-pins did not fail and instead show partial debonding from the laminate and localised plastic shear deformation. The z-pins pull-out at short lengths and rupture at long lengths.

The mode II fatigue resistance was also increased by the carbon fibre and metal z-pins. Irrespective of the z-pin material used, the fatigue strength was improved especially at the low (ΔG_{II} <0.5 kJ/m^2) and high (ΔG_{II} >1 kJ/m^2) cyclic strain energy release rate values. The delamination fatigue resistance was increased with increasing volume content, diameter and decreasing length of z-pins which slowed the crack growth rate. Z-pins increase the mode II fatigue resistance by generating a large-scale extrinsic bridging zone along the fatigue crack. The metal z-pins plastically deformed close to the delamination crack plane by localised cyclic shear flow, but did not fail. The carbon fibre z-pin, permanently deformed close to the crack plane and eventually fractured under cyclic shear loading. Despite these differences in the fatigue responses between the metal and carbon fibre z-pins, this did not change significantly their capacity to increase the mode II delamination failure resistance (except at very low and high ΔG_{II} values when the carbon fibre pins were slightly better).

The work presented has proven that the amount of improvement is controlled from several parameters such as volume content, length, diameter and material properties of z-pins. Loading conditions also affect the performance and failure mechanism of z-pinned laminates. Reported in this thesis was a study on the interlaminar fracture toughness and fatigue resistance properties of z-pinned laminates subjected to mixed-mode I/II interlaminar loadings. When increasing the mode I component, both the delamination toughness and fatigue resistance were improved, and this was due to a transition in the toughening mechanisms. Z-pins are more effective under mode I than mode II because of their capacity to generate higher traction energy associated with pull-out, caused by high friction forces as the pins slide against the laminate.

The effects of the length and material properties of z-pins on the impact damage resistance and compression-after-impact properties was also experimentally investigated. This and other studies have proven that z-pinning is an effective technique to reduce the amount of impact damage and minimise the reduction to the in-plane compression-after-impact properties of carbon-epoxy laminates. Results showed that the z-pins reduce the amount of impact damage by up to about 50% and improved the post-impact compressive strength by about 20%. Z-pins are effective in reducing the impact damage because of the greater amount of energy absorbed by the elastic deformation, debonding and partial pull-out of pins. Increasing the impact energy increases the reduction to the impact damage due to the development of a large-scale bridging zone. The material properties of z-pins do not affect significantly the impact damage resistance

of the laminates. The pre-impact compressive strength and failure mode of the composites were not affected significantly by z-pins.

9.3   Electrical and Thermal Properties of Z-Pinned Composites

This PhD project extended the concept of using z-pinning to provide carbon-epoxy laminates with increased through-thickness electrical conductivity (including damage detection) and thermal conductivity properties.

Experimental tests showed that z-pins are capable of improving the through-thickness electrical conductivity by up to about 6 orders of magnitude. The conductivity increases with the volume content and electrical conductivity of z-pins. The through-thickness conductivity is increased by z-pins creating preferential paths for current flow. However, z-pins had a slight adverse effect on the in-plane electrical conductivity transverse to the fibre direction and this is due to dielectric resin-rich regions surrounding the pin sites disrupting the current flow. The suitability of z-pins for in-situ detection of delamination damage detection was also investigated. The measured through-thickness electrical resistance increases with the mode I delamination crack length. Due to a different conductive mode, the changes in resistivity were larger for the z-pinned laminates compared to the unpinned composite potentially making the delamination detection easier when using z-pins.

A numerical investigation was performed into the effects of the volume content and thermal properties of z-pins on the thermal diffusivity of z-pinned laminates. The through-thickness thermal diffusivity increased linearly with the volume content and thermal diffusivity of the z-pins, which create conductive paths for heat flow through the laminate. However, the z-pins were ineffective at increasing the in-plane (longitudinal and transverse) thermal properties of laminates.

To summarise, this PhD project experimentally characterised a novel multi-functional carbon fibre-epoxy laminate that uniquely combines high delamination resistance with increased thermal and electrical conductivities which can be tailored by judiciously choosing the volume content, diameter, length and material of the z-pins.

9.4   Future Research

For almost 20 years, z-pinning have attracted significant interest from researchers and the composite industry. There is a large body of experimental and numerical work that has

investigated the benefits and drawbacks with z-pins leading to a deeper understanding into their delamination strengthening efficiency and mechanisms, impact damage tolerance and in-plane mechanical properties of carbon fibre epoxy laminates. This PhD project has broadened this knowledge by analysing the static, fatigue and impact properties of z-pinned laminates under loading conditions that were not comprehensively studied. Preliminary studies into the suitability of z-pins at providing polymeric matrix composites with improved through-thickness electrical and thermal properties were performed. However, more research into z-pinned multi-functional composites is needed.

Models have been developed to predict the delamination toughness under mode I and mode II loading conditions, elastic properties and compressive strength, but there are no models that can predict the delamination fatigue performance of z-pinned laminates. Research towards the development of delamination fatigue model is needed which considers the effects of the volume content, diameter, length and material properties of z-pins. More research is also needed to further investigate the effect of z-pins on the electrical and thermal properties of composite.

References

[1]   J. Rouchon, Damage tolerance and fatigue evaluation of structure: The Composite Material Response, 22nd Plantema Memorial Lecture, 2001.

[2]   S. Dutton, A. Baker, D. Kelly. Composite Materials for Aircraft Structures, AIAA Education Series, Blacksburg, Virginia, 2004.

[3]   A. T. Hojo M. Tanaka, T. Adachi, S. Ochiai, Y. Endo. Modes I and II interlaminar fracture toughness and fatigue delamination of CF/epoxy laminates with self-same epoxy interleaf, International Journal of Fatigue. vol. 28, pp. 1154-165, 2006.

[4]   V. J. Argüelles, A. F. Canteli, M. A. Castrillo, J. Bonhomme. Interlaminar crack initiation and growth rate in a carbon–fibre epoxy composite under mode-I fatigue loading, Composite Science & Technology. vol. 68, pp. 2325-2331, 2008.

[5]   L. E. Asp, A. Sjögren, E. S. Greenhalgh. Delamination growth and thresholds in a carbon/epoxy composite under fatigue loading, Journal of Composites Technology and Research. vol. 23, pp. 55-68, 2001.

[6]   K. L. Rugg, B. N. Cox, K. E. Ward, G. O. Sherrick. Damage mechanisms for angled through-thickness rod reinforcement in carbon-epoxy laminates, Composites Part A: Applied Science and Manufacturing. vol. 29, pp. 1603-1613, 1998.

[7]   S. Sihn, A. K. Roy, Enhancement of through-thickness thermal conductivity of nanotube-reinforced composites, Collection of Technical Papers - AIAA/ASME/ASCE/AHS/ASC Structures, Structural Dynamics and Materials Conference, 2008.

[8]   G. Gardiner. Lightning strike protection for composite structures, High-Performance Composites. vol. 14, pp. 44-50, 2006.

[9]   D. Chakraborty. Delamination of laminated fiber reinforced plastic composites under multiple cylindrical impact, Materials and Design. vol. 28, pp. 1142-1153, 2007.

[10]   S. X. Wang, L. Z. Wu, L. Ma. Low-velocity impact and residual tensile strength analysis to carbon fiber composite laminates, Materials and Design. vol. 31, pp. 118-125, 2010.

[11]   F. Cappello, D. Tumino. Numerical analysis of composite plates with multiple delaminations subjected to uniaxial buckling load, Composites Science and Technology. vol. 66, pp. 264-272, 2006.

[12]   Anon. Z-pins strengthen the Super Hornet, save weight and cost, The Integrator. vol. 3, pp. 1-2, 2001.

[13] I. K. Partridge, D. D. R. Cartié, T. Bonnington. Manufacture and performance of z-pinned composites. In: G. Shonaike, S. Advani, editors. Advanced Polymeric Composites, Florida: CRC Press; 2003.

[14] S. McBeath. Safety pins, Racecar Eng. vol. 12, pp. 56-62, 2002.

[15] A. P. Mouritz. Review of z-pinned composite laminates, Composites Part A: Applied Science and Manufacturing. vol. 38, pp. 2383-2397, 2007.

[16] G. Freitas, T. Fusco, T. Campbell, J. Harris, S. Rosenberg. Z-Fibre technology and products for enhancing composite design, Proceedings of the 83rd Meeting of the AGARD SMP Conference on Bolted/Bonded Joints in Polymeric Composites, Florence Italy, Paper 17, pp. 2-3, 1996.

[17] C. A. Steeves, N. A. Fleck. In-plane properties of composite laminates with through-thickness pin reinforcement, International Journal of Solids and Structures. vol. 43, pp. 3197-3212, 2006.

[18] P. Chang. The mechanical properties and failure mechanisms of z-pinned composites. PhD Thesis, RMIT University, 2006.

[19] R. D. Sweeting, R. S. Thomson. The effect of thermal mismatch on z-pinned laminated composite structures, Composite Structures. vol. 66, pp. 189-195, 2004.

[20] P. Chang, A. P. Mouritz, B. N. Cox. Properties and failure mechanisms of pinned composite lap joints in monotonic and cyclic tension, Composites Science and Technology. vol. 66, pp. 2163-2176, 2006.

[21] A. P. Mouritz, P. Chang, H. Kong, B. N. Cox. Tensile properties of z-pinned polymer composites, Proceedings of the 27th international SAMPE Europe conference, 27-29. pp. 371-376, Paris France, 2006.

[22] W. Yan, H. Y. Liu, Y. W. Mai. Mode II delamination toughness of z-pinned laminates, Composites Science and Technology. vol. 64, pp. 1937-1945, 2004.

[23] W. Yan, H. Y. Liu, Y. W. Mai. Numerical study on the mode I delamination toughness of z-pinned laminates, Composites Science and Technology. vol. 63, pp. 1481-1493, 2003.

[24] L. Tong, X. Sun. Bending effect of through-thickness reinforcement rods on mode I delamination toughness of DCB specimen. Linearly elastic and rigid-perfectly plastic models, International Journal of Solids and Structures. vol. 41, pp. 6831-6852, 2004.

[25] K. L. Rugg, B. N. Cox, R. Massabò. Mixed mode delamination of polymer composite laminates reinforced through the thickness by z-fibers, Composites - Part A: Applied Science and Manufacturing. vol. 33, pp. 177-190, 2001.

[26]   P. Robinson, S. Das. Mode I DCB testing of composite laminates reinforced with z-direction pins: A simple model for the investigation of data reduction strategies, Engineering Fracture Mechanics. vol. 71, pp. 345-364, 2004.

[27]   A. Rezai, D. Cartié, I. Partridge, P. Irving, T. Aston, P. Negre. Interlaminar damage resistance of z-fibre™ reinforced structural CFRP, Proceedings of the 13th International Conference on Composite Materials, 25-29 June. 2001.

[28]   K. Pingkarawat, A. P. Mouritz. Improving the mode I delamination fatigue resistance of composites using z-pins, Composites Science and Technology. vol. 92, pp. 70-76, 2014.

[29]   A. P. Mouritz, T. M. Koh. Re-evaluation of mode I bridging traction modelling for z-pinned laminates based on experimental analysis, Composites Part B: Engineering. vol. 56, pp. 797-807, 2014.

[30]   A. P. Mouritz. Delamination properties of z-pinned composites in hot-wet environment, Composites Part A: Applied Science and Manufacturing. vol. 52, pp. 134-142, 2013.

[31]   H. Y. Liu, W. Yan, X. Y. Yu, Y. W. Mai. Experimental study on effect of loading rate on mode I delamination of z-pin reinforced laminates, Composites Science and Technology. vol. 67, pp. 1294-1301, 2007.

[32]   H. Cui, Y. Li, S. Koussios, L. Zu, A. Beukers. Bridging micromechanisms of z-pin in mixed mode delamination, Composite Structures. vol. 93, pp. 2685-2695, 2011.

[33]   B. N. Cox. Snubbing effects in the pullout of a fibrous rod from a laminate, Mechanics of Advanced Materials and Structures. vol. 12, pp. 85-98, 2005.

[34]   D. D. R. Cartié, M. Troulis, I. K. Partridge. Delamination of Z-pinned carbon fibre reinforced laminates, Composites Science and Technology. vol. 66, pp. 855-861, 2006.

[35]   D. D. R. Cartié, J. M. Laffaille, I. K. Partridge, A. J. Brunner. Fatigue delamination behaviour of unidirectional carbon fibre/epoxy laminates reinforced by z-fiber® pinning, Engineering Fracture Mechanics. vol. 76, pp. 2834-2845, 2009.

[36]   D. D. R. Cartié, B. N. Cox, N. A. Fleck. Mechanisms of crack bridging by composite and metallic rods, Composites Part A: Applied Science and Manufacturing. vol. 35, pp. 1325-1336, 2004.

[37]   D. J. Barrett. The mechanics of z-fiber reinforcement, Composite Structures. vol. 36, pp. 23-32, 1996.

[38]   B. N. Cox. Constitutive model for a fiber tow bridging a delamination crack, Mechanics of Composite Materials and Structures. vol. 6, pp. 117-138, 1999.

[39]   B. N. Cox. A constitutive model for through-thickness reinforcement bridging a delamination crack, Advanced Composites Letters. vol. 8, pp. 249-256, 1999.

[40]   B. N. Cox, N. Sridhar. A traction law for inclined fiber tows bridging mixed-mode cracks, Mechanics of Advanced Materials and Structures. vol. 9, pp. 299-331, 2002.

[41]   S. C. Dai, W. Yan, H. Y. Liu, Y. W. Mai. Experimental study on z-pin bridging law by pullout test, Composites Science and Technology. vol. 64, pp. 2451-2457, 2004.

[42]   D. A. Evans, J. S. Boyce, Transverse reinforcement methods for improved delamination resistance, International SAMPE Symposium and Exhibition, pp. 271-282, 1989.

[43]   G. Freitas, C. Magee, P. Dardzinski, T. Fusco. Fiber insertion process for improved damage tolerance in aircraft laminates, Journal of Advanced Matererials. vol. 25, pp. 36-43, 1994.

[44]   M. Grassi, X. Zhang. Finite element analyses of mode I interlaminar delamination in z-fibre reinforced composite laminates, Composites Science and Technology. vol. 63, pp. 1815-1832, 2003.

[45]   H. Y. Liu, W. Yan, Y. W. Mai. Z-pin bridging force in composite delamination, Fracture of Polymers, Composites and Adhesives II. vol. 32, pp. 491-502, 2003.

[46]   R. Massabo, B. N. Cox. Concepts for bridged Mode II delamination cracks, Journal of the Mechanics and Physics of Solids. vol. 47, pp. 1265-1300, 1999.

[47]   V. Dantuluri, S. Maiti, P. H. Geubelle, R. Patel, H. Kilic. Cohesive modeling of delamination in z-pin reinforced composite laminates, Composites Science and Technology. vol. 67, pp. 616-631, 2007.

[48]   G. Allegri, X. Zhang. On the delamination and debond suppression in structural joints by z-fibre pinning, Composites Part A: Applied Science and Manufacturing. vol. 38, pp. 1107-1115, 2007.

[49]   H. Cui, Y. Li, S. Koussios, A. Beukers. Mixed mode cohesive law for Z-pinned composite analyses, Computational Materials Science. vol. 75, pp. 60-68, 2013.

[50]   W. Yan, H. Y. Liu, Y. W. Mai. Numerical study on the mode I delamination toughness of z-pinned laminates, Composites Science and Technology. vol. 63, pp. 1481-1493, 2003.

[51]   D. D. R. Cartié, I. K. Partridge, Delamination behaviour of Z-pinned laminates, European Structural Integrity Society. vol. 27, J. G. Williams, A. Pavan, Elsevier, pp. 27-36, 2000.

[52]   F. Bianchi, X. Zhang. Predicting mode-II delamination suppression in z-pinned laminates, Composites Science and Technology. vol. 72, pp. 924-932, 2012.

[53]   M. Hojo, K. Tanaka, C. G. Gustafson, R. Hayashi. Effect of stress ratio on near-threshold propagation of delimination fatigue cracks in unidirectional CFRP, Composites Science and Technology. vol. 29, pp. 273-292, 1987.

[54]   A. Y. Zhang, H. Y. Liu, A. P. Mouritz, Y. W. Mai. Experimental study and computer simulation on degradation of z-pin reinforcement under cyclic fatigue, Composites Part A: Applied Science and Manufacturing. vol. 39, pp. 406-414, 2008.

[55]   K. Pingkarawat, A. P. Mouritz. Comparative study of metal and composite z-pins for delamination fracture and fatigue strengthening of composites, Engineering Fracture Mechanics. vol. 154, pp. 180-190, 2016.

[56]   X. Zhang, L. Hounslow, M. Grassi. Improvement to low-velocity impact and compression-after-impact performance of z-fibre pinning, Proceeding of the 13th International Conference on Composite Materials, 2003.

[57]   L. Dickinson, G. Farley, M. Hinders. Translaminar reinforced composites: a review, Journal of Composites Technology and Research. vol.21, pp. 3-15, 1999.

[58]   X. Zhang, L. Hounslow, M. Grassi. Improvement of low-velocity impact and compression-after-impact performance by z-fibre pinning, Composites Science and Technology. vol. 66, pp. 2785-2794, 2006.

[59]   M. D. Isa, S. Feih, A. P. Mouritz. Compression fatigue properties of z-pinned quasi-isotropic carbon/epoxy laminate with barely visible impact damage, Composite Structures. vol. 93, pp. 2269-2276, 2011.

[60]   M. Knaupp, F. Baudach, J. Franck, G. Scharr. Impact and post-impact properties of CFRP laminates reinforced with rectangular z-pins, Composites Science and Technology. vol. 87, pp. 218-223, 2013.

[61]   P. Chang, A. P. Mouritz, B. N. Cox. Properties and failure mechanisms of z-pinned laminates in monotonic and cyclic tension, Composites Part A: Applied Science and Manufacturing. vol. 37, pp. 1501-1513, 2006.

[62]   P. Chang, A. P. Mouritz, B. N. Cox. Flexural properties of z-pinned laminates, Composites Part A: Applied Science and Manufacturing. vol. 38, pp. 244-251, 2007.

[63]   L. C. Dickinson, G. L. Farley, M. K. Hinders. Prediction of effective three-dimensional elastic constants of translaminar reinforced composites, Journal Of Composite Materials. vol. 33, pp. 1002-1029, 1999.

[64]   M. Grassi, X. Zhang, M. Meo. Prediction of stiffness and stresses in z-fibre reinforced composite laminates, Composites Part A: Applied Science and Manufacturing. vol. 33, pp. 1653-1664, 2002.

[65]   A. P. Mouritz. Compression properties of z-pinned composite laminates, Composites Science and Technology. vol. 67, pp. 3110-3120, 2007.

[66]   T. K. O'Brien, R. Krueger. Influence of compression and shear on the strength of composite laminates with z-pinned reinforcement, Applied Composite Materials. vol. 13, pp. 173-189, 2006.

[67]   A. P. Mouritz, P. Chang. Tension fatigue of fibre-dominated and matrix-dominated laminates reinforced with z-pins, International Journal of Fatigue. vol. 32, pp. 650-658, 2010.

[68]   N. A. F. Craig A. Steeves. In-plane properties of composite laminates with through-thickness pin reinforcement, International Journal of Solids and Structures. vol. 43, p. 3197-3212, 2005.

[69]   X. Sun, H. Sun, H. Li, H. Peng. Developing polymer composite materials: Carbon nanotubes or graphene?, Advanced Materials. vol. 25, pp. 5153-5176, 2013.

[70]   A. A. Balandin, S. Ghosh, W. Bao, I. Calizo, D. Teweldebrhan, F. Miao, C. N. Lau. Superior thermal conductivity of single-layer graphene, Nano Letters. vol. 8, pp. 902-907, 2008.

[71]   R. A. Hauser, J. A. King, R. M. Pagel, J. M. Keith. Effects of carbon fillers on the thermal conductivity of highly filled liquid-crystal polymer based resins, Journal of Applied Polymer Science. vol. 109, pp. 2145-2155, 2008.

[72]   J. Nanda, C. Maranville, S. C. Bollin, D. Sawall, H. Ohtani, J. T. Remillard, J. M. Ginder. Thermal conductivity of single-wall carbon nanotube dispersions: Role of interfacial effects, Journal of Physical Chemistry C. vol. 112, pp. 654-658, 2008.

[73]   A. Yu, P. Ramesh, X. Sun, E. Bekyarova, M. E. Itkis, R. C. Haddon. Enhanced thermal conductivity in a hybrid graphite nanoplatelet-carbon nanotube filler for epoxy composites, Advanced Materials. vol. 20, pp. 4740-4744, 2008.

[74]   J. Gu, X. Yang, Z. Lv, N. Li, C. Liang, Q. Zhang. Functionalized graphite nano- platelets/epoxy resin nanocomposites with high thermal conductivity, International Journal of Heat and Mass Transfer. vol. 92, pp. 15-22, 2016.

[75]   I. M. Afanasov, D. V. Savchenko, S. G. Ionov, D. A. Rusakov, A. N. Seleznev, V. V. Avdeev. Thermal conductivity and mechanical properties of expanded graphite, Inorganic Materials. vol. 45, pp. 486-490, 2009.

[76]   I. A. Tsekmes, R. Kochetov, P. H. F. Morshuis, J. J. Smit, Thermal conductivity of polymeric composites: A review, Proceedings of IEEE International Conference on Solid Diele- ctrics, ICSD, 2013, pp. 678-681.

[77]   D. L. Gaxiola, J. M. Keith, J. A. King, B. A. Johnson. Nielsen thermal conductivity model for single filler carbon/polypropylene composites, Journal of Applied Polymer Science. vol. 114, pp. 3261-3267, 2009.

[78]   M. Šupová, G. S. Martynková, K. Barabaszová. Effect of nanofillers dispersion in polymer matrices: A review, Science of Advanced Materials. vol. 3, pp. 1-25, 2011.

[79]   A. Ma, W. Chen, Y. Hou, G. Zhang. The preparation and cure kinetics researches of thermal conductivity Epoxy/AlN composites, Polymer-Plastics Technology and Engineering. vol. 49, pp. 354-358, 2010.

[80]   Y. Yao, X. Zeng, K. Guo, R. Sun, J. B. Xu. The effect of interfacial state on the thermal conductivity of functionalized Al_2O_3 filled glass fibers reinforced polymer composites, Composites Part A: Applied Science and Manufacturing. vol. 69, pp. 49-55, 2015.

[81]   D. D. L. Chung. Materials for thermal conduction, Applied Thermal Engineering. vol. 21, pp. 1593-1605, 2001.

[82]   S. M. Firdaus, M. Mariatti. Fabrication and characterization of nano filler-filled epoxy composites for underfill application, Journal of Materials Science: Materials in Electronics. vol. 23, pp. 1293-1299, 2012.

[83]   F. Y. Yuan, H. B. Zhang, X. Li, X. Z. Li, Z. Z. Yu. Synergistic effect of boron nitride flakes and tetrapod-shaped ZnO whiskers on the thermal conductivity of electrically insulating phenol formaldehyde composites, Composites Part A: Applied Science and Manufacturing. vol. 53, pp. 137-144, 2013.

[84]   G. W. Lee, M. Park, J. Kim, J. I. Lee, H. G. Yoon. Enhanced thermal conductivity of polymer composites filled with hybrid filler, Composites Part A: Applied Science and Manufacturing. vol. 37, pp. 727-734, 2006.

[85]   R. B. Ladani, S. Wu, A. J. Kinloch, K. Ghorbani, J. Zhang, A. P. Mouritz, C. H. Wang. Improving the toughness and electrical conductivity of epoxy nanocomposites by using aligned carbon nanofibres, Composites Science and Technology. vol. 117, pp. 146-158, 2015.

[86]   E. T. Thostenson, Z. Ren, T. W. Chou. Advances in the science and technology of carbon nanotubes and their composites: A review, Composites Science and Technology. vol. 61, pp. 1899-1912, 2001.

[87]   M. Rahmat, P. Hubert. Carbon nanotube-polymer interactions in nanocomposites: A review, Composites Science and Technology. vol. 72, pp. 72-84, 2011.

[88]   W. Bauhofer, J. Z. Kovacs. A review and analysis of electrical percolation in carbon nanotube polymer composites, Composites Science and Technology. vol. 69, pp. 1486-1498, 2009.

[89]   S. Shadlou, E. Alishahi, M. R. Ayatollahi. Fracture behavior of epoxy nanocomposites reinforced with different carbon nano-reinforcements, Composite Structures. vol. 95, pp. 577-581, 2013.

[90]   G. Tibbetts, M. L. Lake, K. L. Strong, B. P. Rice. A review of the fabrication and properties of vapor-grown carbon nanofiber/polymer composites, Composites Science and Technology. vol. 67, pp. 1709-1718, 2007.

[91]   M. A. Rafiee, J. Rafiee, I. Srivastava, Z. Wang, H. Song, Z. Z. Yu, N. Koratkar. Fracture and fatigue in graphene nanocomposites, Small. vol. 6, pp. 179-183, 2010.

[92]   S. Chatterjee, F. Nafezarefi, N. H. Tai, L. Schlagenhauf, F. A. Nüesch, B. T. T. Chu. Size and synergy effects of nanofiller hybrids including graphene nanoplatelets and carbon nanotubes in mechanical properties of epoxy composites, Carbon. vol. 50, pp. 5380-5386, 2012.

[93]   A. Argüelles, J. Viña, A. F. Canteli, M. A. Castrillo, J. Bonhomme. Interlaminar crack initiation and growth rate in a carbon-fibre epoxy composite under mode-I fatigue loading, Composites Science and Technology. vol. 68, pp. 2325-2331, 2008.

[94]   H. Masaki, O. Shojiro, C.-G. Gustafson, T. Keisuke. Effect of matrix resin on delamination fatigue crack growth in CFRP laminates, Engineering Fracture Mechanics. vol. 49, pp. 35-47, 1994.

[95]   H. G. Son, Y. B. Park, J. H. Kweon, J. H. Choi. Fatigue behaviour of metal pin-reinforced composite single-lap joints in a hygrothermal environment, Composite Structures. vol. 108, pp. 151-160, 2014.

[96]   M. G. Ko, J. H. Kweon, J. H. Choi. Fatigue characteristics of jagged pin-reinforced composite single-lap joints in hygrothermal environments, Composite Structures. vol. 119, pp. 59-66, 2014.

[97]   Advanced Composite Group Umeco. ACG VTM 260Series variable temperature moulding prepreg system, 2006. [ONLINE] Available at: http://www.lavender-ce.com/wp-content/uploads/pds1154-vtm260-issue5.pdf. [Accessed 10 August 2016].

[98]   ASM Handbooks Online. ASM Handbooks Online, vol 19, 2016. [ONLINE] Available at: http://products.asminternational.org/hbk/index.jsp. [Accessed 2 August 2016].

[99]   F. K. Ko. Braiding, Engineered Materials Handbook. vol. 1, pp. 519-528, 1987.

[100]   C. S. V. M.S. Sham Prasad, T. Jayaraju. Experimental methods of determining fracture toughness of fiber reinforced polymer composites under various loading conditions, Journal of Mineral & Materials Characterization & Engineering. vol. 10, p. 1263-1275, 2011.

[101]   F. Bianchi, X. Zhang. A cohesive zone model for predicting delamination suppression in z-pinned laminates, Composites Science and Technology. vol. 71, pp. 1898-1907, 2011.

[102]   L. W. Byrd, V. Birman. The estimate of the effect of z-pins on the strain release rate, fracture and fatigue in a composite co-cured z-pinned double cantilever beam, Composite Structures. vol. 68, pp. 53-63, 2005.

[103]   L. W. Byrd, V. Birman. Effectiveness of z-pins in preventing delamination of co-cured composite joints on the example of a double cantilever test, Composites Part B: Engineering. vol. 37, pp. 365-378, 2006.

[104]   J. G. Ratcliffe, T. K. O'Brien. Discrete spring model for predicting delamination growth in z-fibre reinforced DCB specimens. NASA Langley Research Center, Hampton, Virginia, U.S.A., 2004.

[105]   F. Warzok, G. Allegri, M. Gude, S. R. Hallett. Experimental characterisation of fatigue damage in single z-pins, Composites Part A: Applied Science and Manufacturing. In press, corrected proof.

[106] M. Yasaee, J. K. Lander, G. Allegri, S. R. Hallett. Experimental characterisation of mixed mode traction–displacement relationships for a single carbon composite z-pin, Composites Science and Technology. vol. 94, pp. 123-131, 2014.

[107] B. Zhang, G. Allegri, M. Yasaee, S. R. Hallett. Micro-mechanical finite element analysis of z-pins under mixed-mode loading, Composites Part A: Applied Science and Manufacturing. vol. 78, pp. 424-435, 2015.

[108] G. Allegri, M. Yasaee, I. K. Partridge, S. R. Hallett. A novel model of delamination bridging via z-pins in composite laminates, International Journal Of Solids and Structures. vol. 51, pp. 3314-3332, 2014.

[109] ASTM D6671/D6671M-06, Standard Test Method for Mixed Mode I-Mode II Interlaminar Fracture Toughness of Unidirectional Fiber Reinforced Polymer Matrix Composites.

[110] M. D. Isa, S. Feih, A. P. Mouritz. Compression fatigue properties of quasi-isotropic z-pinned carbon/epoxy laminate with barely visible impact damage, Composite Structures. vol. 93, pp. 2222-2230, 2011.

[111] X. Zhang, G. A. O. Davies, D. Hitchings. Impact damage with compressive preload and post-impact compression of carbon composite plates, International Journal of Impact Engineering. vol. 22, pp. 485-509, 1999.

[112] J. J. Childress, G. Freitas. Z-direction pinning of composite laminates for increased survivability, Proceedings of the AIAA Aerospace Design Conference. pp. 92-109, 1992.

[113] D. B. Vaidya, U. K. Kopacz. Affordable processing and characterization of multi-functional z-pin reinforced VARTM composites, Proceedings of the 13th international conference on composite materials, Beijing, 2001.

[114] I. K. Partridge, M. Troulis, M. Grassi X. Zhang. Evaluating the mechanical effectiveness of z-pinning, Proceedings of the SAMPE technical conference, 2004.

[115] C. Li, Y. Yan, P. Wang, D. Qi, Y. Wen. Study on compressive properties of z-pinned laminates in RTD and hygrothermal environment, Chinese Journal of Aeronautics. vol. 25, pp. 64-70, 2012.

[116] B. Zhang, G. Allegri, S. R. Hallett. An experimental investigation into multi-functional z-pinned composite laminates, Materials & Design. vol. 108, pp. 679-688, 2016.

[117] Conductive Materials or Metal Conductivity - TIBTECH innovations. Conductive Materials or Metal Conductivity - TIBTECH innovations, 2016. [ONLINE] Available at: http://www.tibtech.com/conductivity.php. [Accessed 26 August 2016].

[118] X. Yang, Z. Wang, M. Xu, R. Zhao, X. Liu. Dramatic mechanical and thermal increments of thermoplastic composites by multi-scale synergetic reinforcement: Carbon fiber and graphene nanoplatelet, Materials and Design. vol. 44, pp. 74-80, 2013.

[119] S. Y. Pak, H. M. Kim, S. Y. Kim, J. R. Youn. Synergistic improvement of thermal conductivity of thermoplastic composites with mixed boron nitride and multi-walled carbon nanotube fillers, Carbon. vol. 50, pp. 4830-4838, 2012.

[120] W. Li, A. Dichiara, J. Bai. Carbon nanotube-graphene nanoplatelet hybrids as high-performance multifunctional reinforcements in epoxy composites, Composites Science and Technology. vol. 74, pp. 221-227, 2013.

[121] J. Kim, J. Kim, B. S. Yim, J. M. Kim. The effects of functionalized graphene nanosheets on the thermal and mechanical properties of epoxy composites for anisotropic conductive adhesives (ACAS), Microelectronics Reliability. vol. 52, pp. 595-602, 2012.

[122] C. Heo, J. H. Chang. Polyimide nanocomposites based on functionalized graphene sheets: Morphologies, thermal properties, and electrical and thermal conductivities, Solid State Sciences. vol. 24, pp. 6-14, 2013.

[123] S. Chatterjee, J. W. Wang, W. S. Kuo, N. H. Tai, C. Salzmann, W. L. Li, R. Hollertz, F. A. Nüesch, B. T. T. Chu. Mechanical reinforcement and thermal conductivity in expanded graphene nanoplatelets reinforced epoxy composites, Chemical Physics Letters. vol. 531, pp. 6-10, 2012.

[124] S. Chandrasekaran, C. Seidel, K. Schulte. Preparation and characterization of graphite nano-platelet (GNP)/epoxy nano-composite: Mechanical, electrical and thermal properties, European Polymer Journal. vol. 49, pp. 3878-3888, 2013.

[125] E. Kandare, A. Khatibi, S. Yoo, R. Wang, J. Ma, P. Olivier, N. Gleizes, C. H. Wang. Improving the through-thickness thermal and electrical conductivity of carbon fibre/epoxy laminates by exploiting synergy between graphene and silver nano-inclusions, Composites Part A: Applied Science and Manufacturing. vol. 69, pp. 72-82, 2015.

[126] S. Han, J. T. Lin, Y. Yamada, D. D. L. Chung. Enhancing the thermal conductivity and compressive modulus of carbon fiber polymer–matrix composites in the through-thickness direction by nanostructuring the interlaminar interface with carbon black, Carbon. vol. 46, pp. 1060-1071, 2008.

[127] S. Han, D. D. L. Chung. Increasing the through-thickness thermal conductivity of carbon fiber polymer–matrix composite by curing pressure increase and filler incorporation, Composites Science and Technology. vol. 71, pp. 1944-1952, 2011.

[128] M. H. Al-Saleh, U. Sundararaj. Review of the mechanical properties of carbon nanofiber/polymer composites, Composites Part A: Applied Science and Manufacturing. vol. 42, pp. 2126-2142, 2011.

[129] J. Schuster, D. Heider, K. Sharp, M. Glowania. Thermal conductivities of three-dimensionally woven fabric composites, Composites Science and Technology. vol. 68, pp. 2085-2091, 2008.

[130] W. Parker, R. Jenkins, C. Butler, G. Abbott. Flash method of determining thermal diffusivity, heat capacity, and thermal conductivity, Journal of Applied Physics. vol. 32, pp. 1679-1684, 1961.

[131] P. E. Specht, M. A. Cooper. Thermal diffusivity and specific heat measurements of titanium potassium perchlorate, titanium subhydride potassium perchlorate, 9013 glass, 7052 glass, sb-14 glass, d c-4000 muscovite mica using the flash technique, 2015. [ONLINE] Available at: http://prod.sandia.gov/techlib/access-control.cgi/2015/150889 .pdf. [Accessed 27 July 2016].

[132] AK Steel. Product data sheet 316/316L Stainless steel UNS S31600 AND UNS S31603, 2016. [ONLINE] Available at: http://www.aksteel.com/pdf/markets_products/ stainless /austenitic/316_316l_data_sheet.pdf. [Accessed 5 July 2016].

[133] Metals and Alloys - Densities. Metals and Alloys Densities, 2016. [ONLINE] Available at: http://www.engineeringtoolbox.com/metal-alloys-densities-d_50.html. [Accessed 26 August 2016].

[134] Mechanical Properties of Carbon Fibre Composite Materials. Mechanical Properties of Carbon Fibre Composite Materials, 2016. [ONLINE] Available at: http://www. performance-composites.com/carbonfibre/mechanicalproperties_2.asp. [Accessed 26 August 2016].

[135] R. D. R. Joven, A. Ahmed, P. Roozbehjavan, B. Minaie. Thermal properties of carbon fiber/epoxy composites with different fabric weaves, Conference: SAMPE International Symposium, Charleston, SC, 2012.

[136] T. Tian. Anisotropic Thermal Property Measurement of Carbon-fiber/Epoxy Composite Materials, PhD Thesis, University of Nebraska, 2011.